Astronomy & Astrophysics manuscript no.
(will be inserted by hand later)

arXiv:astro-ph/0104297v2 20 Apr 2001

The second ROSAT PSPC survey of M31 and the complete ROSAT PSPC source list

R. Supper[1], G. Hasinger[1,2], W.H.G. Lewin[3], E.A. Magnier[4], J. van Paradijs[†5,6], W. Pietsch[1], A.M. Read[1], and J. Trümper[1]

[1] Max-Planck-Institut für extraterrestrische Physik, Postfach 1603, 85740 Garching, Germany
[2] Astrophysikalisches Institut, An der Sternwarte 16, 14482 Potsdam, Germany
[3] CSR and Department of Physics, Massachusetts Institute of Technology, Room 37-627, Cambridge, MA 02139, USA
[4] Canada-France-Hawaii Telescope, 65-1238 Mamalahoa Hwy, Kamuela, HI 96743, USA
[5] Astronomical Institute "Anton Pannekoek", University of Amsterdam, Kruislaan 403, 1098 SJ Amsterdam, Netherlands
[6] Physics Department, University of Alabama in Huntsville, Huntsville, AL 35899, USA

Received date / Accepted date

Abstract. This paper reports the results of the analysis of the second ROSAT PSPC survey of M31 performed in summer 1992. We compare our results with those of the first survey, already published in Supper et al. (1997). Within the ~ 10.7 deg^2 field of view, 396 individual X-ray sources are detected in the second survey data, of which 164 are new detections. When combined with the first survey, this result in a total of 560 X-ray sources in the field of M31. Their (0.1 keV – 2.0 keV) fluxes range from 7×10^{-15} erg cm^{-2} s^{-1} to 7.6×10^{-12} erg cm^{-2} s^{-1}, and of these 560 sources, 55 are tentatively identified with foreground stars, 33 with globular clusters, 16 with supernova remnants, and 10 with radio sources and galaxies (including M32). A comparison with the results of the *Einstein* M31 survey reveals 491 newly detected sources, 11 long term variable sources, and 7 possible transient sources. Comparing the two ROSAT surveys, we come up with 34 long term variable sources and 8 transient candidates. For the M31 sources, the observed luminosities range from 4×10^{35} erg s^{-1} to 4×10^{38} erg s^{-1}. The total (0.1 keV – 2.0 keV) luminosity of M31 is $(3.4 \pm 0.3) \times 10^{39}$ erg s^{-1}, distributed approximately equally between the bulge and disk. Within the bulge region, the luminosity of a possible diffuse component combined with faint sources below the detection threshold is $(2.0 \pm 0.5) \times 10^{38}$ erg s^{-1}. An explanation in terms of hot gaseous emission leads to a maximum total gas mass of $(1.0 \pm 0.3) \times 10^6$ M$_\odot$.

Key words. galaxies: fundamental parameters – galaxies: individual: M31 – galaxies: spiral – X-rays: galaxies

1. Introduction

Before ROSAT, the knowledge of the X-ray properties of M31 was mainly based on the IPC and HRI observations with the *Einstein* observatory. These observations were performed in the years 1979 & 1980 and the main results are described in van Speybroeck et al. (1979), van Speybroeck & Bechtold (1981), Long & van Speybroeck (1983), Crampton et al. (1984), and Trinchieri & Fabbiano (1991, hereafter TF). In 300 ks of total exposure, $\sim 86\%$ of the area of our neighbouring spiral galaxy M31 had been covered to a limiting sensitivity of $\sim 10^{37}$erg s^{-1}. Many of the 108 detected point sources within these *Einstein* observations were measured with a positional accuracy of about $3''$, and were found to be concentrated within a highly confused bulge region and an outer region approximately following the spiral arms. In addition, a variety of possible optical counterparts had been determined, dividing into groups of foreground stars within our own Galaxy, accreting objects and supernova remnants in M31 and background galaxies seen through the disc of M31. Additionally, it had been considered that the luminosity distribution of the M31 disk sources were comparable with that of the bulge sources. The high confusion in the bulge region together with the moderate total number of detected sources made it difficult to justify this statement.

Two deep PSPC surveys of M31 were performed with the ROSAT X-ray observatory, the first in the summer of 1991, the second in the summer of 1992 (with some follow-up observations in the winter of 1992/1993). Both surveys consisted of a number of observations arranged in raster pointings, covering the whole area of M31 and

Send offprint requests to: R. Supper, e-mail:ros@mpe.mpg.de
†Jan van Paradijs passed away on November 2nd, 1999.

beyond. The total observation time of 200 ks for each survey, together with the higher sensitivity of the ROSAT telescope pushed the limiting flux to a factor of $10 - 100$ lower than for the *Einstein* observations. Additionally, several ROSAT HRI M31 pointings were performed, including a very deep one on the bulge. These were discussed by Primini et al. (1993) and Immler (2000).

The results of the first PSPC survey have been described in Supper et al. (1997, hereafter S97). This work led to the detection of 396 X-ray point sources with (0.1 keV - 2.4 keV) fluxes ranging from $\sim 5 \times 10^{-15}$erg cm^{-2} s^{-1} to $\sim 4 \times 10^{-12}$erg cm^{-2} s^{-1}. Several tentative identifications with foreground stars, globular clusters, supernova remnants, and galaxies were found, but the majority of the objects remained unidentified. For the sources in M31, the observed luminosities range from $\sim 3 \times 10^{35}$erg s^{-1} to $\sim 2 \times 10^{38}$erg s^{-1} (at the assumed M31 distance of 690 kpc used throughout this paper; see Capaccioli et al. 1989). Also this very first survey settled the question of whether a difference between the integrated luminosity distribution of the globular cluster sources in M31 and the one in our own Milky Way existed, by showing that they were in fact similar. Also, spectral analyses of the 56 brightest sources were presented, confirming their identifications with optical sources. Additionally, a diffuse component within the bulge region was found, its luminosity estimated to be less than 3.2×10^{38}erg s^{-1}.

For 10 of the brightest sources, and for the bulge as a whole, Trinchieri et al. (1999) presented results from spectral analyses based on data obtained with BeppoSAX. They confirmed that most of the sources correlate with globular clusters and found, for all but one, Low Mass X-ray Binary (LMXB) spectra, typical of X-ray sources in globular clusters. Additionally, they also confirmed the presence of two components in the spectrum of the bulge, though they also stated that it is consistent with a superposition of many LMXB spectra (as Irwin & Bregman 1999 also did using ASCA and ROSAT data). Furthermore they extended the spectral data range up to ~ 30 keV by making use of the PDS instrument. Because of the lower spatial resolution of BeppoSAX compared with ROSAT, they could not resolve the bulge into individual sources. Garcia et al. (2000) reported the separating of the central source into 5 individual sources using Chandra data. They interpreted one of these sources ($1''$ from the centre) as a possible central black hole, although it shows an unusual (soft) spectrum. In contrast, using ROSAT PSPC observations, Borozdin & Priedhorsky (2000) found all the resolved X-ray sources in the core of M31 to be in accordance with LMXB spectra, this after subtracting a soft component (thought to be thermal emission from hot gas) derived from the area around the individual sources.

The second PSPC survey of M31, described in this paper, is an improvement over the first in terms of its higher spatial homogeneity across the entire disk of M31. This has resulted here in the detection of 396 X-ray point sources, leading to a grand total of 560 individual sources

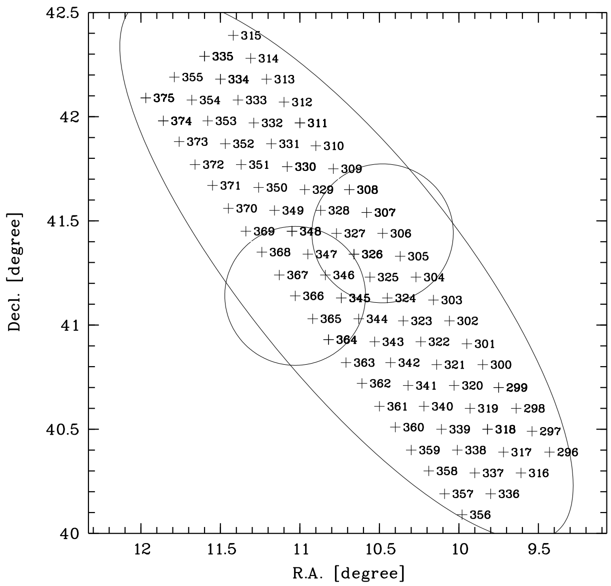

Fig. 1. Locations of the 80 on-axis pointing directions of the second PSPC survey of M31. The numbers beside the crosses give the last three digits of the corresponding ROSAT observation ID. Two PSPC central regions with $20'$ radius are drawn representatively (whereas the total FOV is ~ 3 times larger). The D_{25}-ellipse of M31 is indicated.

on merging the two surveys. Both the list resulting from the here-described analysis of the second survey as well as the merged list of both surveys are presented in this paper. For the majority of the X-ray sources already identified in the first survey, the positional accuracy has been improved. Also, the time interval of approximately one year between the two surveys allows a time variability study to be made, and this is also described in this paper. Spectral analysis is not presented here as it is only suitable for the brightest sources, which were already seen in the first survey, their spectra having been studied in S97.

2. Observations

The analysis in this paper is based on the second pointed M31 survey with the ROSAT PSPC, performed in July/August 1992 together with a few follow-up observations in January 1993. This survey consists of 94 observations of 80 different pointing positions, with 2.5 ks total observation time for each pointing. 15 follow-up observations became necessary to complete the observation time of 14 previously interrupted observations and 1 completely failed observation. The details of the observations are given in Table 4. This entire raster pointing covered the whole disk of M31 (in terms of its D_{25}-ellipse) and more, in 4 strips of 20 pointing directions each. Fig. 1 shows the location of these 80 pointings, crosses marking the on-axis directions of the telescope, and the numbers giving the last three digits of the corresponding ROSAT

observation ID. Follow-up observations are not numbered as they have the same pointings as their corresponding main observations. For two pointings, a $20'$ radius circle is drawn to represent the inner area of the PSPC. The instrument's angular resolution and sensitivity are best within this area, though the total field of view (FOV) of the PSPC is $57'$ in radius. The D_{25}-ellipse of M31 is also drawn for orientation. Just from this image, it can be seen that the whole of M31 is covered by the inner PSPC region, leading to an overall approximately constant sensitivity.

The observations were performed in the normal ROSAT wobble mode which adds a slight positional oscillation of $\sim 3'$ amplitude on the nominal pointing direction. This was done to smooth out the shadow of the PSPC support structure and to prevent point sources being continually hidden behind the main ribs of the structure. This wobble mode, the finely rastered array of the pointing directions, and the fact that the whole disk of M31 was covered with the inner PSPC region explain the higher homogeneity of the second survey compared with the first described in S97.

3. Analysis

For the analysis, the ROSAT energy range from 0.1 to 2.4 keV was divided into five energy bands: a soft band (S: 0.1 - 0.4 keV), two hard bands (H1: 0.5 - 0.9 keV and H2: 0.9 - 2.0 keV), and two combined bands (hard H: 0.5 - 2.0 keV and broad B: 0.1 - 2.0 keV). This energy band splitting was used previously in the analysis of the first M31 survey (S97), except that an upper limit of 2.4 keV was used for the B-band. The change from 2.4 keV to 2.0 keV makes no significant difference due to the drastic drop in effective area for the ROSAT telescope + PSPC instrumentation between 2.0 and 2.4 keV (the count rate in the 0.1-2.0 keV energy band is 2% less than in the 0.1-2.4 keV band, when applying a power law with photon index $\Gamma = -2.0$ and $N_{\rm H} = 9 \times 10^{20}$ cm^{-2} as a spectral model – typical for M31 sources). Therefore the count rates of the two survey analyses are directly comparable.

Parts of the following analysis are based on the Extended Scientific Analysis System (EXSAS; Zimmermann et al. 1993) developed at the Max-Planck-Institute für extraterrestrische Physik.

3.1. Data preparation and images

All the data were inspected for contamination by solar scattered X-rays and particle background. The first originate from Thomson and fluorescent scattering of solar X-ray photons with atoms and molecules in the upper atmosphere along the line of sight. For the ROSAT orbit, these are mainly oxygen, nitrogen, argon, helium, and hydrogen (Jacchia 1972). For the integral solar scatter, the illuminated column density of the atomic oxygen can be used because of the well known fixed ratio of scatter contribution of the other components, as discussed in detail by Snowden & Freyberg (1993). Therefore, for each pointing, the column density of atomic oxygen was calculated from the orientation of the telescope and the sun position during the whole observation. All time intervals with oxygen column densities above 1×10^{15} cm^{-2} (see Snowden & Freyberg 1993 for an explanation of this threshold) were rejected.

Snowden et al. (1992) found a strong correlation between the Master Veto Rate of the ROSAT onboard electronics and the residual particle background not rejected by the veto electronics. Therefore, all time intervals with a Master Veto Rate of more than 170 ct s^{-1} were additionally rejected. Applying these procedures, the rest of the scattered X-rays and residual particle background within the screened intervals was estimated to be less than 1%.

For the following analysis, the photon events of all 94 observations representing the survey were merged into one single event file. This increased the photon statistics and allowed us to make use of the homogeneity of the raster survey. A slight random offset and rotation of each pointing was corrected for by first correlating bright point sources in neighbouring pointings detected by the Standard Analysis Software System (SASS) and delivered with the data. For this purpose, only sources within the inner PSPC region ($20'$ radius) were used where the telescope has its highest spatial resolution. The final source position was calculated as the weighted mean position from the individual source positions in each contributing pointing, with the signal to noise ratio as the weighting factor. In a last step, each contributing pointing was shifted and rotated to fit best this mean source position. The distribution of the shift and rotation offsets over all 94 pointings was found to be gaussian-like, with $\sigma = 5.2''$ in shift and $\sigma = 0.21°$ in rotation. These corrected data were then ready to be merged.

Fig. 2 shows a photon image in the B-band from the merged inner PSPC regions of the 94 pointings with a pixel size of $21.5'' \times 21.5''$. Just from this image, the high homogeneity and the narrow (center of detector) point spread function (PSF; Hasinger et al. 1992) of the second ROSAT M31 survey across the whole galaxy (indicated by the D_{25}-ellipse) can be seen, especially when compared to the image of the first survey (Fig. 2 in S97). Some bright identified sources are also indicated in Fig. 2. Most of them are not members of the M31 system. The bulge region is severely crowded by point sources and confused by an additional diffuse component.

Fig. 3 shows an optical image (taken from the Mount Palomar Sky Survey) of M31 in false colour representation. Size and orientation are as in Fig. 2 and the D_{25}-ellipse of M31 is also marked. The white boxes mark the 560 X-ray source positions from the analyses of both ROSAT PSPC surveys of M31 as described in Sect. 3.3 and listed in Table 6. The 4 box sizes indicate the logarithm of the X-ray luminosities below 36, between 36 and 37, between 37 and 38, and above 38 (from small to large). This corresponds to flux thresholds of $1.76 \times 10^{(-14,-13,-12)}$erg cm^{-2} s^{-1}. For flux calculations, a spectral model of a power law with photon index $\Gamma = -2.0$ and

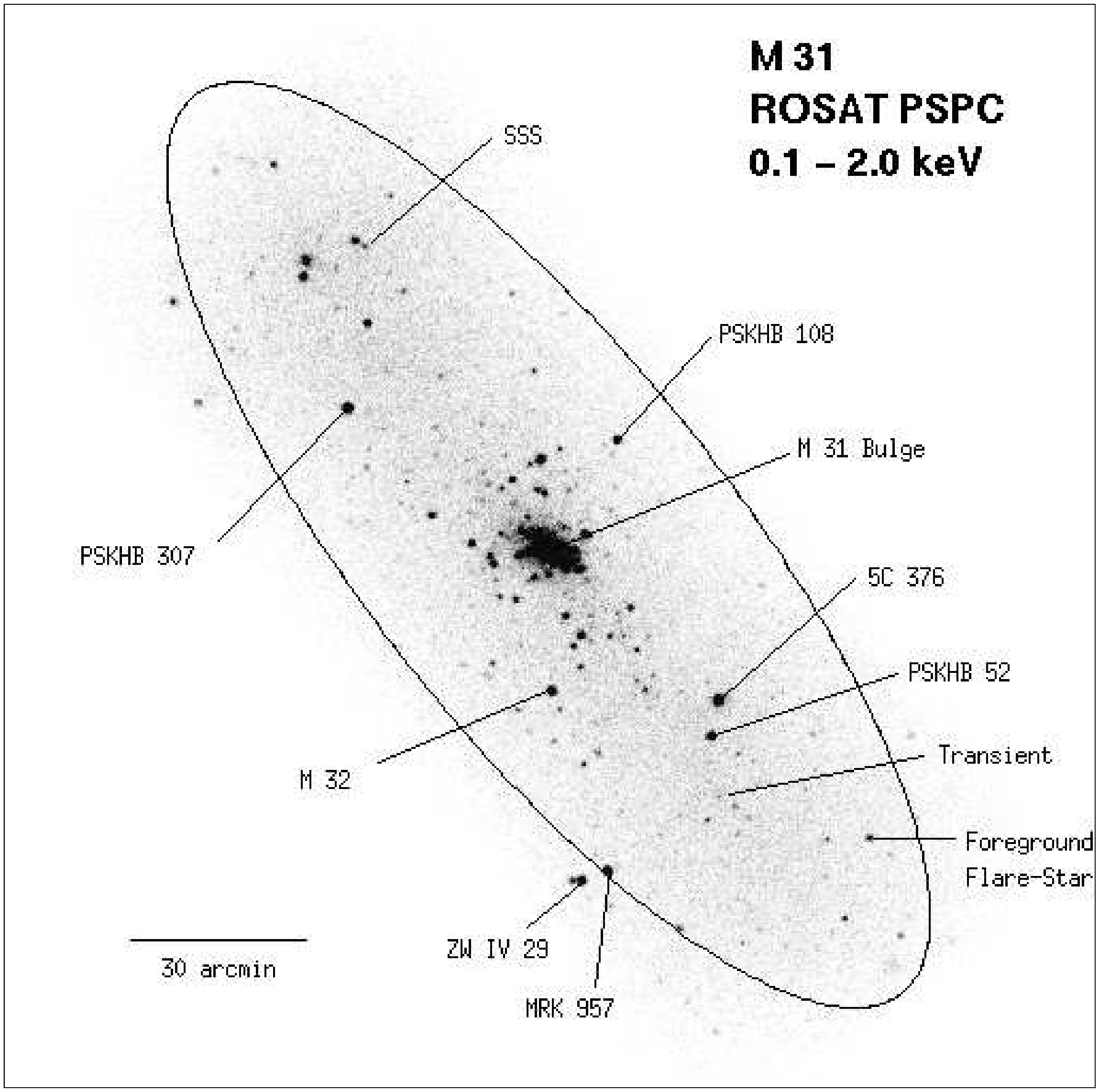

Fig. 2. Projection of the B-band photons of the merged 94 pointings in the inner PSPC regions (20′ radius each) with a pixel size of 21.5″ × 21.5″. The D_{25}-ellipse of M31 is marked. For a few bright sources their identifications are given, 'SSS' standing for 'supersoft source'. During the first ROSAT M31 survey, the here indicated transient source was as bright as PSKHB 52.

$N_{\rm H} = 9 \times 10^{20}$ cm^{-2} has been used which holds for M31-sources but not for foreground or background objects. A distance of 690 kpc for M31 is asumed for the resulting luminosity values.

3.2. Source detection

To make use of the high homogeneity of the second PSPC M31 survey, the source detection was performed on the merged data of the inner PSPC regions of all 94 observations. This guaranteed the best results for the determined source positions and covered approximately the whole D_{25}-area of M31. For detections of sources outside this region, the following source detection procedure was repeated using the merged data of the total FOV. The source detection technique used is similar to the one previously used for the analysis of the first survey and described in detail in S97. Hence, only a brief description will be given here, with emphasis on the differences employed.

The computations can be divided into three steps: a local, a map, and a maximum likelihood detection algo-

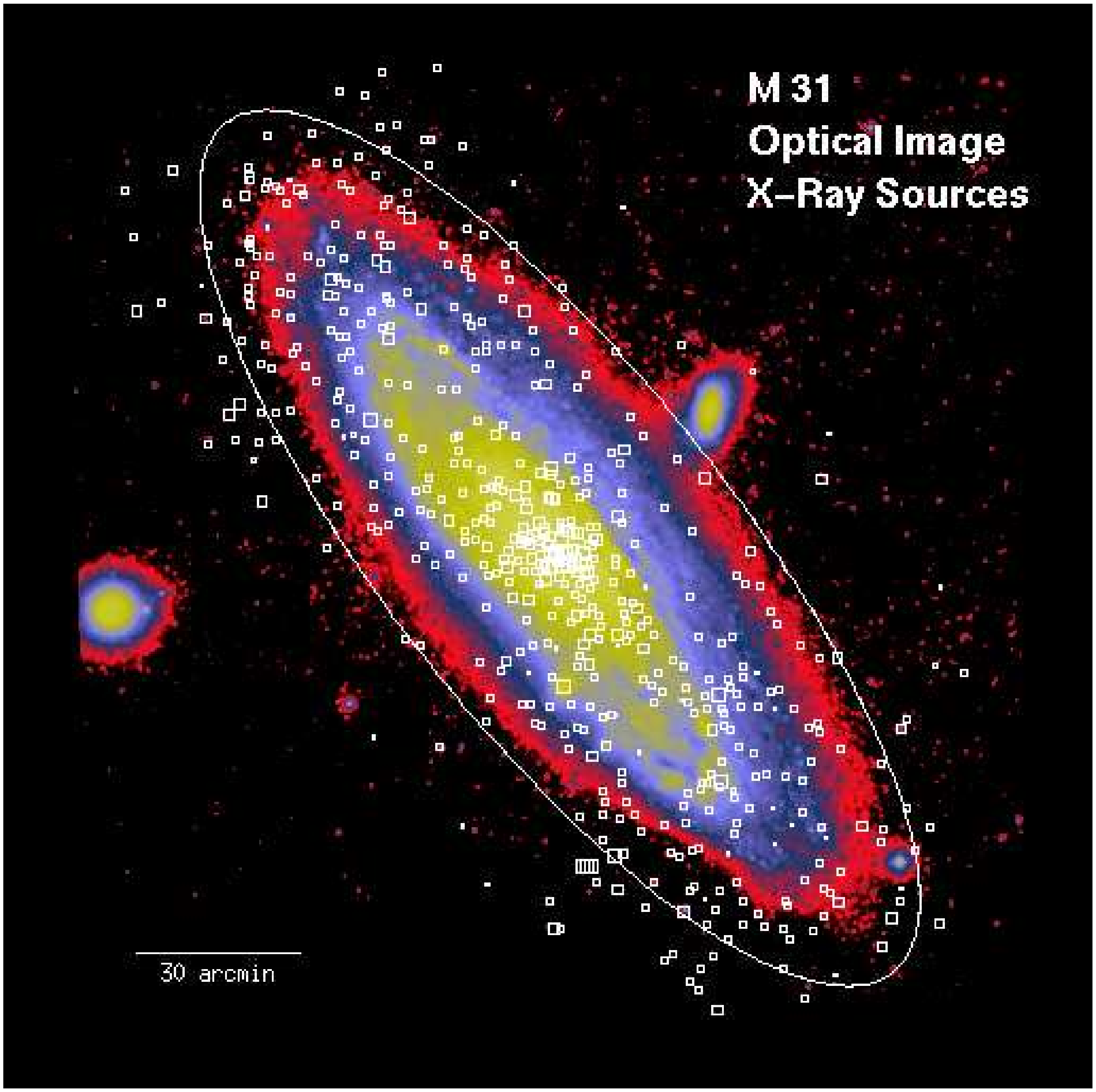

Fig. 3. False colour image of M31 made from an optical photography with the Mount Palomar observatory. Size and orientation are as in Fig. 2 (also the D_{25}-ellipse of M31 is marked). The white boxes give the 560 X-ray source positions from the analyses of the first and second ROSAT PSPC survey of M31 as described in Sect. 3.3 and listed in Table 6. The 4 box sizes indicate the logarithm of the X-ray luminosities below 36, between 36 and 37, between 37 and 38, and above 38 (from small to large). This corresponds to flux thresholds of $1.76 \times 10^{(-14,-13,-12)}$erg cm^{-2} s^{-1}.

rithm. For the local detect algorithm, the merged photon event tables were split into a northern, middle and southern part and for each part, images were created with a pixel size of $15'' \times 15''$ for each of the five energy bands. This led to $3 \times 5 = 15$ images for the three regions and the five energy bands. With a sliding window technique (3×3 pixel box), the images were searched for a significant count excess within the box compared with the surroundings. Only source candidates with a likelihood of existence ≥ 8 were listed, where the likelihood L = -ln(P), P being the probability that the measured number of photons in the box originate from Poissonian background fluctuations.

In the following map detect algorithm, the same procedure was applied to the 15 images, but this time the photon number within the box was compared with the number of photons within a box of equivalent area and position in a background map. These background maps were computed from the photon images by punching out holes at the source positions determined by the local detect algorithm, and applying smoothing procedures before

and afterwards as described in S97. The radius of the holes was set to twice the FWHM of the PSF computed for a $20'$ off-axis angle and for the lowest energy value within the considered energy band (a $40'$ off-axis angle was used for the merged total FOV data). This resulted in a second list of source candidates (also with L ≥ 8).

For the third step, the local and map source candidate lists were merged into one list (separately for each of the five energy bands) and used as input for a maximum likelihood detection procedure (Cruddace et al. 1988). Here only sources with a likelihood L ≥ 10 were accepted and the background maps described above were used. All resulting lists were merged into one final list such that sources separated by less than 2σ of the PSF (referring to the lowest energy value within the considered energy band) were substituted by one single source, its position set to the position of the original source with the highest likelihood. This list was used as input for a repeated maximum likelihood process to compute upper limits in the energy bands where a source was below our detection threshold (but above in any of the other energy bands).

3.3. The catalogue of detected X-ray sources

The source detection yielded the 396 sources listed in Table 5, which has the same structure as the first survey source list given in Table 5 of S97. Column 1 gives the source number, columns 2 - 7 list the centroid position (epoch J2000) after correction for a systematic offset (see below) and column 8 shows the 1σ uncertainty of the source position in arcseconds. The calculation of this positional uncertainty is based on the maximum likelihood algorithm and incorporates the effects of statistical errors depending on the number of source counts, together with the blur radius of the PSF at the off-axis angle and the mean photon energy of the source. We also set a minimum threshold of $5''$ to account for a systematic positional error. The parameter in column 9 represents a classification of the quality of the detection and is differently defined than for the first survey due to the different homogeneity and sensitivity of the second survey: class '1' indicates sources detected in the inner PSPC region ($20'$ radius) and class '4' sources outside this region. Column 10 in Table 5 gives the highest likelihood of existence found in any of the five energy bands computed with the maximum likelihood method. Finally, columns 11 to 15 list the count rates with their 1σ errors (in counts per kilosecond) within the five energy bands (B, S, H, H1, and H2; see beginning of Sect. 3). The listed count rate errors are only statistical errors, whereas the systematical errors are expected to be less than $\pm 15\%$. Because some faint sources were not detected in all energy bands (i.e., these sources had a likelihood below the threshold value of 10 in one or more energy bands), we present 1σ upper limits to their count rates. The upper limits are computed from the 1σ fluctuations (Poissonian statistics) of the background counts at the source position and are indicated by a preceding '<' symbol.

The 396 X-ray sources found in the second PSPC survey underwent a correlation with a positionally accurate (optical) reference catalogue to determine a systematic offset in source position. This was done in the same manner as for the sources in the first survey, and is described in detail in S97. Here, for reference, we also used the optical globular cluster catalogue of Magnier et al. (1994a; Table 2) which revealed a slight systematic offset in our source positions of $\Delta R.A. = 5.8''$ and $\Delta Dec. = 1.2''$. Table 5 lists the offset-corrected source positions.

The fact that the total number of detected sources in the second PSPC survey is identical with the total number of detected sources in the first PSPC survey (S97) is purely accidental. The source lists are different and contain only 239 common sources. The detection of common sources in the two surveys is due to the fact that approximately the same region of sky was observed over (in some areas) similar integrated exposure time. The differences in the source lists are mainly due to different sensitivity characteristics: the first survey has its highest sensitivity along a line following the main axis of the M31 ellipse, whereas the second survey has an approximately constant and high sensitivity across the whole galaxy. Therefore, the detected sources are concentrated within different regions of each survey. Additionally, the slight differences in the source detection procedures and statistical fluctuations cause some departures close to the detection threshold.

Merging of the two survey lists (see Sect. 4.1.1 for details) yielded a final catalogue containing 560 PSPC detected X-ray sources in the field of M31. This is presented in Table 6, which has a similar structure to Table 5 described above. The only differences are that column 1 gives the RXJ-number of the source and column 2 lists the source number of the first survey (as listed in Table 5 of S97) if a correlation was found. Here four possible cases are indicated; (i) number followed by '+': source was found in both surveys and the listed data are from the first survey, (ii) number followed by '-': source was found in both surveys and listed data are from the second survey, (iii) number without any additions: source was found only in the first survey, the listed data being from there, and (iv) no number at all: source was found only in the second survey, the listed data being from there. For the criteria of which data are listed in cases of correlation see Sect. 4.1.1. The following columns 3 - 16 are identical with columns 2 - 15 of Table 5, and have been described above. For sources found in the first survey, the classification parameter listed in column 10 is as follows: class '1' identifies sources detected in the central region of the PSPC with off-axis angles $\leq 20'$, class '2' defines locations of sources found between $20'$ and $40'$, and class '3' contains sources with off-axis angles $> 40'$. As mentioned in Sect. 2 of S97, the source position was derived from the pointing in which it appears at the lowest off-axis angle, i.e., the best class (though not under a PSPC rib). For sources in class

Table 1. Summary of the correlation analysis. N_{total} gives the number of all possible correlations within a distance of 2σ of the combined positional error, $N_{\text{acc.}}$ gives the number of statistically expected accidental correlations, and $N_{\text{fin.}}$ gives the final accepted correlations. For a detailed explanation see Sect. 4.2.

Type	Databases	N_{total}	$N_{\text{acc.}}$	$N_{\text{fin.}}$
X-ray	*Einstein* (TF)	82	12.7	69
GC	BA87, BA93, MA94a	43	11.6	33
Extragalactic	NED	10	0.6	10
Foreground	MA92, SIMBAD	72	40.4	55
SNR	DO80, BW93, MA95	22	4.1	16
Novae	SA91, SA92	0	0.8	–

'2' and especially class '3', any upper limit in count rate listed in columns 11 - 15 can even be an underestimation due to the wider PSF and the therefore higher possibility of rib influencies. For sources found in the second survey, the listed classification parameter for the quality of detection is defined as described above: class '1' for sources detected in the inner PSPC region (20$'$ radius) and class '4' for sources outside this region.

The caveats for the first survey source catalogue mentioned in S97 are still valid where these sources are not substituted by second survey detections.

4. Comparisons with other source catalogues

For all correlations with other catalogues described in this section, the final source list of Table 6 was used. Table 1 summarises the results of the correlation analysis for different catalogues and these are discussed in more detail in the following subsections. From the description (in S97) of the correlation process itself, we simply summarise here that it yields not only the total number of correlating sources (N_{total}) but also the amount of expected accidental correlations ($N_{\text{acc.}}$) within a 1σ confidence level.

4.1. Comparisons with previous X-ray source catalogues

4.1.1. Comparison with the first ROSAT survey of M31

The source list of the second M31 survey was merged with that of the first to obtain the final ROSAT PSPC X-ray source list of M31 (Table 6). For this purpose the above-mentioned correlation process was applied to both lists to identify common sources. The 'radius of acceptance' (r_{a}) – the important correlation parameter – was iteratively determined as follows: the correlation procedure was repeatly carried out, with r_{a} increasing successively from $r_{\text{a}} = \sigma_{\text{comb.}}$ (here, $\sigma_{\text{comb.}} = \sqrt{\sigma_1^2 + \sigma_2^2}$, the combined positional error of the correlating sources, where the single positional error of each source is given by the maximum likelihood detect algorithm). This iterative process was stopped just before the occurrence of multi-identifications (one source in one catalogue correlating with more than one source in the other catalogue) for sources with likelihood ≥ 20 (to exclude sources near the detection threshold), and outside confused regions. In this way, most potential common sources have been uncovered, without risking having to accept multi-identifications for bright isolated point sources.

This process yielded 239 correlations (with $r_{\text{a}} = 4\sigma_{\text{comb.}}$, corresponding to a 99.99% probability of all real identifications having been found) with an expected number of 23 chance coincidences (1σ-value). A few multi-correlations were accepted (see below) because they either occur within confused regions or have likelihoods < 20 or at least one of the correlating sources is covered by the PSPC rib structure.

For sources correlated within the two surveys, the one with the better quality of detection (i.e. with the lowest classification parameter listed in column 10 of Table 6, class '4' of the second survey being considered the same as classes '2' and '3' of the first) was taken and the other was rejected as being identical with the first. In cases where the correlating sources were of the same class, the one with the higher likelihood was taken and, if the likelihood was also the same, the source from the second survey was taken because of its better positional accuracy[1]. The same procedure was applied to the few multi-correlations to clarify their situation. With this only one multi-correlation remained: source #379 of the first survey (see Table 5 in S97) correlates with sources #380 and #384 of the second survey (see Table 5 in this paper). Applying the rules mentioned above for both correlations we would have to accept source #379 from the first survey and would have to reject both sources from the second survey. Here we decided only to accept the correlation with the least distance as a true identification and left source #384 as a new one.

Conversely, 158 sources from the first survey and 163 from the second do not correlate with any other source (and we extend to 164 for the second survey due to the reasons mentioned above). To consider all these sources as transients would ignore the different spatial sensitivity distributions and different sky coverage of the two surveys. Therefore, a more explicit investigation of transients is presented in Sect. 5.

4.1.2. Comparison with the *Einstein* catalogue

The 560 X-ray sources in the merged source list of the two ROSAT PSPC surveys exceeds the number of X-ray sources detected with the *Einstein* observatory in this region of sky by a factor of more than 5. On the one hand, it is the result of the $\sim$ 10 times higher sensitivity of

[1] As a concequence of this data quality based decision variable sources are preferentially listed in their luminous state which may have different spectral characteristics compared with their less luminous state. Therefore sources detected as variable (see Tables 2 and 3) are marked with a '$\sim$'-sign in front of their RXJ-number.

ROSAT and the larger exposure of the disk region in the second ROSAT survey. On the other hand, both ROSAT surveys covered a more complete and therefore larger portion of the M31 field than the *Einstein* observations did. The number of sources detected with the ROSAT PSPC in the M31 bulge region (within 1 kpc from the centre) increased from 22 in the first survey to 31 using the data from both surveys. The fact that this is still less than the 48 sources found with the *Einstein* observatory in this region, as listed by Trinchieri & Fabbiano (1991, hereafter TF), is due to the large fraction of sources in TF's list which were detected with the higher spatial resolution *Einstein* HRI. Primini et al. (1993) reported 45 sources found with the ROSAT HRI within the bulge region of M31 and Immler (2000), again using the ROSAT HRI observations, counted 63 sources within a $5'$ circle around the centre.

As already described in S97, the list of *Einstein* X-ray sources in the field of M31 reported by TF contains 108 sources, with 81 sources taken from the *Einstein* HRI data with an assumed positional error of $3''$ (reported by Crampton et al. 1984), and 27 sources based on *Einstein* IPC data with a $45''$ positional error. Applying the above mentioned correlation procedure to the 560 ROSAT sources and the 108 *Einstein* sources reported by TF yields $N_{\rm total} = 82$ correlations with a probable contamination of $N_{\rm acc.} = 12.7$ chance coincidences, here accepting a source separation of up to twice the combined positional error (2σ). 12 ROSAT sources each correlated with several *Einstein* sources, due mainly to the large positional error of the *Einstein* IPC. To clarify their situation, only the correlation with the smallest separation (between the correlating counterparts) was taken into account. This reduced the number of finally accepted correlations to 69, which is in good agreement with the number of statistically expected true correlations (i.e. $N_{\rm total} - N_{\rm acc.} = 69.3$).

All 69 identifications are listed in Table 7. Column 1 gives the ROSAT RXJ-number (ref. Table 6), column 2 gives the fluxes and 1σ errors of the ROSAT sources using the spectral model of TF (thermal bremsstrahlung with $kT = 5$ keV and $N_{\rm H} = 7 \times 10^{20}$ cm^{-2} in the 0.2-4.0 keV energy band), column 3 lists the *Einstein* source numbers (ref. Table 2A of TF), column 4 the fluxes and 1σ errors given by TF, and columns 5 and 6 the distances between the ROSAT source positions and the *Einstein* source positions in arcseconds and in units of their combined positional errors (σ) respectively. The last column shows the ratio between the fluxes obtained with ROSAT and *Einstein* and can be considered as a long term variability check between the epochs of the two observations. More detailed investigations into long time variabilities are described in Sect. 5.

Comparing this correlation list to the one using only ROSAT sources found in the first survey as published in S97 (Table 6), a few remarks should be made. Using only the data of the first survey we had to manually extend the correlation list by one entry (ROSAT source #67 correlating with *Einstein* source #3) as mentioned in S97. This had been necessary because of the poorly–known PSF and the therefore uncertain positioning at the source position. The second PSPC survey now gave us the opportunity to determine much more precisely the position of this source (RXJ0040.2+4050), turning out in fact to be only $3.6''$ away from the position of the *Einstein* HRI source #3. Therefore no manual extension of the correlation list had to be made in this paper.

The listed flux ratio ($F_{\rm R}/F_{\rm E}$) between ROSAT and *Einstein* which can be used as a long term variability indicator should be inspected carefully for sources in the bulge region (marked with a $\star$ preceding the ROSAT source number). Because of the heavy confusion in this region, the flux determination of these sources is very uncertain.

With the help of the second PSPC survey, some positions of X-ray sources already found in the first survey could be improved. Therefore, the 69 identifications listed in Table 7 show a very good positional agreement between the PSPC source positions and the ones listed by TF, which were largely obtained with the *Einstein* HRI. In fact, the mean source separation of the 43 ROSAT PSPC–detected sources correlating with sources also found with the *Einstein* HRI is $5.9'' \pm 3.2''$.

Excluding the heavily confused bulge region and the sources therein, we found a good ROSAT confirmation (90%) of the sources detected with the *Einstein* observatory as, out of the 60 of the 108 *Einstein* sources outside the bulge region, 54 could be confirmed by ROSAT. For the 6 *Einstein*-only detected sources, we give ROSAT flux upper limits and discuss their transient nature in Sect. 5.1. Over and above this, 491 new sources have been found with ROSAT which were not detected with *Einstein*.

4.2. Correlations with optical and radio sources

To identify and classify individual sources, the merged ROSAT source list of both surveys (Table 6) was correlated with the same catalogues previously used for the sources of the first survey in S97. For completeness and to simplify the discussions, we summarise the public data bases and catalogues used as follows:

- **globular clusters:** the two lists of Battistini et al. (1987, 1993; hereafter BA87, BA93) and the lists of Magnier et al. (1994a; Table 2; hereafter MA94a),
- **extragalactic objects:** the NASA Extragalactic Database (version date: 30. Dec. 1992; hereafter NED),
- **foreground stars:** the catalogue of stellar photometry described by Magnier et. al. (1992), hereafter MA92, and Haiman et al. (1994) and the SIMBAD catalogue (Centre de Données astronomiques de Strasbourg; version date: Dec. 1989; hereafter SIMBAD),
- **supernova remnants:** the lists of d'Odorico et al. (1980; hereafter DO80), Braun & Walterbos (1993; hereafter BW93), and Magnier et al. (1995; hereafter MA95).

– **novae:** the two lists of Sharov & Alksnis (1991, 1992; hereafter SA91, SA92).

Information regarding the characteristics of these catalogues, especially the individual positional errors used in the correlation processes, can be found in S97. We adopted them except for the SNR catalogues: D'Odorico et al. (1980) report general position errors of 8″ in declination and 15″ in right ascension. In S97 we assumed a mean position error of 12″ whereas in this paper we decided to use a geometric mean of 17″. For the SNR list of Braun & Walterbos (1993) and also for the list of Magnier et al. (1995) we used 5″ as a systematic position error for our correlations.

Table 8 shows the result of the correlations. The columns are defined as follows. Column 1 gives the ROSAT RXJ source number (ref. Table 6). Column 2 lists the object class, of which four exist: 'Star' for galactic foreground stars followed in brackets by their type if available, 'EO' for extragalactic objects, mainly background galaxies, 'GC' for sources belonging to globular clusters, and 'SNR' for supernova remnants. Column 3 lists the identification, using the abbreviations of the correlated catalogues as defined above. The number following in brackets gives the name/entry number of the object as listed in the relevant catalogue (for details see the remarks to the individual catalogues below). Finally, columns 4 & 5 give the distance between the ROSAT source position and the correlated object in the catalogue, both in arcseconds and in σ units. For the distance expressed in sigma, the combined positional error of the ROSAT source and the correlated catalogue source was used.

Concerning this list, the following should be noted. If one ROSAT source correlates with more than one catalogue source of the same catalogue, only the correlation with the smallest positional separation is listed. If the correlating catalogue sources belong to different catalogues of the same source class then all correlations are listed, separated by commas. In a few cases, multi-correlations between one ROSAT source and catalogue sources of different source classes were found. Here, spectral considerations clarified the situation, especially for distinguishing between foreground stars and globular clusters. Rejections of a good spatial correlation in place of a poorer spatial correlation only took place when the more distant counterpart was spectrally consistent with the ROSAT source and the closer counterpart very inconsistent.

In contrast, no rejection was performed in cases of perfect positional single–correlations, even of moderate coincident spectral characteristics. Additionally, we did not accept identifications with supernova remnants for ROSAT sources with a hardness ratio $HR_1 + \sigma_{\mathrm{HR}_1} \leq -0.80$, because we consider these sources as supersoft sources (see S97 and Greiner et al. 1996)[2]. The hardness ratio HR_1 is defined as $HR_1 = (H - S)/(H + S)$, where S and H stand for the source counts in the relevant energy bands calculated with the maximum likelihood algorithm (and listed in Table 6). With these criteria, 114 identifications with optical and radio sources were found, corresponding to an identification quota of 20.4%. Some quantitative comments on the various object classes are as follows:

Foreground Stars (Star): Among the $N_{\mathrm{total}} = 72$ correlations within the 2σ error level, 17 had to be rejected due to the above criteria, leading to $N_{\mathrm{fin.}} = 55$ finally accepted identifications. The high density of foreground stars within the HA94 catalogue yields a relatively high number of possible chance coincidences, $N_{\mathrm{acc.}} = 40.3$. The resulting statistically expected number of true identifications is $N_{\mathrm{i}} = 31.8 \pm 6.3$, which is too low when compared with the finally accepted 55 identifications. As already discussed in S97, from the *Einstein* and ROSAT medium and deep surveys we know the foreground source luminosity function, and this can be used to derive an upper limit of 54 expected foreground sources within the region covered by the HA94–catalogue. This value is in good agreement with our finally accepted number of identifications.

Background Galaxies (EO): None of the $N_{\mathrm{total}} = 10$ found correlations had to be rejected due to the above criteria. The remaining number of $N_{\mathrm{fin.}} = 10$ finally accepted identifications is in good agreement with the statistically expected number of $N_{\mathrm{i}} = 9.4 \pm 0.8$. The dwarf galaxy M32 can be found among the identifications, correlating with ROSAT source RXJ0042.6+4052.

Globular Clusters (GC): Within the 2σ error level we found $N_{\mathrm{total}} = 43$ correlations (with $N_{\mathrm{acc.}} = 11.6$ chance coincidences), from which 10 had to be rejected due to the above criteria. The remaining 33 finally accepted identifications are in good agreement with the statistically expected number of $N_{\mathrm{i}} = 31.4 \pm 3.4$ true identifications. Among the 10 rejected correlations, 2 accounted for double–correlations with globular clusters, while the remaining 8 were rejected on spectral grounds, showing soft spectral characteristics incompatible with the known relatively hard spectra of X-ray sources belonging to globular clusters.

Supernova Remnants (SNR): Among the $N_{\mathrm{total}} = 22$ correlations within the 2σ error level, 6 had to be rejected due to the above criteria, leading to $N_{\mathrm{fin.}} = 16$ finally accepted identifications. This is in good agreement with the statistically expected number of $N_{\mathrm{i}} = 17.9 \pm 2.0$ true identifications. One important comment concerning the SNR-correlations listed in S97: Due to a misuse of the SNR list of Magnier et al. (abbreviated as MA94b in S97) a few SNR miss-correlations are listed in S97. This is repaired in this paper.

Novae: The extension of the ROSAT source catalogue of the first M31 survey (S97) with the sources found in the

[2] Kahabka (1999) used not only HR_1 but also HR_2 and L_X (with reference to the local N_H-value at the source position) and their respective ratios to discriminate supersoft sources. Using these criteria and the source list of S97, he came up with an additional 26 new supersoft source candidates, 4 of them correlated with foreground stars in S97 and 4 with supernova remnants. Excluding these 8 sources, 18 additional supersoft source candidates in M31 remain.

second survey does not uncover a single correlation with one of the known novae in M31.

5. Time variability

The two ROSAT PSPC surveys of M31, separated by $\sim$ 1 year, and the *Einstein* survey from $\sim$ 11 years before the first ROSAT survey can be used to search for long term variability within the sources. We treat this here in two different subsections. Readers who wish to investigate long term variabilities or the search for transients should refer to both subsections (5.1 and 5.2), and are strongly recommended to read Sect. 4.1 in S97.

Concerning any two catalogues 1 and 2 which refer to the same sources, we used for a quantitative study of possible long term variabilities a linear significance parameter following Primini et al. (1993), which is defined as:

$$S(F_1 - F_2) = \frac{|F_1 - F_2|}{\sqrt{\sigma^2_{\mathrm{F}_1} + \sigma^2_{\mathrm{F}_2}}}\,, \qquad (1)$$

where F_1 and F_2 represent the X-ray flux in the first and second source catalogues and σ_{F_1} and σ_{F_2} give the corresponding flux errors. This definition is useful in that, in cases where an inappropriate spectral model has been used to compute the two fluxes, any systematic errors are disregarded. We state time variability only for sources with $S \geq 3\sigma$. Additionally, sources within the bulge and other confused or 'handicapped' regions (e.g. beneath the ribs of the PSPC support structure) were excluded on cautionary grounds.

5.1. Comparison with the *Einstein* sources

As already described in Sect. 4.1.2, we compared the complete ROSAT PSPC source list of M31 (Table 6) with the *Einstein* source list published by TF. The results are listed in Table 7, where, besides the fluxes (using the spectral model of TF), the flux ratios are also given. Here, we extend these calculations by the significance parameter given in formula (1), where catalogue 1 is set to the ROSAT source list and catalogue 2 is set to the *Einstein* source list. Applying the criteria mentioned above to accept sources only with $S \geq 3\sigma$ and outside confused regions, we come up with the remaining sources listed in Table 2. Additionally, this table contains potential transients (see below). The meanings of the columns are: columns 1 and 3 give the ROSAT source number (RXJ; see Table 6) and the correlating *Einstein* source (TF's source list) respectively, columns 2 and 4 list the (unabsorbed) flux and flux error of the sources as measured with ROSAT and *Einstein* respectively, the spectral model of TF having been applied (thermal bremsstrahlung with $kT = 5$ keV and $N_{\mathrm{H}} = 7\times10^{20}$ cm^{-2} in the 0.2-4.0 keV energy band), column 5 lists the flux ratio between the ROSAT and the *Einstein* observations, and column 6 gives the significance parameter as described above, or a transient indicator 'T' (see below).

Table 2. List of X-ray sources showing flux variability between the *Einstein* observation and the ROSAT observations. F_{R} gives the ROSAT source flux using the *Einstein* spectral model of TF (thermal bremsstrahlung with $kT = 5$ keV and $N_{\mathrm{H}} = 7\times10^{20}$ cm^{-2} in the 0.2-4.0 keV energy band) and F_{E} gives the *Einstein* source flux of the correlated *Einstein* source. Column "S" lists the significance of the variability as described in the text. A "T" in this column indicates bright transients or possible faint transients when enclosed in brackets (see Sect. 5.1 for a detailed explanation).

ROSAT RXJ-No.	F_{R} ($\times10^{13}$) (cgs)	*Ein.* No.	F_{E} ($\times10^{13}$) (cgs)	$F_{\mathrm{R}}/F_{\mathrm{E}}$	S
0040.2+4034	19.87 ± 0.29		< 10.00	> 2.00	T
0041.7+4134	14.38 ± 0.49	9	8.72 ± 1.08	1.65 ± 0.21	3.66
0041.8+4021	24.25 ± 0.76	11	15.54 ± 0.88	1.56 ± 0.10	5.69
0042.2+4019	40.38 ± 1.23	15	48.83 ± 1.61	0.83 ± 0.04	3.89
0042.2+4101	9.53 ± 0.32	16	3.88 ± 0.75	2.46 ± 0.48	4.48
0042.2+4112	9.04 ± 0.25	19	4.26 ± 0.54	2.12 ± 0.28	4.45
0042.2+4118	9.71 ± 0.32	14	3.23 ± 0.51	3.01 ± 0.49	6.09
0042.6+4052	32.45 ± 0.53	51	9.16 ± 1.01	3.54 ± 0.40	15.33
0042.8+4131	18.62 ± 0.45	67	11.95 ± 1.10	1.56 ± 0.15	4.30
0043.1+4118	7.54 ± 0.24	82	2.03 ± 0.31	3.72 ± 0.58	6.69
0043.3+4117	4.44 ± 0.25	88	1.31 ± 0.34	3.39 ± 0.89	3.66
0046.4+4201	10.08 ± 0.31	105	5.52 ± 0.89	1.83 ± 0.30	3.33
	SI: < 0.35	12	2.56 ± 0.50	< 0.14	(T)
	SI: < 0.44	40	1.59 ± 0.62	< 0.28	(T)
	SII: < 2.01	75	4.02 ± 0.56	< 0.50	(T)
	SI: < 0.40	84	1.99 ± 0.49	< 0.82	(T)
	SI: < 0.35	96	3.50 ± 0.94	< 0.10	(T)
	SI: < 0.39	106	0.71 ± 0.22	< 0.55	(T)

Variable sources:
Table 2 lists 11 (long term) variable sources. From a comparison between the *Einstein* detected sources reported by TF and the sources found in the *first* ROSAT survey of M31 we reported 15 potentially variable sources in S97. Actually, 10 of the S97-reported 15 sources vanish from the variability list, and 6 new variable sources join the list. Among the 10 vanished sources, 6 lay within the bulge region (*Einstein* sources #33, #58, #68, #76, #79, and #80) and have therefore been rejected from our very stringent list (we were not so restrictive for Table 3 of S97). For 2 sources (*Einstein* sources #70 and #348), the fluxes of the corresponding ROSAT sources have been substituted with the data from the second PSPC survey, which were closer to the *Einstein* fluxes, and the significance of variability therefore fell below our threshold. *Einstein* source #2 now correlates with ROSAT source RXJ0040.0+4031 (formerly ROSAT source #55) instead of ROSAT source RXJ0040.0+4033 (formerly ROSAT source #57) because we obtained an improved position from the second PSPC survey data, cancelling the prior correlation. Finally, we deleted by hand the correlation pair of *Einstein* source #27 with ROSAT source #172 because it lies close to the bulge within a confused region.

Among the 6 new variable sources, 3 came into the list due to their newly determined fluxes from the second PSPC survey data (ROSAT sources RXJ0041.8+4021, RXJ0043.1+4118, and RXJ0046.4+4201), 2 joined the list because of the now improved positions of the correlating

ROSAT sources (RXJ0042.2+4112 and RXJ0042.2+4118) and the last one (RXJ0043.3+4117) was newly discovered within the second survey data.

In cases where a change in determined flux (between the first and second PSPC survey) is responsible for changes in the variable source list, one should bear in mind that this might be due to a *real* flux change (variability) of the particular source within the time gap between the two ROSAT surveys (∼1 year). In assembling Table 2, we assumed that the changes are due to the better flux determination within the data of the second PSPC survey compared to the first. Readers who wish to investigate the variable sources are therefore recommended to examine all sources in both lists.

The two variable sources reported by Collura et al. (1990) have been discussed already in S97. Including the second PSPC survey data has added nothing of significance as regards these.

Transients:
Table 2 lists 7 possible (bright) transient sources. We define bright transients as those sources which are detected in one catalogue, and are bright enough to be detected in the other, but which are not seen. ROSAT sources with fluxes $\geq 10^{-12}$ erg cm^{-2} s^{-1} (applying the spectral model of TF) should have been seen during the *Einstein* observations. Conversely, *Einstein* sources with fluxes $\geq 10^{-12}$ erg cm^{-2} s^{-1} should have been seen in the ROSAT surveys.

From a comparison between the *Einstein* detected sources reported by TF and the sources found in the *first* ROSAT survey of M31, we reported 9 potentially transient sources in S97. In detail, we have now 'lost' 5 of these transients, 3 of them because the relevant *Einstein* sources (#81, #93, and #100) were found to correlate with sources detected within the second PSPC survey data, and the other two because they lay within confused regions. On the other hand, we included 3 new transients in our list (*Einstein* sources #12, #75, and #84) because, within the first PSPC survey their positions were near the PSPC support structure and therefore we formally excluded them from the list at that time. With the help of the second PSPC survey and its more homogeneous exposure, we were able to verify their potential transient nature. For all transients, we list in Table 2 a flux upper limit. In the case of the ROSAT fluxes, we compute these limits from the known background fluxes at the source positions making use of the most sensitive survey (indicated by SI/SII for the first/second PSPC survey). Although 3 sources were partially obstructed by the PSPC support structure within the first survey (see above), for 2 of them we calculated their upper limits from these data because these positions still received more exposure within the first survey than within the second. In these cases, we simply used the second survey and its homogeneity as a proof to clarify their transient nature.

We list all 6 transients at the bottom of Table 2 as faint transients ('T' within brackets) as they have luminosities below our bright transient threshold given above, even though their *Einstein* luminosities are above the detection threshold of the ROSAT surveys.

For the one transient in Table 2 not seen by *Einstein* (ROSAT source RXJ0040.2+4034), we give our transient threshold of 10^{-12} erg cm^{-2} s^{-1} as an upper limit because TF did not mention the limiting flux of the individual *Einstein* observations. With this value, we are surely above the sensitivity of the *Einstein* observations.

5.2. Comparison between the two ROSAT PSPC surveys

In Sect. 3.3 we described the merge of the two source lists assembled from the first and second PSPC surveys of M31. Sources which were found in both lists have been tested for variability in flux. To indicate a possible variability we have applied the following criteria: (1) The source must reside outside the bulge and outside other confused regions, (2) the significance parameter (eq. (1)) must hold with $S \geq 3$ (F_1 and F_2 being the fluxes of the source determined from the first and second surveys), (3) sources with an upper limit to the count rate in the B–band in either of the two surveys have been excluded (in other words, the count rate must have been determinable), (4) sources behind/near the PSPC support structure within the first survey have been excluded (i.e. sources marked with a †-symbol in Table 5 of S97, (5) the sources have to belong to source class '1' in both surveys, and (6) the detection likelihood of the source has to be ≥ 20 in both surveys. Criterion (1) prevents any pseudo-variability occurring due to uncertain flux determinations within confused regions, criterion (2) ensures a sufficient significance, and with criteria (3) to (6), the influence of any systematic errors should be widely excluded.

With these criteria, 34 possible long term variable sources were found, as listed in Table 3. Column (1) gives the ROSAT RXJ–number of the source, column (2) and (3) list the count rate in the B–band determined from the data of the first and second surveys respectively, column (4) gives the ratio in count rate between the first and second survey, and column (5) gives the value of the significance parameter, following eq. (1).

Additionally, Table 3 contains possible transients, marked with a 'T' in column (5). For this, the sensitive flux limit was determined within the survey in which the source was *not* found, using the source position from the other survey (i.e. where the source *was* detected). If this value was below the count rate minus the 1σ count rate error determined from the survey where the source was found, then this source was considered as a possible transient. To prevent false diagnoses being made, the same criteria as above for the variable source search were applied except for criterion (2) which was dropped, and criterion (3), which was substituted as just described. With this, no transients were found which could be seen only in the first survey but not in the second. This is mainly due to the exclusion of regions near the PSPC support structure within

Table 3. List of all the potentially long term variable sources found via a comparison of the first and second ROSAT PSPC surveys of M31. Column "S" lists the significance of the variability as described in text. Additionally, possible transients are tabled, marked with 'T' in this column.

ROSAT No.	$\mathrm{Rate_{SI}}$ ($\mathrm{ct}*\mathrm{ks}^{-1}$)	$\mathrm{Rate_{SII}}$ ($\mathrm{ct}*\mathrm{ks}^{-1}$)	$\mathrm{Rate_{SI/SII}}$	S
RXJ0038.4+4012	12.61 ± 0.66	9.03 ± 0.78	1.40 ± 0.14	3.51
RXJ0040.7+3959	< 2.81	5.54 ± 1.01	< 0.51	T
RXJ0041.1+4002	1.96 ± 0.64	5.57 ± 1.01	0.35 ± 0.13	3.04
RXJ0041.5+4105	< 1.27	12.36 ± 0.69	< 0.10	T
RXJ0041.6+4101	1.49 ± 0.31	3.10 ± 0.40	0.48 ± 0.12	3.20
RXJ0041.8+4015	3.18 ± 0.58	7.02 ± 1.04	0.45 ± 0.11	3.24
RXJ0041.8+4021	60.52 ± 1.22	90.56 ± 2.85	0.67 ± 0.02	9.68
RXJ0041.8+4101	11.73 ± 0.71	6.25 ± 0.51	1.88 ± 0.19	6.28
RXJ0041.8+4122	6.11 ± 0.58	2.69 ± 0.43	2.27 ± 0.42	4.75
RXJ0042.1+4110	4.20 ± 0.46	6.83 ± 0.65	0.62 ± 0.09	3.28
RXJ0042.1+4118	13.85 ± 0.79	35.01 ± 1.21	0.40 ± 0.03	14.68
RXJ0042.2+4039	3.90 ± 0.39	8.12 ± 0.71	0.48 ± 0.06	5.24
RXJ0042.2+4055	10.13 ± 0.69	6.59 ± 0.52	1.54 ± 0.16	4.10
RXJ0042.2+4101	35.60 ± 1.18	29.59 ± 1.02	1.20 ± 0.06	3.85
RXJ0042.2+4112	24.95 ± 1.02	33.74 ± 0.95	0.74 ± 0.04	6.33
RXJ0042.2+4118	11.31 ± 0.73	36.25 ± 1.21	0.31 ± 0.02	17.64
RXJ0042.3+4113	18.74 ± 0.87	66.18 ± 0.96	0.28 ± 0.01	36.58
RXJ0042.4+4104	6.95 ± 0.56	17.85 ± 0.83	0.39 ± 0.04	10.87
RXJ0042.4+4112	22.09 ± 0.94	44.15 ± 0.76	0.50 ± 0.02	18.34
RXJ0042.5+4048	1.69 ± 0.32	3.91 ± 0.46	0.43 ± 0.10	3.97
RXJ0042.6+4052	121.17 ± 1.99	58.12 ± 1.50	2.08 ± 0.06	25.28
RXJ0042.8+4125	14.75 ± 0.84	21.27 ± 0.98	0.69 ± 0.05	5.05
RXJ0042.9+4146	3.55 ± 0.53	7.64 ± 0.72	0.46 ± 0.08	4.57
RXJ0043.1+4048	< 2.27	5.53 ± 0.62	< 0.41	T
RXJ0043.1+4112	3.06 ± 0.41	5.63 ± 0.56	0.54 ± 0.09	3.69
RXJ0043.1+4118	5.58 ± 0.57	28.17 ± 0.91	0.20 ± 0.02	21.05
RXJ0043.3+4120	6.74 ± 0.62	10.07 ± 0.91	0.67 ± 0.09	3.02
RXJ0043.4+4118	6.86 ± 0.62	11.96 ± 0.76	0.57 ± 0.06	5.20
RXJ0043.4+4126	< 1.50	5.87 ± 0.52	< 0.26	T
RXJ0043.7+4124	< 1.53	3.72 ± 0.50	< 0.41	T
RXJ0043.7+4136	7.04 ± 0.56	2.16 ± 0.36	3.26 ± 0.60	7.35
RXJ0043.9+4122	4.82 ± 0.48	2.07 ± 0.36	2.33 ± 0.47	4.56
RXJ0044.3+4145	1.17 ± 0.35	3.07 ± 0.42	0.38 ± 0.12	3.51
RXJ0044.4+4121	29.77 ± 1.12	25.10 ± 1.02	1.19 ± 0.07	3.08
RXJ0044.8+4225	< 2.74	4.85 ± 1.11	< 0.56	T
RXJ0045.6+4208	19.18 ± 0.92	25.83 ± 1.11	0.74 ± 0.05	4.63
RXJ0045.7+4139	147.96 ± 1.91	134.43 ± 1.96	1.10 ± 0.02	4.95
RXJ0046.4+4201	29.58 ± 1.14	37.64 ± 1.15	0.79 ± 0.04	4.99
RXJ0046.4+4204	20.61 ± 0.99	33.17 ± 1.16	0.62 ± 0.04	8.24
RXJ0047.4+4152	< 2.08	3.35 ± 0.54	< 0.62	T
RXJ0047.8+4142	< 2.70	7.02 ± 1.15	< 0.38	T
RXJ0048.4+4157	46.28 ± 1.64	35.30 ± 2.16	1.31 ± 0.09	4.05

the first survey which results in a reduction in area and may have removed a few transient candidates from our (conservative) list. Additionally, the second survey with its homogeneous exposure is more sensitive in the outer region of M31 than the first survey. As a consequence of these two effects, we found 8 transients which were seen in the second survey but not in the first. Because of the very different conditions of both surveys (mainly the influence of the PSPC support structure in the first survey), we desist from a quantitative analysis of a transient rate and its comparison with expected theoretical values.

If we readopt criterion (2) in a slightly changed form, that the upper flux limit for transient sources also represents the error in flux, we would come up with values for the significance parameter always below our threshold of 3 except for source RXJ0041.5+4105 where $S = 7.67$. Here, we could quote source RXJ0041.5+4105 as a strong candidate for a transient, whereas all the others must be considered as weak candidates.

Some words concerning ROSAT source RXJ0040.2+4034: In Sect. 5.1, from a comparison with the *Einstein* source list of TF, we have indicated this source as a possible transient. If the increase in flux between the *Einstein* observations and the first ROSAT survey is based on a short–time outburst of this transient source, we would expect this source to appear much fainter during the second PSPC survey or even disappear. Actually, with the criteria applied to merge both source lists as described in Sect. 3.3, the source seemed to disappear, as no correlating source could be found within the second survey. Nevertheless, a visual inspection suggested an identification of ROSAT source RXJ0040.2+4034, only found within the first survey (source #69, Table 5 in S97), with ROSAT source RXJ0040.2+4033, only detected within the second survey. Both sources are listed separately in Table 6. Under the assumption that these two sources are the same source we note a large decrease in count rate (by over a factor of 40) between the first and second surveys. This would tie in with the possible transient nature of this source. On the other hand, the fact that these two sources are separated by $57''$ and are both good quality detections argues against this treatement. We therefore list both sources as individual sources in our list.

6. Total luminosity and diffuse emission

From the first ROSAT PSPC survey of M31 we had already derived quantities for the total luminosity of M31 and a possible gaseous component (S97). Because the first survey had to be corrected for several caveats such as the dominant influence of the PSPC support structure, the inhomogeneous exposure, and the rapid decrease of sensitivity from the centre of M31 to the outer regions, we improved the determination of the total luminosity and diffuse component with the data from the much more homogeneous second survey. One of the big advantages of the second survey is its more or less constant exposure and therefore constant flux limit over the whole D_{25}-area of the galaxy. This allows an improved determination of the background around M31 and, as a consequence, a more reliable flux determination of components within M31. Furthermore, it reduces systematical errors in the case of large scale analysis, as discussed in this section. The following description has some overlap with procedures already described in S97, but we decided to briefly summarise them here for completeness.

In this section we will use the term "diffuse component" to mean the sum of the emission from a truly diffuse (gaseous) emitter and from unresolved point sources. We will refer to "total emission" as the sum of the diffuse component and the emission from resolved point sources.

As already described in Sect. 3.1, all the data have been cleaned of contamination by solar scattered X-rays and particle background. The resulting photon event files remain contaminated by these components, but only to less than 1% in each pointing. This is up to ten times bet-

ter than in the worst case of the first PSPC survey. For the analysis in this section, the data were binned into an image with a $30'' \times 30''$ pixel size. For the determination of count rates within the D_{25}-area of M31, the merged inner regions of the PSPC with $20'$ radius have been used, whereas for the outer area around M31, a merge of the total photon event files has been used. The resulting images were divided by exposure maps with the same pixel size to obtain count rate images corrected for the effects of the rib structure, vignetting and dead time. These exposure maps were calculated in the following manner: the B-band was divided into 10 energy slices for which EXSAS provides instrument maps for the PSPC detector response. Together with the photon event files, exposure maps for each of these energy slices were created, considering also dead time effects. A weighted addition of these single exposure maps yields the final exposure maps. The pulse height spectra in the 10 energy slices of the photon event files were used as the weighting factors.

From the image of the merged inner PSPC regions we derived count rates for the bulge (1 kpc around the centre) and the M31 disk region (i.e. outside the bulge up to the D_{25}-ellipse). "Background count rates" were taken from the image of the merged total PSPC FOV and within an area far outside and around the D_{25} ellipse of M31 – explicitly the area between the ellipse with major and minor axes 0.15° larger than the D_{25} ellipse of M31 and the ellipse 0.30° larger. Sources within this area were cut out to a radius of three times the PSF at the source position. With this, we derived count rates for the bulge, disk, and "background" of (46.86 ± 2.5), (4.278 ± 0.04), and (3.311 ± 0.038) ct s^{-1} deg^{-2} respectively, in the broad (0.1 - 2.0 keV) energy band.

Considering the bulge, a subtraction of the background count rate and a multiplication with the bulge area of 0.026 deg^2 yields (1.132 ± 0.065) ct s^{-1}. Applying a power law with $\Gamma = -2.0$ for the spectral model and a galactic foreground absorption of $N_{\rm H} = 6 \times 10^{20}$ cm^{-2} yields $(2.88 \pm 0.17) \times 10^{-11}$ erg cm^{-2} s^{-1} for the total flux of the bulge region, which corresponds to a luminosity of $\sim 1.6 \times 10^{39}$ erg s^{-1}, assuming a distance of 690 kpc to M31. A summation over the count rates of all 22 bulge sources detected in the second PSPC survey data in this area initially yields (2.78 ± 0.02) ct s^{-1}. This is much higher than the total emission derived above. The reason is the way the source detection algorithm works. In highly confused regions it tends to overestimate the count rate of each source due to overlapping of the photon extraction circles of neighbouring sources. By determining the individual extraction radii the detection algorithm has used, and the amount of overlapping area under the assumption of a gaussian PSF for the instrumentation, we can globally correct for this effect. With this, we obtain (0.893 ± 0.006) ct s^{-1} for the resolved emission of the bulge. A comparison with the above derived total emission uncovers an unresolved component of (0.239 ± 0.065) ct s^{-1}. Assuming that this component completely originates from thermal emission of hot gas, and applying a spectral model for an optically-thin thermal plasma (MEKAL) with $kT = 0.35$ keV (as determined from XMM-Newton observations, e.g. see Shirey et al. 2001) and a galactic foreground absorption of $N_{\rm H} = 6 \times 10^{20}$ cm^{-2}, we derive $(3.4 \pm 0.9) \times 10^{-12}$ erg cm^{-2} s^{-1} for a diffuse X-ray flux. For a distance of 690 kpc to M31, this corresponds to a luminosity of $(2.0 \pm 0.5) \times 10^{38}$ erg s^{-1} and would indicate a gas mass of $(1.0 \pm 0.3) \times 10^{6}$ M$_\odot$, assuming the gas fills uniformly the bulge region, a sphere with 1 kpc radius (using the power per unit emission integral as a function of temperature for a low density plasma reported by Kato 1976). Because a luminosity function derived from the detected sources in the heavily confused bulge region would be very uncertain, we cannot trust any estimation of the emission from non-detected sources below our detection threshold by extrapolating such a luminosity function. As a consequence, the above derived luminosity (and gas mass) of the diffuse emission must be considered as an upper limit.

Considering the disk, a subtraction of the background count rate and a multiplication with the disk area of 2.6 deg^2 yields (1.68 ± 0.14) ct s^{-1}. A summation of the count rates of all the sources detected in the disk within the second PSPC survey data yields (2.06 ± 0.31) ct s^{-1}. Here no correction had to be applied, as no important source confusion exists. This value is slightly higher than the one derived from the total emission. It may indicate a possible diffuse absorption of background photons by M31. Although both derived count rates are comparable within their 1σ errors, this is an effect of the integral consideration of the whole disk. A division into several annular regions indicates an absorption at the 1σ significance level in some of these regions. A more detailed report will be the subject of a future paper. In the following discussion, we neglect a possible (slight) absorption in the M31 disk.

As already mentioned in Sect. 4.2, a fair number of the detected sources do not belong to M31, but are foreground sources or background sources shining through the galaxy. Therefore, the derived flux of all the resolved disk sources mentioned above (or the sum of the flux in the disk area) cannot be used for a determination of the total X-ray luminosity of the disk of M31. Following the procedure described in S97 we use the there derived logN-logS distribution for sources truly belonging to M31 (from a statistical point of view). We come up with (1.26 ± 0.20) ct s^{-1} for the resulting count rate, or a total flux of $(1.7 \pm 0.3) \times 10^{-11}$ erg cm^{-2} s^{-1} for the disk of M31 (using the above spectral model). This corresponds to a total luminosity of $(1.8 \pm 0.3) \times 10^{39}$ erg s^{-1}.

All together, applying a power law spectral model with photon index $\Gamma = -2.0$ and a galactic foreground absorption of $N_{\rm H} = 6 \times 10^{20}$ cm^{-2}, we obtain for the total (0.1−2.0 keV) luminosity of M31, $(3.4 \pm 0.3) \times 10^{39}$ erg s^{-1}, approximately equally distributed between the bulge and disk.

Comparison with earlier results:

A comparison with the results derived from the first ROSAT PSPC survey of M31 (S97) uncovered a difference in the bulge luminosities. For the total emission as well as for the sum of the resolved flux of detected sources we determined slightly higher values from the second PSPC survey data. Although the difference in significance for the total emission is less than 1.5σ, we decided to take the new value from the second survey as the better one due to the above mentioned reasons. Because the flux of the resolved emission increased approximately by the same (small) amount we would obtain nearly the same value for a possible gaseous component in the bulge of M31 as previously derived from the first survey data when applying the same spectral model as used in S97 (now $(4.4 \pm 1.2) \times 10^{-12}$ erg cm^{-2} s^{-1}, compared to $(4.6 \pm 1.1) \times 10^{-12}$ erg cm^{-2} s^{-1} in S97). It shows, that the change of the here newly given value ($(3.4 \pm 0.9) \times 10^{-12}$ erg cm^{-2} s^{-1}) is mainly due to the new spectral model used (optically-thin thermal plasma with $kT = 0.35$ keV), which we adopted from recent results of XMM-Newton observations (Shirey et al. 2001). With this, the ROSAT derived diffuse luminosity within $5'$ of the nucleus of M31 is comparable to the luminosity found for the same bulge area with the Chandra (Garcia et al. 2000) and the XMM-Newton observation (Shirey et al. 2001). It is commonly assumed that the hot component of the interstellar medium (ISM) is created by winds from massive young stars and supernova explosions in star-forming regions. The diffuse emission from the hot ISM in M31 is less pronounced than that detected from the inner spiral arms in the neighboring Local Group galaxy M33. For this galaxy ROSAT HRI (Shulman & Bregman 1994) and PSPC observations (Long et al. 1996) show diffuse emission with a luminosity of about 10^{39} erg s^{-1} that traces the spiral arms within $15'$ of the nucleus and has a temperature of $kT = 0.4$ keV. Galaxies with high star-forming activity may be even brighter in diffuse X-rays by factors of more than 10 (see e.g. Read et al. 1997, Vogler & Pietsch 1999a). The low diffuse X-ray luminosity in M31 therefore supports the view that the galaxy is in a phase of low star-forming activity.

For the determination of the disk luminosity we adopted the procedure from our previous calculations used in the first survey. Hence, we obtained the same results. Also the considerations concerning the normalized luminosity distribution of the discrete X-ray sources in the disk of M31 are still valid (see S97). A comparison with the luminosity distributions (normalized to bulge luminosity) of other nearby spiral galaxies like M33, M51, M83, M100, M101, NGC253, NGC1566, NGC4258, NGC4559, NGC4565, and NGC4631 (see Vogler & Pietsch 1999b) shows no significant differencies in shape and reveals the distribution of M31 as being typical for this class of galaxy. However, we do not find super-luminous sources (SLS) above several times 10^{38}erg s^{-1}, as is also the case in M33 and NGC253, but not for the other (star-forming) galaxies mentioned above. Although NGC253 is a (bulge) star-forming galaxy it shows no SLSs in its disk population. Therefore it is difficult to interpret the absence of SLSs in M31, but it perhaps tends to show that M31 is not in a star-forming phase.

The discussion of the comparison of our results with those obtained from the *Einstein* observatory and reported by TF also changes slightly under the transition from the first to the second PSPC survey. For the total luminosity of M31, TF found a value of $\sim 3 \times 10^{39}$ erg s^{-1}. To compare with our values, one has to take into account the different spectral models, energy ranges, and especially the different fields of M31 investigated. TF derived the luminosities from the *Einstein* data by applying a thermal bremsstrahlung spectrum in the energy band 0.2 keV - 4.0 keV with $kT = 5$ keV and $N_{\rm H} = 7 \times 10^{20}$ cm^{-2}. They integrated the count rates within an ellipse of $\sim 2.5° \times 1.0°$ which is a bit smaller than the D_{25} ellipse we used for our calculations. A conversion of our results to the spectral model and reduced area of TF yields for the total luminosity $(3.3 \pm 0.3) \times 10^{39}$ erg s^{-1}. The 1σ agreement with the value reported by TF, however, is somewhat coincidental: while our observations covered the whole galaxy, those of TF did not. On the other hand, TF did not correct for background sources.

Comparing the total luminosity of the bulge region, TF reported $\sim 1.5 \times 10^{39}$ erg s^{-1}, which is in agreement with our value of 1.6×10^{39} erg s^{-1} (in this case the effect of the different assumed spectral models is below the errors and therefore negligible). In contrast, for the disk alone we found a somewhat higher luminosity ($(1.8 \pm 0.3) \times 10^{39}$ erg s^{-1}) than TF ($\sim 1.5 \times 10^{39}$ erg s^{-1}), though there is still a 1σ agreement. Considering the fact that TF did not describe the errors and furthermore did not explicitly quote the values for the bulge and disk emission, but simply mentioned that "the emission is roughly equally divided between the bulge and the disk", as well as their neglecting to compensate for background/foreground sources, we desist from a more quantitative comparison, noting that the agreement is surprisingly good. Our results tend to show that TF determined the disk luminosity too low and with it, the total luminosity of M31. With the improved capabilities of ROSAT, the complete coverage of the total galaxy, and our considerations of statistical errors, we were able to clarify the luminosities in M31 at a more reliable level.

As already mentioned, the second survey data did not (significantly) change the results concerning a possible diffuse emission component in the bulge region (from $(2.6 \pm 0.6) \times 10^{38}$ erg s^{-1} to $(2.5 \pm 0.7) \times 10^{38}$ erg s^{-1}, when using the spectral model of S97). The exhaustive discussion of the comparison with the value reported by TF ($\sim 3.8 \times 10^{38}$ erg s^{-1}) and the reasons for the difference have already been undertaken in S97, and are still valid.

7. Summary and conclusions

The second pointed ROSAT PSPC survey of M31 has extended our knowledge concerning the X-ray nature of this

spiral galaxy beyond that already derived from the first survey described in S97 (Supper et al. 1997). Merging the two point source lists of the two surveys led to a total of 560 X-ray sources in the ~ 10.7 deg^2 M31 FOV, 31 located in the very confused bulge region. Their luminosities range from 4×10^{35} erg s^{-1} to 4×10^{38} erg s^{-1}, assuming a distance of 690 kpc to M31. Of these sources, 55 have been identified with known foreground stars, 33 with globular clusters, 16 with supernova remnants, and 10 correlate with known background objects such as background galaxies. None of our M31 sources could be assigned to known novae. A comparison with the *Einstein* source list reported by TF confirms 69 *Einstein* sources. The much improved homogeneity of the second PSPC survey compared with the first and the resulting fewer problems with the PSPC support structure, allowed better flux determinations for a couple of sources. Combined with the higher positional precision in some regions, the list of variable sources when compared with the reported *Einstein* source fluxes could be restricted to 11 candidates, and 7 transients were discovered. Comparisons of the *Einstein* source list with the two ROSAT survey source lists separately, may yield up to 10 transients. Finally, of the 60 sources reported by TF outside the heavily confused bulge region, we could confirm 54, or 90% of these sources. In total, 39 *Einstein* sources could not be confirmed, while 491 new sources were found with ROSAT.

Comparing the first and second PSPC surveys of M31, 34 possible long term variable sources and 8 possible transients (with some overlap with the transients obtained from the comparison with the *Einstein* detected sources) are reported.

For the bulge region, we can give an upper limit to the diffuse component luminosity of $(2.0 \pm 0.5) \times 10^{38}$ erg s^{-1} when using an optically-thin thermal plasma (MEKAL) with $kT = 0.35$ keV for the spectral model. This is a factor of ~ 1.5 lower than the value reported by TF (after transforming to their spectral model). If we assume this luminosity as completely originating from hot gas within the bulge region, this would indicate a gas mass upper limit of $(1.0 \pm 0.3) \times 10^6$ M$_\odot$. For the total $(0.1 - 2.0$ keV) luminosity of M31, we obtain $(3.4 \pm 0.3) \times 10^{39}$ erg s^{-1}, for the bulge alone 1.6×10^{39} erg s^{-1} and for the disk $(1.8 \pm 0.3) \times 10^{39}$ erg s^{-1}. With these improved values, we find an equal distribution of luminosity between the bulge and disk, in agreement with TF, but a higher value for the total luminosity than reported in TF.

Several results from the first PSPC survey of M31 reported in S97 have not been significantly altered by the inclusion of the second survey data and remain valid. These include: 1) the integral luminosity distribution of the globular cluster sources and its comparison to that of the Milky Way, 2) the statistical estimation of the fraction of background and foreground sources among the detected X-ray sources, and 3) the spectral analysis of the brightest sources.

Acknowledgements. We thank the MPE ROSAT group for their support. Parts of our analysis used the SASS and EXSAS data analysis software. The authors would like to thank the referee for carefully reading this paper and making useful comments and suggestions. We thank NASA and the Centre de Données astronomiques for the online access to their data bases. WHGL is grateful for support from NASA.
RS remembers J. v. Paradijs as an always gentle and helpful excellent scientist who sadly passed away well ahead of his time – a great loss for the astronomical community.
The ROSAT project has been supported by the Bundesministerium für Bildung und Forschung (BMBF/DLR) and the Max-Planck-Gesellschaft (MPG).

References

Battistini P.L., Bònoli F., Braccesi A., et al., 1987, A&AS 67, 447
Battistini P.L., Bònoli F., Casavecchia M., et al., 1993, A&A 272, 77
Borozdin K.N., Priedhorsky W.C., 2000, ApJ 542, L13
Braun R., Walterbos R.A.M., 1993, A&AS 98, 327
Capaccioli M., Della Valle M., D'Onofrio M., et al., 1989, AJ 97, 1622
Collura A., Reale F., Peres G., 1990, ApJ 356, 119
Crampton D., Cowley A.P., Hutchings J.B., Schade D.J., Speybroeck L.P.van, 1984, ApJ 284, 663
Cruddace R.G., Hasinger G.R., Schmitt J.H., 1988, The Application of a Maximum Likelihood Analysis to Detection of Sources in the Rosat Data base. In: Murtagh F., Heck A. (eds.) Astronomy from Large Databases. ESO Conference and Workshop Proceedings No. 28, Garching/Germany, p. 177
D'Odorico S., Dopita M.A., Benevenuti P., 1980, A&AS 40, 67
Garcia M.R., Murray S.S., Primini F.A., et al., 2000, ApJ 537, L23
Greiner J., Supper R., Magnier E.A., 1996, Supersoft X-ray Sources in M31. In: Greiner J. (ed.) Supersoft X-ray Sources, Springer Verlag, p. 75
Haiman Z, Magnier E.A., Lewin W.H.G., et al., 1994, A&A, 286, 725
Hasinger G., et al., 1992, GSFC OGIP Calibration Memo, CAL/ROS/92-001
Immler S., 2000, "The X-Ray Source Population of Nearby Spiral Galaxies", PhD thesis, Ludwig–Maximilians–Universität München, Germany
Irwin J.A., Bregman J.N, 1999, ApJ 527, 125
Jacchia L.G., 1972, in CIRA 1972: COSPAR International Reference Atmosphere 1972, compiled by The Committee for CIRA of Cospar Working Group 4. Akademie-Verlag, Berlin, p. 227
Kahabka P., 1999, A&A 344, 459
Kato T., 1976, ApJS 30, 397
Long K.S., Speybroeck L.P.van, 1983, X-Ray Emission from Normal Galaxies. In: Lewin W.H.G., Heuvel E.P.J.van den (eds.) Accretion Driven Stellar X-Ray Sources. Cambridge University Press, Cambridge, p. 117
Long K.S., Charles P.A., Blair W.P., et al., 1996, ApJ 466, 750L
Magnier E.A., Lewin W.H.G., van Paradijs J., et al., 1992, A&AS 96, 379
Magnier E.A., Lewin W.H.G., van Paradijs J., et al., 1994a, A&AS, submitted

Magnier E.A., Prins S., van Paradijs J., et al., 1995, A&AS, 114, 215
Primini F.A., Forman W., Jones C., 1993, ApJ 410, 615
Read A.M., Ponman T.J., Stickland D.K., 1997, MNRAS 286, 626
Sharov A.S., Alksnis A., 1991, Ap&SS 180, 273
Sharov A.S., Alksnis A., 1992, Ap&SS 190, 119
Shirey R., Soria R., Borozdin K., et al., 2001, A&AL, 365, 195
Shulman E., Bregman J.N., 1994, ROSAT HRI Observations of M33. In: Schlegel E.M., Robert P. (eds.) The Soft X-ray Cosmos. AIP Conference Proceedings #313, AIP, New York, p. 345
Snowden S.L., Plucinsky P.P., Briel U., Hasinger G., Pfeffermann E., 1992, ApJ 393, 819
Snowden S.L., Freyberg M.J., 1993, ApJ 404, 403
van Speybroeck L.P., Epstein A., Forman W., et al., 1979, ApJ 234, L45
van Speybroeck L.P., Bechtold J., 1981, X-Ray Emission from Normal Galaxies. In: Giacconi R. (ed.) X-Ray Astronomy with the Einstein Satellite. Reidel, Dordrecht, p. 153
Supper R., Hasinger G., Pietsch W., et al., 1997, A&A 317, 328 [S97]
Trinchieri G., Fabbiano G., 1991, ApJ 382, 82 [TF]
Trinchieri G., Israel G.L., Chippetti L., et al., 1999, A&A 348, 43
Vogler A., Pietsch W., 1999a, A&A 342, 101
Vogler A., Pietsch W., 1999b, A&A 352, 64
Zimmermann H.U., Belloni T., Izzo C., Kahabka P., Schwentker O., 1993, MPE Report 244, Ed. 3

Table 4. Log of the 94 single observations forming the second ROSAT PSPC survey of M31. Pointing numbers ending with "-1" or "-2" indicate follow-up observations.

Pointing	Date	R.A. (J2000)[1]			Dec. (J2000)[1]			Exposure
		(h)	(m)	(s)	(°)	(′)	(″)	(s)
WG600296P	25.-26. July 1992	0	37	43.2	40	23	24	2 512
WG600297P	25.-25. July 1992	0	38	9.6	40	29	24	2 536
WG600316P	21.-21. July 1992	0	38	26.3	40	17	24	2 672
WG600298P	05.-05. Aug. 1992	0	38	33.5	40	36	00	2 640
WG600317P	20.-20. July 1992	0	38	52.7	40	23	24	2 616
WG600299P	05.-05. Aug. 1992	0	39	0.0	40	42	0	1 576
WG600299P-1	01.-11. Jan. 1993	0	39	0.0	40	42	0	1 448
WG600336P	29.-30. July 1992	0	39	12.0	40	11	24	2 752
WG600318P	06.-06. Aug. 1992	0	39	16.7	40	30	0	1 416
WG600318P-1	31.-31. Dec. 1992	0	39	16.7	40	30	0	1 312
WG600300P	05.-05. Aug. 1992	0	39	24.0	40	48	36	2 456
WG600337P	30.-30. Dec. 1992	0	39	36.0	40	17	24	2 096
WG600319P	06.-06. Aug. 1992	0	39	43.2	40	36	00	1 816
WG600301P	22.-22. July 1992	0	39	48.0	40	54	36	2 688
WG600356P	03.-04. Aug. 1992	0	39	55.2	40	5	24	1 976
WG600338P	03.-03. Aug. 1992	0	40	2.4	40	24	0	2 168
WG600320P-1	01.-01. July 1993	0	40	7.2	40	42	36	2 744
WG600302P	30.-31. Dec. 1992	0	40	14.3	41	1	12	2 568
WG600357P	30.-30. Dec. 1992	0	40	21.6	40	11	24	2 720
WG600339P	25.-25. July 1992	0	40	26.3	40	30	0	2 840
WG600321P	29.-30. July 1992	0	40	33.5	40	48	36	2 848
WG600303P	27.-28. July 1992	0	40	38.4	41	7	12	2 416
WG600358P	26.-26. July 1992	0	40	45.5	40	18	00	2 864
WG600340P	06.-06. Aug. 1992	0	40	52.7	40	36	36	2 560
WG600322P	06.-06. Aug. 1992	0	40	57.5	40	55	12	2 584
WG600304P	31.-31. Dec. 1992	0	41	4.8	41	13	48	1 872
WG600359P	06.-07. Aug. 1992	0	41	12.0	40	24	0	2 600
WG600341P	23.-23. July 1992	0	41	16.7	40	42	36	2 712
WG600323P	05.-06. Aug. 1992	0	41	24.0	41	1	12	2 560
WG600305P	06.-07. Aug. 1992	0	41	28.7	41	19	48	2 216
WG600360P	23.-24. July 1992	0	41	36.0	40	30	36	2 864
WG600342P	05.-05. Aug. 1992	0	41	43.2	40	49	12	3 416
WG600324P	07.-07. Jan. 1993	0	41	48.0	41	7	48	2 960
WG600306P	07.-08. Aug. 1992	0	41	55.2	41	26	24	2 424
WG600361P	05.-06. Aug. 1992	0	42	0.0	40	36	36	2 744
WG600343P	04.-04. Jan. 1993	0	42	7.1	40	55	12	2 744
WG600325P	02.-02. Jan. 1993	0	42	14.3	41	13	48	2 848
WG600307P	01.-01. Jan. 1993	0	42	19.2	41	32	24	720
WG600307P-1	05.-09. July 1993	0	42	19.2	41	32	24	2 032
WG600362P	06.-06. Aug. 1992	0	42	26.3	40	43	12	2 448
WG600344P	07.-07. Aug. 1992	0	42	31.2	41	1	48	1 744
WG600326P	07.-07. Aug. 1992	0	42	38.4	41	20	24	1 704
WG600326P-2	18.-18. July 1993	0	42	38.4	41	20	24	696
WG600308P	07.-07. Aug. 1992	0	42	45.5	41	39	0	1 512
WG600308P-1	03.-11. Jan. 1993	0	42	45.5	41	39	0	1 768
WG600363P	03.-03. Jan. 1993	0	42	50.4	40	49	12	1 944
WG600345P	01.-01. Jan. 1993	0	42	57.5	41	7	48	1 592
WG600345P-1	22.-22. July 1993	0	42	57.6	41	7	48	1 712
WG600327P	07.-07. Aug. 1992	0	43	4.8	41	26	24	2 112

Pointing	Date	R.A. (J2000)[1]			Dec. (J2000)[1]			Exposure
		(h)	(m)	(s)	(°)	(′)	(″)	(s)
WG600309P	07.-08. Aug. 1992	0	43	9.6	41	45	0	2 576
WG600364P	07.-07. Aug. 1992	0	43	16.7	40	55	48	416
WG600364P-2	04.-04. July 1993	0	43	16.8	40	55	48	3 296
WG600346P	06.-06. Aug. 1992	0	43	21.6	41	14	24	1 968
WG600328P	02.-02. Jan. 1993	0	43	28.7	41	33	00	2 320
WG600310P	05.-05. Jan. 1993	0	43	36.0	41	51	36	2 720
WG600365P	02.-02. Jan. 1993	0	43	40.7	41	1	48	3 144
WG600347P	03.-03. Jan. 1993	0	43	48.0	41	20	24	2 936
WG600329P	08.-08. Aug. 1992	0	43	52.7	41	39	0	1 760
WG600311P	08.-08. Aug. 1992	0	44	0.0	41	58	12	1 352
WG600311P-1	01.-01. Jan. 1993	0	44	0.0	41	58	12	1 240
WG600366P	07.-07. Aug. 1992	0	44	7.1	41	8	24	1 776
WG600348P	31.-31. Dec. 1992	0	44	12.0	41	27	0	1 696
WG600348P-1	22.-22. July 1993	0	44	12.0	41	27	0	1 800
WG600330P	08.-08. Aug. 1992	0	44	19.2	41	45	36	1 624
WG600330P-1	14.-14. Jan. 1993	0	44	19.2	41	45	36	944
WG600312P	08.-08. Aug. 1992	0	44	24.0	42	4	12	2 416
WG600367P	04.-04. Jan. 1993	0	44	31.2	41	14	24	2 624
WG600349P	06.-06. Jan. 1993	0	44	38.4	41	33	00	2 824
WG600331P	04.-04. Jan. 1993	0	44	43.2	41	52	12	2 872
WG600313P	09.-09. Jan. 1993	0	44	50.4	42	10	48	2 672
WG600368P	03.-03. Jan. 1993	0	44	57.5	41	21	00	2 912
WG600350P	05.-05. Jan. 1993	0	45	2.4	41	39	36	2 680
WG600332P	11.-11. Jan. 1993	0	45	9.6	41	58	12	2 944
WG600314P	10.-10. Jan. 1993	0	45	14.3	42	16	48	2 704
WG600369P	09.-09. Jan. 1993	0	45	21.6	41	27	0	2 520
WG600351P	02.-02. Jan. 1993	0	45	28.7	41	46	12	2 824
WG600333P	11.-11. Jan. 1993	0	45	33.5	42	4	48	3 040
WG600315P	06.-10. Jan. 1993	0	45	40.7	42	23	24	3 024
WG600370P	06.-06. Jan. 1993	0	45	48.0	41	33	36	2 864
WG600352P	10.-10. Jan. 1993	0	45	52.7	41	52	12	2 632
WG600334P	09.-09. Aug. 1992	0	46	0.0	42	10	48	720
WG600334P-1	07.-07. Jan. 1993	0	46	0.0	42	10	48	2 168
WG600371P	08.-09. Aug. 1992	0	46	12.0	41	40	12	2 080
WG600353P	11.-11. Jan. 1993	0	46	19.2	41	58	48	3 008
WG600335P	09.-09. Aug. 1992	0	46	24.0	42	17	24	728
WG600335P-1	10.-10. Jan. 1993	0	46	24.0	42	17	24	2 368
WG600372P	03.-03. July 1993	0	46	38.4	41	46	12	3 088
WG600354P	08.-08. Aug. 1992	0	46	43.2	42	4	48	2 368
WG600373P	11.-12. Jan. 1993	0	47	2.4	41	52	48	3 144
WG600355P	09.-09. Aug. 1992	0	47	9.6	42	11	24	1 920
WG600374P	09.-09. Aug. 1992	0	47	26.3	41	58	48	680
WG600374P-1	04.-04. Jan. 1993	0	47	26.3	41	58	48	2 008
WG600375P	09.-09. Aug. 1992	0	47	52.7	42	5	24	1 080
WG600375P-1	15.-15. Jan. 1993	0	47	52.7	42	5	24	2 112

[1]The coordinates give the centre of the FOV (nominal pointing direction).

Table 5. List of all X-ray sources in M31 detected in the second ROSAT PSPC survey (SII). The meaning of the different columns is described in Sect. 3.3. The listed count rate errors are only statistical. The systematic errors are expected to be less than ∼ 15%. For sources not detected in a considered energy band 1σ upper limits have been calculated indicated by a '<'-symbol in front of the upper limit value. A conversion of count rates into fluxes depends on the assumed spectral shape. For M31-sources a power law with $\Gamma = -2.0$ and $N_{\rm H} = 9 \times 10^{20}$ cm^{-2} may be used, leading to the conversion factor 1 cts ksec^{-1} = 3.00×10^{-14} erg cm^{-2} sec^{-1} in the 0.1 - 2.0 keV band (B-band). For foreground stars the application of this conversion factor leads to an over-estimate of the fluxes.

⋆ Bulge sources

SII No. (1)	R.A. (h) (2)	(m) (3)	(J2000) (s) (4)	(°) (5)	Dec. (′) (6)	(″) (7)	$\sigma_{\rm Pos}$ (″) (8)	Cl. (9)	Maxlik (LH) (10)	Rate (B) ($ct \cdot ks^{-1}$) (11)	Rate (S) ($ct \cdot ks^{-1}$) (12)	Rate (H) ($ct \cdot ks^{-1}$) (13)	Rate (H_1) ($ct \cdot ks^{-1}$) (14)	Rate (H_2) ($ct \cdot ks^{-1}$) (15)
1	0	36	21.7	40	53	37	13	4	69.7	< 0.61	< 0.20	5.73 ± 0.65	< 1.70	4.22 ± 0.53
2	0	36	43.0	41	9	2	19	4	27.1	< 0.43	< 0.16	3.18 ± 0.71	< 0.87	3.56 ± 0.61
3	0	36	49.6	40	55	12	18	4	11.8	< 0.13	< 0.14	1.72 ± 0.42	< 0.99	< 1.20
4	0	36	49.8	40	8	52	12	1	45.0	10.62 ± 1.82	< 3.50	7.46 ± 1.43	< 3.59	3.74 ± 1.04
5	0	36	57.4	40	26	10	12	1	12.2	< 2.13	< 0.62	1.34 ± 0.43	< 0.81	< 1.30
6	0	37	11.4	40	22	10	11	1	10.5	< 1.65	< 0.70	< 1.13	< 0.63	< 0.55
7	0	37	18.7	40	29	47	8	1	82.4	3.43 ± 0.65	< 0.30	3.90 ± 0.60	2.02 ± 0.43	1.79 ± 0.41
8	0	37	22.5	40	43	49	9	1	86.3	10.19 ± 1.34	5.09 ± 0.98	4.93 ± 0.90	2.97 ± 0.69	1.82 ± 0.56
9	0	37	26.2	40	13	7	10	1	20.6	2.16 ± 0.60	< 0.79	1.63 ± 0.43	< 0.54	1.22 ± 0.36
10	0	37	34.6	40	9	55	7	1	238.8	11.48 ± 1.16	< 1.25	9.49 ± 0.97	3.63 ± 0.61	5.63 ± 0.75
11	0	37	38.5	39	38	42	16	4	81.2	< 6.05	< 0.62	10.39 ± 1.17	< 3.21	8.48 ± 0.96
12	0	37	41.5	40	25	45	10	1	15.9	< 1.62	< 0.59	0.78 ± 0.25	< 0.36	0.51 ± 0.19
13	0	37	42.6	40	37	50	10	1	15.9	< 1.86	< 0.73	0.90 ± 0.28	< 0.45	0.58 ± 0.22
14	0	37	43.3	40	23	44	8	1	52.3	2.97 ± 0.54	< 1.30	2.12 ± 0.39	1.64 ± 0.34	< 0.62
15	0	37	43.5	40	4	55	11	1	44.0	19.11 ± 2.03	< 2.32	14.48 ± 1.49	4.25 ± 0.89	8.80 ± 1.15
16	0	38	0.5	40	26	34	6	1	578.9	16.59 ± 0.99	9.23 ± 0.78	7.05 ± 0.61	3.24 ± 0.41	3.86 ± 0.45
17	0	38	20.1	40	40	29	10	1	17.2	< 1.39	< 0.50	0.75 ± 0.23	< 0.22	0.60 ± 0.20
18	0	38	21.3	40	56	40	9	1	52.1	7.23 ± 1.16	3.23 ± 0.92	3.99 ± 0.80	1.42 ± 0.50	2.49 ± 0.63
19	0	38	21.5	40	18	32	12	1	12.8	< 0.92	< 0.33	0.54 ± 0.19	< 0.22	0.52 ± 0.18
20	0	38	23.5	40	12	59	7	1	327.8	9.03 ± 0.78	< 1.67	7.21 ± 0.64	3.08 ± 0.42	4.17 ± 0.49
21	0	38	27.7	41	36	55	23	4	14.6	< 0.17	< 0.17	< 2.86	< 0.46	< 0.68
22	0	38	34.5	41	28	51	8	4	2093.6	55.28 ± 0.96	< 0.40	63.69 ± 1.42	21.82 ± 0.91	35.02 ± 1.17
23	0	38	34.8	40	10	34	10	1	22.9	< 2.03	< 0.55	1.32 ± 0.32	< 0.51	1.07 ± 0.27
24	0	38	38.6	40	26	21	7	1	144.6	3.87 ± 0.46	< 0.84	2.85 ± 0.35	1.77 ± 0.27	1.06 ± 0.22
25	0	38	38.6	40	56	54	11	1	26.0	2.59 ± 0.71	< 0.48	2.57 ± 0.57	< 0.82	2.25 ± 0.53
26	0	38	39.0	40	43	25	10	1	11.7	< 0.80	< 0.25	< 0.77	< 0.18	0.44 ± 0.17
27	0	38	40.0	40	20	5	11	1	19.4	1.52 ± 0.36	1.63 ± 0.36	< 0.25	< 0.18	< 0.11
28	0	38	40.8	40	44	57	9	1	20.3	1.46 ± 0.39	< 0.98	0.78 ± 0.24	< 0.18	0.69 ± 0.21
29	0	38	48.2	40	8	3	10	1	23.9	1.50 ± 0.44	< 0.60	1.39 ± 0.33	< 1.20	0.64 ± 0.21
30	0	38	48.6	40	38	12	8	1	39.5	1.28 ± 0.31	< 0.26	1.18 ± 0.24	0.43 ± 0.15	0.73 ± 0.19
31	0	38	50.1	40	44	18	8	1	111.0	3.28 ± 0.49	< 0.45	3.25 ± 0.43	< 0.87	2.70 ± 0.38
32	0	38	56.0	39	55	51	10	1	26.2	2.52 ± 0.74	< 0.66	2.07 ± 0.59	< 0.73	1.57 ± 0.50
33	0	38	56.3	40	34	52	9	1	43.3	1.69 ± 0.34	< 0.50	1.35 ± 0.25	< 0.42	1.03 ± 0.21
34	0	39	3.6	40	47	43	9	1	10.9	< 1.03	< 0.37	0.59 ± 0.20	< 0.30	0.39 ± 0.15
35	0	39	9.1	40	6	23	12	1	12.8	< 0.85	< 0.36	< 0.87	< 0.19	0.58 ± 0.21
36	0	39	11.6	40	35	34	10	1	16.8	< 1.11	< 0.30	0.66 ± 0.18	0.51 ± 0.16	< 0.23
37	0	39	12.8	40	13	8	10	1	14.9	< 1.36	< 0.63	0.56 ± 0.19	< 0.20	0.46 ± 0.16
38	0	39	15.4	40	8	21	9	1	44.8	2.04 ± 0.46	< 0.37	2.10 ± 0.38	0.92 ± 0.25	1.24 ± 0.28
39	0	39	16.5	40	1	6	9	1	25.0	2.21 ± 0.61	< 2.02	1.69 ± 0.44	< 0.96	1.53 ± 0.42
40	0	39	16.6	40	51	17	8	1	35.4	1.64 ± 0.38	< 0.42	1.33 ± 0.28	< 0.78	0.84 ± 0.21
41	0	39	17.9	41	3	0	10	1	33.8	1.62 ± 0.47	< 0.26	2.17 ± 0.45	< 1.00	1.40 ± 0.36
42	0	39	25.0	41	5	20	11	1	12.3	< 1.80	< 0.54	0.98 ± 0.32	< 0.47	0.66 ± 0.26
43	0	39	25.1	40	50	30	9	1	25.1	1.88 ± 0.38	< 1.33	0.81 ± 0.21	0.45 ± 0.15	< 0.51
44	0	39	29.2	40	35	55	10	1	11.5	< 1.09	< 0.43	0.50 ± 0.16	< 0.27	< 0.61
45	0	39	34.6	41	9	34	8	1	93.4	5.04 ± 0.81	< 0.53	4.87 ± 0.72	1.09 ± 0.36	3.75 ± 0.63
46	0	39	38.0	40	48	3	9	1	18.7	1.02 ± 0.30	< 1.18	0.78 ± 0.20	< 0.38	0.54 ± 0.16
47	0	39	38.3	40	11	6	9	1	26.2	1.86 ± 0.41	< 0.93	1.04 ± 0.25	0.65 ± 0.20	0.45 ± 0.16
48	0	39	39.9	40	35	37	9	1	31.6	1.18 ± 0.28	< 0.33	1.00 ± 0.21	< 0.50	0.66 ± 0.16
49	0	39	42.6	40	39	48	9	1	24.5	1.03 ± 0.26	< 0.34	0.79 ± 0.18	0.62 ± 0.16	< 0.31
50	0	39	43.0	41	16	3	20	1	15.0	< 11.52	< 0.87	4.67 ± 1.13	< 2.19	3.11 ± 0.87
51	0	39	47.5	40	30	17	9	1	28.4	1.89 ± 0.34	1.68 ± 0.32	< 0.34	< 0.28	< 0.12
52	0	39	48.8	41	10	8	9	1	22.6	< 2.03	< 0.35	1.51 ± 0.39	< 0.88	0.88 ± 0.29
53	0	39	53.8	40	9	1	7	1	85.1	3.03 ± 0.49	< 0.58	2.60 ± 0.40	1.17 ± 0.28	1.47 ± 0.30
54	0	39	56.1	40	41	6	7	1	100.5	2.44 ± 0.34	< 0.36	1.91 ± 0.26	1.15 ± 0.20	0.76 ± 0.17
55	0	39	56.4	41	11	39	10	1	14.0	< 1.55	< 0.33	1.15 ± 0.36	< 1.27	< 0.53
56	0	39	57.5	40	27	31	8	1	57.6	2.08 ± 0.35	< 0.44	1.61 ± 0.26	0.84 ± 0.20	0.80 ± 0.18
57	0	39	57.6	40	16	32	9	1	20.8	1.23 ± 0.32	< 1.64	0.74 ± 0.19	< 0.38	0.49 ± 0.15
58	0	39	58.1	39	29	33	37	4	10.3	< 0.70	< 0.55	< 3.01	< 1.01	< 3.21
59	0	39	59.2	40	32	8	8	1	104.0	2.97 ± 0.39	< 0.68	2.85 ± 0.34	0.74 ± 0.18	2.00 ± 0.27
60	0	39	59.5	41	1	3	11	1	20.2	< 2.13	< 0.27	2.20 ± 0.40	1.35 ± 0.31	< 1.13
61	0	40	7.6	40	6	28	14	1	11.5	< 2.23	< 1.24	< 1.27	< 0.18	< 1.34
62	0	40	7.6	40	53	3	12	1	10.2	< 0.64	< 0.20	0.70 ± 0.21	< 0.47	< 0.50
63	0	40	11.3	40	59	30	9	1	16.7	< 1.32	< 0.37	0.78 ± 0.22	< 0.40	0.51 ± 0.18
64	0	40	13.5	40	50	10	5	1	16287.	118.14 ± 1.78	1.72 ± 0.36	124.12 ± 1.94	23.39 ± 0.87	103.45 ± 1.86
65	0	40	13.9	40	33	52	8	1	59.8	1.84 ± 0.32	< 0.26	1.59 ± 0.25	0.81 ± 0.19	0.90 ± 0.18

⋆ Bulge sources

SII	R.A.		(J2000)		Dec.		$\sigma_{\rm Pos}$	Cl.	Maxlik	Rate (B)	Rate (S)	Rate (H)	Rate (H_1)	Rate (H_2)
No.	(h)	(m)	(s)	(°)	(′)	(″)	(″)		(LH)	($ct \cdot ks^{-1}$)	($ct \cdot ks^{-1}$)	($ct \cdot ks^{-1}$)	($ct \cdot ks^{-1}$)	($ct \cdot ks^{-1}$)
(1)	(2)	(3)	(4)	(5)	(6)	(7)	(8)	(9)	(10)	(11)	(12)	(13)	(14)	(15)
66	0	40	14.8	40	15	17	11	1	11.0	< 1.06	< 0.36	0.63 ± 0.21	< 0.61	< 0.44
67	0	40	17.7	39	53	54	8	1	99.8	9.65 ± 1.45	< 2.27	7.97 ± 1.26	4.25 ± 0.91	3.67 ± 0.87
68	0	40	19.9	40	44	5	5	1	6379.9	52.34 ± 1.27	1.39 ± 0.28	48.99 ± 1.21	14.45 ± 0.65	34.80 ± 1.02
69	0	40	21.5	40	3	20	13	1	10.6	< 1.87	< 0.38	< 1.90	< 0.28	1.07 ± 0.35
70	0	40	22.6	40	36	17	10	1	19.2	< 1.01	< 0.24	0.71 ± 0.18	< 0.29	0.54 ± 0.14
71	0	40	22.9	40	53	15	9	1	26.9	1.61 ± 0.32	< 0.73	0.97 ± 0.21	0.59 ± 0.17	< 0.51
72	0	40	23.7	40	29	53	7	1	187.0	4.21 ± 0.45	< 0.56	3.44 ± 0.36	0.93 ± 0.20	2.47 ± 0.30
73	0	40	25.3	40	34	30	10	1	11.2	< 0.82	< 0.35	< 0.60	< 0.19	0.35 ± 0.12
74	0	40	25.8	41	29	12	12	1	35.6	8.58 ± 1.51	< 1.31	7.79 ± 1.28	< 1.64	6.94 ± 1.18
75	0	40	32.1	40	1	12	11	1	16.0	2.12 ± 0.63	< 1.23	1.49 ± 0.46	< 1.14	< 0.99
76	0	40	32.4	40	33	28	16	1	12.4	< 1.08	< 0.42	< 0.73	< 0.16	< 0.94
77	0	40	35.6	39	57	18	12	1	10.4	2.55 ± 0.80	< 3.27	< 0.99	< 0.44	< 0.60
78	0	40	38.1	41	19	39	14	1	11.1	< 3.20	< 2.72	< 1.70	< 0.77	< 1.05
79	0	40	41.0	40	22	29	11	1	12.8	< 1.26	< 0.49	0.68 ± 0.21	< 0.45	0.44 ± 0.16
80	0	40	41.8	41	8	8	19	1	10.8	< 1.64	< 0.45	< 2.27	< 0.30	< 1.40
81	0	40	42.3	39	59	7	8	1	50.8	5.54 ± 1.01	< 1.89	3.97 ± 0.77	2.55 ± 0.63	1.54 ± 0.47
82	0	40	42.3	40	32	41	12	1	10.4	< 0.97	< 0.39	< 0.75	< 0.24	0.54 ± 0.16
83	0	40	44.3	39	37	1	12	4	135.1	11.01 ± 1.57	< 0.85	15.23 ± 1.32	6.17 ± 0.88	8.30 ± 0.97
84	0	40	46.2	40	51	38	9	1	26.5	1.16 ± 0.27	< 0.34	0.98 ± 0.21	< 0.44	0.68 ± 0.17
85	0	40	48.0	41	53	2	15	4	35.2	< 0.81	< 0.11	3.59 ± 0.53	1.21 ± 0.31	3.60 ± 0.49
86	0	40	48.7	40	30	44	8	1	37.4	1.55 ± 0.33	< 0.61	1.00 ± 0.22	< 0.28	0.81 ± 0.18
87	0	40	49.4	40	11	32	7	1	267.7	14.64 ± 1.10	9.49 ± 0.90	4.31 ± 0.57	1.98 ± 0.39	2.26 ± 0.42
88	0	40	51.6	40	21	12	9	1	15.5	< 1.04	< 0.23	0.75 ± 0.22	< 0.58	< 0.53
89	0	40	53.3	41	32	46	11	1	20.0	2.26 ± 0.67	< 0.90	2.03 ± 0.54	< 1.20	1.32 ± 0.44
90	0	40	58.6	40	3	45	11	1	10.6	< 2.23	< 0.67	1.08 ± 0.39	< 0.75	< 0.82
91	0	41	4.8	41	23	58	10	1	24.4	2.86 ± 0.60	< 1.87	2.12 ± 0.48	1.19 ± 0.33	< 1.32
92	0	41	5.4	40	27	17	8	1	44.0	1.79 ± 0.38	< 0.36	1.43 ± 0.28	0.50 ± 0.17	0.90 ± 0.22
93	0	41	6.9	40	2	51	10	1	45.4	5.57 ± 1.01	< 1.49	4.08 ± 0.80	1.42 ± 0.47	3.04 ± 0.70
94	0	41	7.3	40	50	57	9	1	20.8	1.11 ± 0.27	< 0.44	0.72 ± 0.18	< 0.33	0.47 ± 0.13
95	0	41	11.8	40	54	25	7	1	70.2	1.94 ± 0.32	< 0.37	1.60 ± 0.25	< 0.45	1.30 ± 0.21
96	0	41	14.7	40	49	1	12	1	10.7	1.00 ± 0.27	< 1.12	< 0.27	< 0.11	< 0.22
97	0	41	15.8	41	1	7	8	1	46.7	1.81 ± 0.33	< 0.40	1.37 ± 0.24	< 0.65	0.92 ± 0.19
98	0	41	15.9	40	16	48	9	1	23.4	1.73 ± 0.46	< 0.60	1.26 ± 0.32	< 0.78	0.71 ± 0.24
99	0	41	18.3	40	51	59	7	1	212.8	4.93 ± 0.44	< 0.82	3.88 ± 0.36	1.81 ± 0.24	2.14 ± 0.27
100	0	41	24.8	41	36	51	11	1	12.4	< 1.51	< 0.49	1.07 ± 0.34	0.80 ± 0.28	< 0.37
101	0	41	25.7	40	58	48	6	1	328.3	6.34 ± 0.50	< 0.68	5.04 ± 0.41	1.58 ± 0.24	3.52 ± 0.34
102	0	41	26.0	40	53	30	7	1	87.6	2.78 ± 0.36	< 0.70	2.00 ± 0.27	0.97 ± 0.19	1.03 ± 0.19
103	0	41	28.5	40	25	51	9	1	17.6	< 1.37	< 0.36	0.91 ± 0.26	< 0.44	0.58 ± 0.20
104	0	41	31.3	41	5	55	6	1	901.2	12.36 ± 0.69	< 0.19	11.92 ± 0.64	2.84 ± 0.32	9.27 ± 0.56
105	0	41	32.6	41	17	48	9	1	22.2	1.40 ± 0.34	< 0.54	0.99 ± 0.24	< 0.41	0.71 ± 0.20
106	0	41	34.6	40	28	56	10	1	14.3	< 1.50	< 0.70	0.71 ± 0.22	< 0.21	0.57 ± 0.19
107	0	41	35.9	41	40	6	11	1	14.3	< 1.95	< 0.51	1.03 ± 0.35	0.91 ± 0.30	< 0.28
108	0	41	37.6	41	1	13	8	1	85.8	3.10 ± 0.40	< 1.31	2.30 ± 0.30	0.71 ± 0.18	1.56 ± 0.24
109	0	41	41.1	40	31	22	10	1	28.4	1.75 ± 0.42	< 0.54	1.46 ± 0.30	0.64 ± 0.20	0.72 ± 0.21
110	0	41	41.3	41	0	10	5	1	16.5	< 2.12	< 0.33	1.76 ± 0.36	< 0.16	0.56 ± 0.16
111	0	41	41.4	41	3	32	8	1	46.6	1.84 ± 0.33	< 0.36	1.45 ± 0.25	0.66 ± 0.17	0.80 ± 0.19
112	0	41	43.1	41	4	59	8	1	71.0	2.90 ± 0.39	< 0.81	2.06 ± 0.29	1.23 ± 0.22	0.82 ± 0.19
113	0	41	43.2	41	34	22	6	1	3463.9	53.70 ± 1.83	< 1.12	51.53 ± 1.75	14.74 ± 0.94	37.07 ± 1.49
114	0	41	44.1	41	21	19	10	1	26.2	1.11 ± 0.33	< 0.62	1.60 ± 0.34	< 0.14	0.92 ± 0.23
115	0	41	44.7	40	22	0	5	1	52.1	19.66 ± 1.52	< 3.94	5.15 ± 0.70	2.37 ± 0.48	2.58 ± 0.49
116	0	41	45.2	41	26	25	8	1	49.2	2.37 ± 0.46	< 0.55	1.91 ± 0.35	0.77 ± 0.23	1.01 ± 0.25
117	0	41	45.5	40	34	31	9	1	20.6	< 1.27	< 0.30	0.88 ± 0.22	< 0.64	0.42 ± 0.15
118	0	41	45.7	40	36	24	10	1	10.6	< 0.98	< 0.92	< 0.56	< 0.12	0.33 ± 0.13
119	0	41	47.2	41	31	55	9	1	53.5	3.08 ± 0.56	< 0.54	3.00 ± 0.46	0.95 ± 0.27	1.62 ± 0.34
120	0	41	48.7	40	28	14	10	1	13.0	< 1.08	< 0.42	0.73 ± 0.25	< 0.27	0.61 ± 0.21
121	0	41	48.9	41	22	33	7	1	94.1	2.69 ± 0.43	< 0.30	2.57 ± 0.37	< 0.70	2.03 ± 0.32
122	0	41	49.6	41	1	8	6	1	299.0	6.25 ± 0.51	< 0.58	5.22 ± 0.43	1.69 ± 0.24	3.62 ± 0.35
123	0	41	49.9	40	15	26	8	1	62.0	7.02 ± 1.04	2.80 ± 0.76	3.60 ± 0.68	< 2.33	2.20 ± 0.51
124	0	41	50.6	41	13	34	9	1	18.3	< 1.25	< 0.20	0.83 ± 0.22	< 0.26	0.71 ± 0.19
125	0	41	51.3	41	51	53	11	1	14.3	3.28 ± 0.91	< 1.80	1.94 ± 0.66	< 1.43	< 1.17
126	0	41	51.9	41	14	49	8	1	46.2	1.85 ± 0.36	< 0.40	1.84 ± 0.31	0.63 ± 0.18	1.21 ± 0.25
127	0	41	52.6	40	21	24	6	1	3614.5	90.56 ± 2.85	10.27 ± 1.06	76.44 ± 2.59	36.93 ± 1.80	41.22 ± 1.91
128	0	41	54.7	41	33	38	8	1	45.1	2.10 ± 0.44	< 0.48	1.76 ± 0.34	0.78 ± 0.23	0.91 ± 0.24
129	0	41	55.6	40	46	49	15	1	15.1	< 2.96	< 0.17	2.82 ± 0.42	< 0.92	1.22 ± 0.25
130	0	42	0.7	40	41	24	7	1	142.7	6.47 ± 0.61	5.62 ± 0.58	1.44 ± 0.27	1.09 ± 0.23	< 0.49
131	0	42	2.6	40	31	18	10	1	16.0	< 1.40	< 0.49	0.77 ± 0.24	< 0.52	< 0.57
132	0	42	2.7	40	46	15	8	1	42.1	1.50 ± 0.32	< 0.44	1.06 ± 0.22	< 0.83	0.91 ± 0.19
133	0	42	3.0	40	24	16	10	1	45.9	3.24 ± 0.68	< 0.62	3.79 ± 0.64	1.56 ± 0.41	2.06 ± 0.47
134	0	42	3.2	40	28	56	8	1	46.0	2.19 ± 0.47	< 0.37	1.84 ± 0.37	0.77 ± 0.24	1.03 ± 0.28
135	0	42	3.3	40	33	8	10	1	12.3	< 1.15	< 0.39	0.67 ± 0.22	< 0.66	< 0.32
136	0	42	6.3	41	2	47	8	1	37.4	2.17 ± 0.37	< 1.76	1.39 ± 0.25	< 0.69	0.93 ± 0.20
137	0	42	7.1	41	0	19	8	1	66.3	2.37 ± 0.37	< 0.43	2.16 ± 0.31	< 0.46	2.01 ± 0.28
138	0	42	7.8	41	4	39	8	1	63.1	3.20 ± 0.43	< 2.79	2.13 ± 0.31	0.88 ± 0.20	1.19 ± 0.23
139	0	42	9.0	41	18	19	5	1	970.6	35.01 ± 1.21	< 0.32	27.80 ± 1.01	5.76 ± 0.48	21.32 ± 0.88
140	0	42	9.3	41	20	58	10	1	13.5	1.33 ± 0.36	< 0.50	0.99 ± 0.26	< 0.48	< 0.84
141	0	42	9.6	40	16	47	9	1	36.0	4.96 ± 1.07	< 1.17	3.77 ± 0.83	1.66 ± 0.55	2.06 ± 0.60

⋆ Bulge sources

SII No. (1)	R.A. (h) (2)	(J2000) (m) (3)	(s) (4)	Dec. (°) (5)	(′) (6)	(″) (7)	σ_{Pos} (″) (8)	Cl. (9)	Maxlik (LH) (10)	Rate (B) ($ct \cdot ks^{-1}$) (11)	Rate (S) ($ct \cdot ks^{-1}$) (12)	Rate (H) ($ct \cdot ks^{-1}$) (13)	Rate (H_1) ($ct \cdot ks^{-1}$) (14)	Rate (H_2) ($ct \cdot ks^{-1}$) (15)
142	0	42	10.9	41	10	46	9	1	80.0	6.83 ± 0.65	< 1.58	3.65 ± 0.42	1.32 ± 0.27	2.33 ± 0.33
143	0	42	12.0	41	15	17	5	1	34.7	< 3.37	< 0.41	4.53 ± 0.50	< 1.60	2.82 ± 0.38
144	0	42	12.4	41	18	31	5	1	1492.6	36.25 ± 1.21	< 0.38	33.07 ± 1.10	8.65 ± 0.60	29.48 ± 1.04
145	0	42	13.5	40	39	25	6	1	329.3	8.12 ± 0.71	< 1.30	6.62 ± 0.59	2.20 ± 0.34	4.45 ± 0.48
146	0	42	15.2	40	19	45	6	1	3894.8	150.77 ± 4.58	14.56 ± 1.57	125.26 ± 4.09	43.66 ± 2.43	80.55 ± 3.27
147	0	42	15.6	41	1	16	6	1	2651.4	29.59 ± 1.02	< 0.83	27.56 ± 0.95	3.63 ± 0.36	23.98 ± 0.88
148	0	42	15.6	41	20	31	8	1	47.9	2.06 ± 0.37	< 0.27	1.79 ± 0.30	0.56 ± 0.17	1.18 ± 0.24
149	0	42	16.0	41	31	19	11	1	11.1	< 0.96	< 0.26	0.81 ± 0.24	< 0.52	< 0.59
150	0	42	16.2	40	55	54	6	1	362.7	6.59 ± 0.52	< 0.44	5.83 ± 0.45	1.53 ± 0.24	4.38 ± 0.39
151	0	42	16.3	40	48	18	11	1	13.9	< 1.22	< 0.43	0.84 ± 0.22	0.57 ± 0.17	< 0.27
152	0	42	16.6	41	29	1	12	1	13.8	< 0.83	< 0.65	< 1.45	< 0.21	1.17 ± 0.27
153	0	42	17.7	41	12	29	5	1	2282.0	33.74 ± 0.95	3.22 ± 0.51	35.36 ± 1.11	13.32 ± 0.68	21.68 ± 0.87
154	0	42	19.3	41	14	0	5	1	812.8	66.18 ± 0.96	2.59 ± 0.50	22.41 ± 0.80	9.39 ± 0.60	18.04 ± 0.82
155	0	42	20.2	41	47	46	12	1	10.1	< 1.12	< 0.39	0.79 ± 0.30	< 0.47	< 0.72
156	0	42	20.3	41	26	41	9	1	27.9	1.69 ± 0.37	< 0.40	1.37 ± 0.28	< 0.63	0.91 ± 0.23
157	0	42	22.2	40	59	25	6	1	589.7	9.73 ± 0.62	< 0.57	8.72 ± 0.55	2.89 ± 0.32	5.86 ± 0.45
158	0	42	22.6	40	44	18	9	1	35.1	1.26 ± 0.32	< 0.48	0.96 ± 0.23	< 0.19	0.90 ± 0.21
⋆159	0	42	22.8	41	15	43	5	1	2830.2	71.08 ± 0.81	1.68 ± 0.38	44.28 ± 1.06	16.12 ± 0.74	33.13 ± 1.05
⋆160	0	42	22.9	40	19	42	7	1	815.9	94.42 ± 4.08	6.63 ± 1.45	48.60 ± 2.78	16.05 ± 1.63	30.90 ± 2.20
161	0	42	22.9	41	13	34	5	1	651.3	93.27 ± 1.12	3.55 ± 0.53	75.40 ± 1.45	59.85 ± 1.46	52.47 ± 1.39
162	0	42	23.1	41	7	33	9	1	21.1	1.65 ± 0.35	< 0.71	0.92 ± 0.23	< 1.29	0.59 ± 0.17
163	0	42	24.3	40	57	17	9	1	20.2	< 1.22	< 0.23	0.84 ± 0.20	< 0.40	0.58 ± 0.16
164	0	42	24.8	39	47	38	26	4	10.2	< 0.78	< 0.32	< 3.91	< 0.85	2.58 ± 0.67
165	0	42	25.0	40	28	30	14	1	12.3	< 2.00	< 0.35	< 2.31	< 0.33	< 2.18
166	0	42	26.4	41	25	54	7	1	128.8	4.21 ± 0.50	< 0.25	3.95 ± 0.43	0.85 ± 0.21	3.02 ± 0.37
167	0	42	26.9	41	45	30	10	1	15.3	< 1.04	< 0.22	1.06 ± 0.31	< 0.56	0.66 ± 0.23
⋆168	0	42	27.6	41	19	21	5	1	131.9	9.20 ± 0.62	< 0.40	8.01 ± 0.59	2.25 ± 0.34	5.37 ± 0.48
169	0	42	28.4	41	12	22	5	1	1533.1	44.15 ± 0.76	4.08 ± 0.54	26.47 ± 0.92	9.74 ± 0.59	16.72 ± 0.76
170	0	42	29.1	41	4	35	6	1	1118.4	17.85 ± 0.83	< 1.17	15.22 ± 0.74	5.04 ± 0.43	10.24 ± 0.60
171	0	42	29.2	41	8	26	8	1	43.0	2.41 ± 0.39	< 2.06	1.59 ± 0.28	0.64 ± 0.18	0.98 ± 0.21
172	0	42	29.6	41	29	3	8	1	51.7	1.52 ± 0.35	< 0.39	1.63 ± 0.28	0.54 ± 0.17	1.15 ± 0.23
⋆173	0	42	29.7	41	14	30	5	1	317.8	154.67 ± 1.01	7.28 ± 0.68	97.14 ± 1.08	35.21 ± 1.10	42.28 ± 1.04
⋆174	0	42	31.4	41	16	17	5	1	897.3	51.43 ± 0.57	8.92 ± 0.71	104.70 ± 0.95	37.20 ± 1.02	20.30 ± 0.67
⋆175	0	42	32.1	41	19	35	5	1	263.9	8.48 ± 0.56	< 0.51	10.64 ± 0.66	3.54 ± 0.39	7.42 ± 0.56
176	0	42	32.2	41	55	45	9	1	38.1	3.64 ± 0.77	< 1.11	2.61 ± 0.56	1.61 ± 0.44	0.88 ± 0.34
⋆177	0	42	32.3	41	13	16	5	1	611.1	121.82 ± 0.99	7.95 ± 0.67	53.14 ± 1.22	23.41 ± 0.94	35.42 ± 1.14
178	0	42	33.5	41	21	49	10	1	18.0	1.30 ± 0.34	< 0.24	1.16 ± 0.26	0.85 ± 0.21	< 0.41
179	0	42	34.4	41	32	53	6	1	287.1	6.30 ± 0.58	< 0.45	5.68 ± 0.51	0.91 ± 0.21	4.93 ± 0.47
180	0	42	34.5	40	48	40	7	1	171.8	3.91 ± 0.46	< 0.33	3.54 ± 0.39	1.34 ± 0.24	2.28 ± 0.31
181	0	42	35.0	40	40	35	11	1	12.9	< 1.26	< 0.44	0.82 ± 0.25	< 0.41	0.60 ± 0.21
⋆182	0	42	36.7	41	14	1	5	1	611.8	171.71 ± 0.99	10.17 ± 0.76	93.39 ± 1.05	29.82 ± 0.93	33.16 ± 0.92
183	0	42	38.8	41	10	16	11	1	18.4	6.38 ± 0.66	< 2.67	2.07 ± 0.40	1.59 ± 0.32	< 0.61
⋆184	0	42	39.1	41	16	3	5	1	4245.6	361.41 ± 1.29	26.98 ± 1.03	242.68 ± 1.24	74.53 ± 1.25	138.36 ± 1.21
185	0	42	39.4	41	59	52	13	1	19.2	3.04 ± 0.84	< 1.04	3.74 ± 0.81	1.38 ± 0.48	< 1.14
186	0	42	39.5	40	43	20	8	1	75.2	3.96 ± 0.53	1.36 ± 0.36	2.43 ± 0.37	1.44 ± 0.28	0.97 ± 0.24
⋆187	0	42	40.4	41	13	29	5	1	701.9	112.89 ± 0.87	7.23 ± 0.65	61.78 ± 0.87	26.80 ± 1.00	32.18 ± 1.09
188	0	42	41.8	40	51	53	5	1	5446.2	58.12 ± 1.50	4.21 ± 0.47	51.83 ± 1.38	18.10 ± 0.81	33.92 ± 1.12
189	0	42	41.8	42	3	16	13	1	13.1	< 3.45	< 1.00	2.01 ± 0.66	< 1.23	< 1.79
⋆190	0	42	41.9	41	18	26	5	1	215.8	81.41 ± 0.78	4.20 ± 0.57	47.10 ± 0.80	19.54 ± 0.86	22.07 ± 0.93
191	0	42	42.7	41	28	21	12	1	17.6	< 0.56	< 0.31	< 1.29	< 0.19	1.23 ± 0.26
192	0	42	43.5	40	8	34	24	4	10.4	< 0.84	< 0.12	< 1.82	< 1.18	1.33 ± 0.33
193	0	42	44.1	41	21	28	11	1	31.1	5.61 ± 0.64	< 0.59	3.46 ± 0.46	< 2.41	1.55 ± 0.30
⋆194	0	42	44.6	41	11	43	6	1	1077.8	17.36 ± 0.69	3.62 ± 0.53	18.33 ± 0.80	8.14 ± 0.54	9.74 ± 0.58
⋆195	0	42	45.5	41	16	28	5	1	2468.3	332.40 ± 1.24	39.91 ± 1.24	278.71 ± 1.33	55.02 ± 1.07	141.34 ± 1.23
196	0	42	47.2	40	58	32	10	1	12.2	< 1.38	< 0.65	0.60 ± 0.18	< 0.47	< 0.40
⋆197	0	42	47.3	41	15	24	5	1	1843.7	423.34 ± 1.43	48.24 ± 1.36	198.84 ± 1.13	68.29 ± 1.21	94.76 ± 1.02
198	0	42	48.6	41	25	26	6	1	776.3	21.27 ± 0.98	< 0.60	15.13 ± 0.76	3.68 ± 0.40	11.12 ± 0.64
199	0	42	51.6	41	31	9	5	1	6523.9	66.34 ± 1.60	< 0.76	63.28 ± 1.52	14.96 ± 0.74	48.51 ± 1.34
⋆200	0	42	52.2	41	18	57	5	1	1868.8	71.46 ± 0.82	3.50 ± 0.53	59.15 ± 1.37	26.19 ± 1.00	22.63 ± 0.88
201	0	42	52.7	40	53	27	10	1	11.6	< 0.92	< 0.29	0.58 ± 0.18	< 0.35	< 0.51
202	0	42	53.2	40	13	20	11	4	135.7	< 1.81	< 0.09	7.40 ± 0.58	4.00 ± 0.42	5.53 ± 0.47
⋆203	0	42	53.3	41	15	49	5	1	1250.4	253.68 ± 1.13	30.40 ± 1.09	136.85 ± 1.07	45.88 ± 1.01	45.55 ± 1.03
204	0	42	53.6	40	48	18	10	1	10.4	< 0.95	< 0.35	< 0.73	< 0.39	0.36 ± 0.14
205	0	42	53.7	41	49	32	5	1	13.2	< 2.38	< 0.92	1.59 ± 0.40	< 1.31	< 0.65
206	0	42	54.4	41	25	55	6	1	606.8	11.39 ± 0.72	< 0.36	12.22 ± 0.69	3.96 ± 0.40	8.20 ± 0.56
⋆207	0	42	54.5	41	13	36	5	1	98.0	65.09 ± 0.82	4.70 ± 0.57	8.44 ± 0.53	6.73 ± 0.52	1.46 ± 0.27
⋆208	0	42	56.1	41	17	1	5	1	298.8	31.59 ± 0.48	15.27 ± 0.86	92.18 ± 1.06	35.71 ± 1.03	40.83 ± 1.09
209	0	42	57.4	41	11	5	6	1	857.1	16.97 ± 0.81	1.10 ± 0.31	13.15 ± 0.67	4.96 ± 0.42	8.10 ± 0.53
210	0	42	57.8	41	46	6	7	1	212.7	7.64 ± 0.72	2.11 ± 0.47	5.17 ± 0.55	3.04 ± 0.42	2.16 ± 0.36
⋆211	0	42	58.8	41	19	11	5	1	618.2	79.32 ± 1.06	4.33 ± 0.59	20.47 ± 0.86	17.73 ± 0.87	10.68 ± 0.64
212	0	43	1.0	41	30	17	7	1	249.9	6.87 ± 0.58	< 0.44	6.06 ± 0.50	1.50 ± 0.26	4.33 ± 0.42
⋆213	0	43	1.5	41	13	55	5	1	138.3	57.23 ± 0.95	< 2.66	9.58 ± 0.58	4.96 ± 0.45	4.49 ± 0.44
⋆214	0	43	1.6	41	15	32	5	1	1555.2	133.44 ± 1.01	8.41 ± 0.69	35.88 ± 0.89	32.31 ± 1.08	27.70 ± 0.96
215	0	43	1.9	40	44	58	9	1	57.5	2.99 ± 0.54	< 0.48	2.83 ± 0.43	0.94 ± 0.25	1.74 ± 0.33
216	0	43	2.9	41	21	20	7	1	232.3	9.74 ± 0.61	< 1.16	6.94 ± 0.54	3.36 ± 0.37	3.26 ± 0.37
⋆217	0	43	3.0	41	18	4	5	1	843.9	77.56 ± 0.90	7.31 ± 0.65	36.56 ± 1.08	14.76 ± 0.78	24.42 ± 0.99

$\star$ Bulge sources

SII	R.A.		(J2000)		Dec.		$\sigma_{\rm Pos}$	Cl.	Maxlik	Rate (B)	Rate (S)	Rate (H)	Rate (H_1)	Rate (H_2)
No.	(h)	(m)	(s)	(°)	(′)	(″)	(″)		(LH)	($ct \cdot ks^{-1}$)	($ct \cdot ks^{-1}$)	($ct \cdot ks^{-1}$)	($ct \cdot ks^{-1}$)	($ct \cdot ks^{-1}$)
(1)	(2)	(3)	(4)	(5)	(6)	(7)	(8)	(9)	(10)	(11)	(12)	(13)	(14)	(15)
218	0	43	7.7	41	45	51	8	1	28.9	1.55 ± 0.38	< 0.57	1.12 ± 0.26	< 0.38	0.85 ± 0.22
219	0	43	7.8	41	12	58	5	1	60.8	5.63 ± 0.56	< 0.52	2.17 ± 0.31	1.70 ± 0.28	0.81 ± 0.20
220	0	43	8.8	41	52	8	9	1	22.5	1.40 ± 0.42	< 0.43	1.10 ± 0.29	< 0.62	0.92 ± 0.28
221	0	43	9.3	40	59	28	8	1	27.5	1.50 ± 0.33	< 1.04	0.90 ± 0.21	< 0.32	0.68 ± 0.17
222	0	43	9.5	41	19	0	5	1	1217.7	28.17 ± 0.91	2.91 ± 0.54	24.21 ± 0.94	12.81 ± 0.74	15.33 ± 0.75
223	0	43	10.4	41	14	49	5	1	2311.9	31.25 ± 0.89	2.87 ± 0.44	32.60 ± 1.05	12.33 ± 0.65	19.83 ± 0.82
224	0	43	10.7	41	55	41	10	1	18.4	< 1.68	< 0.47	1.03 ± 0.30	< 0.33	0.82 ± 0.26
225	0	43	11.8	40	48	35	7	1	169.0	5.53 ± 0.62	< 1.03	4.31 ± 0.50	1.70 ± 0.31	2.62 ± 0.39
226	0	43	13.4	41	17	15	5	1	73.1	11.08 ± 0.69	3.55 ± 0.53	6.00 ± 0.55	3.04 ± 0.39	2.60 ± 0.37
227	0	43	13.9	41	7	21	6	1	634.7	11.88 ± 0.70	< 1.01	10.31 ± 0.62	2.91 ± 0.34	7.44 ± 0.53
228	0	43	15.4	40	54	6	11	1	10.8	< 1.02	< 0.42	0.53 ± 0.18	< 0.34	< 0.44
229	0	43	15.5	41	3	43	10	1	17.0	1.24 ± 0.32	< 0.73	0.74 ± 0.20	< 0.40	0.49 ± 0.16
230	0	43	15.6	41	23	41	9	1	75.6	6.34 ± 0.63	4.29 ± 0.49	< 2.94	< 1.97	< 0.64
231	0	43	17.2	41	12	28	12	1	12.7	1.53 ± 0.38	< 0.34	< 1.43	0.87 ± 0.22	< 0.28
232	0	43	17.2	41	27	44	6	1	1165.6	17.30 ± 0.81	< 0.88	15.37 ± 0.73	5.61 ± 0.44	9.78 ± 0.59
233	0	43	18.0	41	59	8	7	1	185.4	7.12 ± 0.84	< 0.45	6.65 ± 0.74	2.12 ± 0.43	4.53 ± 0.61
234	0	43	19.4	40	48	38	10	1	21.6	< 1.85	< 0.52	1.39 ± 0.33	< 0.53	0.90 ± 0.25
235	0	43	20.2	41	20	25	10	1	42.6	10.07 ± 0.91	< 1.26	4.29 ± 0.54	1.79 ± 0.30	< 0.35
236	0	43	21.0	41	17	49	5	1	114.2	16.60 ± 0.94	2.17 ± 0.42	12.21 ± 0.81	2.95 ± 0.37	3.50 ± 0.44
237	0	43	23.0	41	31	47	8	1	35.7	1.68 ± 0.33	< 0.52	1.22 ± 0.24	< 0.43	0.98 ± 0.21
238	0	43	23.8	41	14	19	10	1	10.5	< 1.26	< 0.26	0.72 ± 0.21	< 0.75	< 0.42
239	0	43	25.9	41	53	12	14	1	10.3	< 1.47	< 0.51	< 1.45	< 0.26	1.07 ± 0.30
240	0	43	26.6	41	26	14	7	1	218.4	5.87 ± 0.52	< 0.39	4.78 ± 0.43	1.26 ± 0.23	3.53 ± 0.37
241	0	43	26.7	41	18	27	7	1	271.8	11.96 ± 0.76	< 1.71	7.20 ± 0.54	5.13 ± 0.44	1.90 ± 0.30
242	0	43	28.4	41	7	48	6	1	281.2	5.97 ± 0.52	< 0.32	5.60 ± 0.47	1.25 ± 0.24	4.42 ± 0.41
243	0	43	28.4	42	22	12	14	4	24.5	< 0.21	< 0.15	2.46 ± 0.44	< 1.29	1.88 ± 0.36
244	0	43	31.7	41	10	37	7	1	78.0	2.44 ± 0.36	< 0.43	1.88 ± 0.28	< 0.31	1.71 ± 0.26
245	0	43	32.3	42	4	58	12	1	10.0	< 1.91	< 0.77	< 1.59	< 0.37	0.91 ± 0.35
246	0	43	32.9	41	16	14	12	1	39.9	10.76 ± 1.01	3.58 ± 0.50	< 2.20	< 0.71	< 0.43
247	0	43	33.9	41	13	25	6	1	1258.7	21.31 ± 0.90	< 1.69	17.98 ± 0.79	6.52 ± 0.48	11.20 ± 0.62
248	0	43	34.4	40	56	30	7	1	219.6	6.06 ± 0.59	< 0.91	4.62 ± 0.47	2.40 ± 0.34	2.21 ± 0.32
249	0	43	36.7	41	14	42	6	1	1048.8	19.14 ± 0.87	4.72 ± 0.71	15.26 ± 0.74	4.94 ± 0.42	10.03 ± 0.60
250	0	43	38.7	41	26	52	8	1	78.0	3.53 ± 0.44	< 0.61	2.57 ± 0.33	1.68 ± 0.26	0.80 ± 0.20
251	0	43	38.7	42	1	26	10	1	21.8	1.81 ± 0.53	< 0.58	1.63 ± 0.40	< 0.69	1.21 ± 0.33
252	0	43	40.3	40	54	36	9	1	55.3	4.08 ± 0.59	< 2.45	2.38 ± 0.38	< 1.20	1.42 ± 0.28
253	0	43	41.6	41	53	13	11	1	15.5	< 1.41	< 0.42	1.09 ± 0.29	0.72 ± 0.22	< 0.42
254	0	43	43.0	41	28	52	8	1	48.0	2.54 ± 0.39	< 0.58	1.92 ± 0.30	< 0.72	1.40 ± 0.25
255	0	43	43.1	41	12	27	8	1	33.4	1.82 ± 0.35	< 0.27	1.40 ± 0.26	0.69 ± 0.18	0.68 ± 0.19
256	0	43	44.1	41	24	8	9	1	60.0	3.72 ± 0.50	< 0.36	2.55 ± 0.35	1.43 ± 0.30	1.35 ± 0.25
257	0	43	44.9	41	37	0	8	1	49.7	2.16 ± 0.36	< 0.46	1.52 ± 0.26	0.50 ± 0.16	1.00 ± 0.21
258	0	43	48.6	41	27	46	48	1	10.0	< 1.98	< 0.47	< 0.97	< 0.27	0.51 ± 0.17
259	0	43	49.7	40	49	49	12	1	15.8	< 1.74	< 0.43	1.37 ± 0.37	< 0.70	< 1.03
260	0	43	52.5	40	16	29	20	4	10.4	< 0.13	< 0.13	< 1.95	< 0.59	< 1.37
261	0	43	53.1	41	11	53	11	1	10.3	< 1.20	< 0.56	< 0.72	0.56 ± 0.18	< 0.13
262	0	43	53.2	41	16	54	6	1	1565.6	23.50 ± 0.96	1.32 ± 0.32	20.69 ± 0.88	7.17 ± 0.51	13.57 ± 0.71
263	0	43	53.7	41	6	13	9	1	25.6	1.36 ± 0.34	< 0.43	1.15 ± 0.26	0.55 ± 0.17	0.57 ± 0.18
264	0	43	54.6	40	45	38	9	1	53.9	3.17 ± 0.70	< 0.61	3.36 ± 0.62	0.91 ± 0.34	2.40 ± 0.52
265	0	43	54.8	41	52	53	9	1	24.3	1.40 ± 0.37	< 0.54	1.03 ± 0.25	0.63 ± 0.19	< 0.55
266	0	43	55.6	41	22	2	8	1	32.6	2.07 ± 0.36	< 0.74	1.19 ± 0.25	< 0.40	0.90 ± 0.21
267	0	43	57.4	41	27	25	9	1	22.2	1.42 ± 0.31	< 0.71	0.95 ± 0.22	< 0.41	0.64 ± 0.17
268	0	43	57.6	41	30	53	8	1	31.5	1.41 ± 0.30	< 0.42	1.03 ± 0.21	< 0.42	0.73 ± 0.17
269	0	43	57.8	41	13	45	11	1	10.4	< 0.79	< 0.21	< 0.72	0.46 ± 0.15	< 0.22
270	0	43	58.8	41	57	17	8	1	28.3	< 1.35	< 0.28	0.97 ± 0.26	< 0.20	0.88 ± 0.23
271	0	44	0.9	40	56	13	10	1	52.8	2.73 ± 0.55	< 0.82	2.81 ± 0.46	0.77 ± 0.24	1.82 ± 0.34
272	0	44	4.3	41	49	5	12	1	10.2	< 1.33	< 0.43	0.82 ± 0.24	< 0.68	< 0.46
273	0	44	4.5	41	21	18	9	1	16.7	< 1.15	< 0.46	< 0.71	< 0.11	0.61 ± 0.17
274	0	44	5.8	41	52	1	10	1	17.2	< 1.41	< 1.10	0.67 ± 0.21	< 0.14	0.67 ± 0.19
275	0	44	7.8	41	56	7	9	1	20.6	< 1.41	< 0.52	0.92 ± 0.25	< 0.47	0.73 ± 0.21
276	0	44	10.2	42	5	5	10	1	15.4	1.74 ± 0.48	< 0.81	1.10 ± 0.32	< 0.57	0.76 ± 0.26
277	0	44	12.3	41	31	39	11	1	12.3	< 0.67	< 0.13	0.62 ± 0.18	< 0.20	0.53 ± 0.16
278	0	44	13.7	42	8	44	11	1	10.1	< 1.46	< 0.66	< 1.08	< 0.82	< 0.91
279	0	44	13.8	41	57	51	9	1	14.3	< 0.99	< 0.56	< 0.60	< 0.10	0.54 ± 0.18
280	0	44	13.8	42	14	4	11	1	17.4	< 3.01	< 1.14	1.48 ± 0.47	< 0.53	1.35 ± 0.41
281	0	44	14.9	42	6	34	12	1	12.0	< 1.88	< 0.62	1.25 ± 0.36	< 0.51	1.00 ± 0.31
282	0	44	15.3	40	26	50	20	4	23.5	< 0.48	< 0.10	2.30 ± 0.41	1.28 ± 0.30	1.18 ± 0.31
283	0	44	15.9	41	26	22	10	1	14.3	1.22 ± 0.30	< 0.75	0.60 ± 0.18	< 0.37	< 0.48
284	0	44	16.4	41	11	14	10	1	12.1	< 0.90	< 0.36	< 0.68	< 0.09	0.46 ± 0.16
285	0	44	20.2	41	34	12	10	1	10.2	0.98 ± 0.28	< 0.74	< 0.63	< 0.22	< 0.44
286	0	44	22.3	41	45	7	8	1	86.4	3.07 ± 0.42	< 0.60	2.40 ± 0.32	0.73 ± 0.18	1.65 ± 0.26
287	0	44	23.7	42	0	15	9	1	12.5	< 1.35	< 0.69	0.67 ± 0.21	< 0.41	< 0.55
288	0	44	25.0	41	31	55	9	1	31.7	1.54 ± 0.32	< 0.40	1.24 ± 0.24	< 0.62	0.74 ± 0.18
289	0	44	25.6	41	36	30	8	1	42.1	1.86 ± 0.34	< 0.48	1.33 ± 0.24	0.64 ± 0.17	0.70 ± 0.17
290	0	44	29.2	41	21	34	6	1	1795.5	25.10 ± 1.02	1.10 ± 0.31	22.54 ± 0.94	6.86 ± 0.52	15.71 ± 0.78
291	0	44	29.5	41	15	31	14	1	11.2	< 1.92	< 0.41	1.08 ± 0.29	< 0.98	< 0.43
292	0	44	31.8	42	7	31	10	1	10.2	< 1.47	< 0.81	< 0.78	< 0.23	0.49 ± 0.18
293	0	44	35.7	42	10	47	12	1	10.1	< 1.52	< 0.62	< 1.18	< 0.46	< 0.86

$\star$ Bulge sources

SII	R.A.		(J2000)		Dec.		$\sigma_{\rm Pos}$	Cl.	Maxlik	Rate (B)	Rate (S)	Rate (H)	Rate (H_1)	Rate (H_2)
No.	(h)	(m)	(s)	(°)	(′)	(″)	(″)		(LH)	$(ct \cdot ks^{-1})$	$(ct \cdot ks^{-1})$	$(ct \cdot ks^{-1})$	$(ct \cdot ks^{-1})$	$(ct \cdot ks^{-1})$
(1)	(2)	(3)	(4)	(5)	(6)	(7)	(8)	(9)	(10)	(11)	(12)	(13)	(14)	(15)
294	0	44	36.7	41	45	8	10	1	13.6	< 0.79	< 0.36	< 0.82	< 0.15	0.51 ± 0.15
295	0	44	42.0	41	13	42	10	1	11.2	< 1.05	< 0.60	< 0.64	< 0.14	0.51 ± 0.18
296	0	44	45.5	42	43	2	15	4	38.9	< 2.03	< 0.38	6.19 ± 0.91	< 3.03	3.96 ± 0.67
297	0	44	47.5	41	22	52	8	1	36.7	1.51 ± 0.33	< 0.35	1.24 ± 0.25	0.48 ± 0.16	0.74 ± 0.19
298	0	44	48.2	42	29	54	12	1	11.2	< 5.17	< 1.95	< 4.17	2.83 ± 1.01	< 0.67
299	0	44	50.2	41	28	59	9	1	33.4	1.53 ± 0.32	< 0.33	1.23 ± 0.24	0.47 ± 0.15	0.70 ± 0.18
300	0	44	52.0	41	17	11	10	1	13.5	< 1.01	< 0.30	0.60 ± 0.19	< 0.29	0.41 ± 0.15
301	0	44	52.0	41	27	17	7	1	116.2	2.94 ± 0.38	< 0.36	2.24 ± 0.30	0.41 ± 0.14	1.79 ± 0.26
302	0	44	52.0	42	25	10	9	1	24.3	4.85 ± 1.11	< 1.41	3.04 ± 0.77	< 1.72	1.91 ± 0.60
303	0	44	55.1	41	34	38	10	1	16.5	< 1.12	< 0.42	0.54 ± 0.17	< 0.14	0.55 ± 0.16
304	0	44	55.9	41	59	34	7	1	102.4	4.71 ± 0.51	2.15 ± 0.42	2.46 ± 0.33	1.28 ± 0.24	1.16 ± 0.22
305	0	44	56.5	40	59	11	8	1	58.1	3.12 ± 0.65	< 0.56	2.78 ± 0.53	1.11 ± 0.34	1.64 ± 0.41
306	0	44	57.4	41	23	38	7	1	62.2	1.80 ± 0.34	< 0.22	1.66 ± 0.28	0.48 ± 0.16	1.18 ± 0.23
307	0	45	0.4	41	14	38	10	1	11.9	< 1.50	< 0.58	0.63 ± 0.21	< 0.25	0.46 ± 0.17
308	0	45	0.8	41	26	48	10	1	11.2	< 0.87	< 0.25	0.52 ± 0.17	< 0.37	< 0.38
309	0	45	8.5	42	15	42	7	1	176.6	6.62 ± 0.74	< 0.79	5.57 ± 0.61	2.39 ± 0.42	3.19 ± 0.46
310	0	45	9.2	42	2	31	9	1	22.5	1.23 ± 0.31	< 0.49	0.84 ± 0.20	0.58 ± 0.17	< 0.43
311	0	45	10.1	41	0	15	12	1	12.9	2.17 ± 0.62	< 1.76	1.05 ± 0.37	< 0.53	0.67 ± 0.28
312	0	45	10.4	41	45	53	8	1	29.1	1.59 ± 0.34	< 1.17	1.14 ± 0.24	< 0.79	0.78 ± 0.18
313	0	45	12.3	42	20	26	9	1	16.8	< 1.83	< 0.44	1.18 ± 0.36	< 0.73	0.64 ± 0.25
314	0	45	13.2	41	36	11	8	1	33.7	1.49 ± 0.31	< 0.71	1.03 ± 0.21	0.66 ± 0.17	0.35 ± 0.13
315	0	45	17.1	42	17	10	10	1	11.0	< 1.86	< 0.98	< 0.91	< 0.21	0.47 ± 0.19
316	0	45	26.5	41	32	45	8	1	50.7	1.81 ± 0.35	< 0.22	1.77 ± 0.29	0.45 ± 0.15	1.41 ± 0.25
317	0	45	27.4	41	39	0	10	1	18.6	1.57 ± 0.35	< 1.15	0.82 ± 0.21	< 0.32	0.66 ± 0.18
318	0	45	27.4	42	10	56	9	1	27.5	< 1.69	< 0.26	1.18 ± 0.27	< 0.58	0.88 ± 0.22
319	0	45	27.8	41	29	38	7	1	126.7	3.68 ± 0.46	< 0.49	2.93 ± 0.37	0.87 ± 0.21	2.05 ± 0.31
320	0	45	28.0	41	20	37	8	1	39.3	1.57 ± 0.36	< 0.33	1.32 ± 0.28	< 0.39	1.03 ± 0.24
321	0	45	28.3	41	46	4	10	1	11.2	< 1.21	< 1.47	< 0.48	< 0.11	0.36 ± 0.13
322	0	45	28.7	41	54	6	6	1	2703.3	29.63 ± 0.98	2.87 ± 0.37	23.80 ± 0.85	18.78 ± 0.75	4.91 ± 0.39
323	0	45	30.4	42	1	45	11	1	10.0	< 0.76	< 0.38	< 0.50	< 0.12	0.37 ± 0.13
324	0	45	31.8	42	7	6	8	1	147.7	7.75 ± 0.69	7.41 ± 0.66	< 0.45	< 0.32	< 0.18
325	0	45	32.6	42	27	48	11	1	13.3	< 3.12	< 3.44	1.30 ± 0.50	< 0.34	1.16 ± 0.45
326	0	45	34.1	42	41	44	19	4	11.2	< 0.62	< 0.28	2.35 ± 0.63	< 0.98	1.69 ± 0.47
327	0	45	34.5	42	17	55	9	1	22.9	< 1.36	< 0.37	0.90 ± 0.28	< 0.20	0.90 ± 0.26
328	0	45	38.1	42	31	53	12	1	10.5	4.59 ± 1.40	< 3.50	< 3.01	< 2.07	< 1.30
329	0	45	38.2	41	19	30	10	1	21.6	< 1.57	< 0.38	1.12 ± 0.29	< 0.59	0.69 ± 0.22
330	0	45	38.3	42	12	39	10	1	11.8	1.43 ± 0.40	< 0.98	0.64 ± 0.21	< 0.25	0.50 ± 0.18
331	0	45	40.2	42	8	5	6	1	1122.7	25.83 ± 1.11	11.23 ± 0.79	13.77 ± 0.77	6.70 ± 0.54	7.01 ± 0.55
332	0	45	41.1	41	27	49	8	1	34.3	1.58 ± 0.36	< 1.21	1.13 ± 0.25	< 0.62	0.67 ± 0.19
333	0	45	42.1	41	23	52	9	1	19.5	< 1.13	< 0.24	0.86 ± 0.24	< 0.66	< 0.56
334	0	45	42.6	42	23	28	10	1	13.1	2.01 ± 0.60	< 1.43	0.93 ± 0.34	< 0.32	0.74 ± 0.28
335	0	45	42.9	41	20	25	8	1	51.6	2.18 ± 0.44	< 0.50	1.78 ± 0.34	0.92 ± 0.24	0.83 ± 0.23
336	0	45	45.4	41	39	37	5	1	17930.	134.43 ± 1.96	4.71 ± 0.47	133.47 ± 2.10	38.77 ± 1.15	95.71 ± 1.82
337	0	45	55.8	41	48	35	10	1	13.9	< 0.93	< 0.30	0.55 ± 0.17	< 0.23	0.43 ± 0.14
338	0	45	55.9	41	56	33	10	1	22.5	1.55 ± 0.32	1.50 ± 0.30	< 0.21	< 0.25	< 0.08
339	0	45	56.0	42	12	32	9	1	20.2	1.39 ± 0.39	< 2.41	0.91 ± 0.25	< 0.28	0.72 ± 0.21
340	0	45	57.6	42	3	10	8	1	65.3	3.03 ± 0.42	< 1.50	1.89 ± 0.28	0.83 ± 0.19	1.06 ± 0.21
341	0	45	57.6	42	26	42	11	1	12.6	< 2.94	< 1.05	1.43 ± 0.49	< 0.97	0.98 ± 0.37
342	0	46	0.2	41	33	10	10	1	17.5	1.06 ± 0.31	< 0.37	0.79 ± 0.22	< 0.46	0.47 ± 0.16
343	0	46	5.9	41	51	37	11	1	10.2	< 1.34	< 0.64	< 0.69	< 0.14	0.43 ± 0.14
344	0	46	10.9	42	3	53	9	1	40.7	1.67 ± 0.35	< 0.37	1.28 ± 0.25	< 0.54	0.88 ± 0.19
345	0	46	11.6	41	58	58	10	1	15.2	< 1.21	< 0.42	0.53 ± 0.16	< 0.15	0.49 ± 0.14
346	0	46	12.0	42	8	27	7	1	80.3	2.73 ± 0.43	< 0.50	2.29 ± 0.34	0.56 ± 0.18	1.73 ± 0.29
347	0	46	13.3	41	50	37	10	1	11.6	< 0.99	< 0.46	< 0.60	< 0.54	0.38 ± 0.13
348	0	46	14.8	42	21	34	12	1	11.2	< 1.24	< 0.54	< 1.55	< 0.13	0.82 ± 0.29
349	0	46	15.7	41	24	9	13	1	11.6	< 1.29	< 0.46	1.00 ± 0.32	< 0.73	< 0.55
350	0	46	19.9	42	14	36	9	1	13.2	< 0.89	< 0.24	0.70 ± 0.22	< 0.47	< 0.53
351	0	46	24.2	42	4	38	6	1	1690.2	33.17 ± 1.16	< 0.71	29.36 ± 1.02	6.85 ± 0.50	22.29 ± 0.88
352	0	46	24.3	42	9	53	9	1	29.4	1.79 ± 0.42	< 1.12	2.45 ± 0.46	< 0.48	1.16 ± 0.27
353	0	46	25.6	41	16	30	13	1	16.0	2.42 ± 0.73	< 1.76	1.83 ± 0.54	< 1.30	< 1.23
354	0	46	26.7	42	1	51	6	1	3781.8	37.64 ± 1.15	< 1.28	34.53 ± 1.06	10.53 ± 0.59	24.08 ± 0.88
355	0	46	31.5	42	44	2	16	4	10.2	< 1.40	< 0.42	1.99 ± 0.57	< 0.74	< 1.99
356	0	46	34.1	42	7	29	10	1	15.3	< 1.44	< 0.47	0.70 ± 0.20	< 1.24	0.52 ± 0.17
357	0	46	36.6	41	29	0	11	1	12.7	< 1.45	< 0.52	0.80 ± 0.27	< 0.57	< 0.60
358	0	46	38.0	41	46	17	11	1	11.5	< 0.92	< 0.42	< 0.61	< 0.12	0.40 ± 0.14
359	0	46	39.6	42	25	16	9	1	18.7	< 2.49	< 0.71	1.63 ± 0.49	< 0.76	1.10 ± 0.39
360	0	46	44.8	42	30	38	10	1	16.7	< 5.19	< 1.39	2.76 ± 0.84	< 2.21	< 1.66
361	0	46	46.9	41	49	8	10	1	12.6	< 1.14	< 0.47	0.59 ± 0.19	< 0.58	< 0.40
362	0	46	47.3	42	8	56	9	1	28.9	1.60 ± 0.38	< 0.57	1.16 ± 0.26	< 0.43	0.95 ± 0.23
363	0	46	55.1	42	20	47	6	1	730.9	23.18 ± 1.50	< 0.77	20.88 ± 1.33	7.71 ± 0.81	13.02 ± 1.05
364	0	46	56.8	41	52	33	9	1	33.3	0.98 ± 0.29	< 0.27	0.83 ± 0.21	< 0.12	0.87 ± 0.20
365	0	47	0.8	41	41	7	10	1	19.0	< 1.47	< 0.40	0.98 ± 0.27	0.65 ± 0.22	< 0.46
366	0	47	1.0	41	51	24	9	1	23.7	1.21 ± 0.33	< 0.48	0.88 ± 0.22	< 0.29	0.70 ± 0.19
367	0	47	3.4	41	58	8	11	1	10.7	1.21 ± 0.34	< 1.25	< 0.52	< 0.46	< 0.13
368	0	47	3.4	42	4	55	8	1	43.7	1.89 ± 0.37	< 0.53	1.39 ± 0.27	< 0.58	1.05 ± 0.23
369	0	47	13.8	42	2	13	8	1	68.9	3.67 ± 0.50	1.47 ± 0.37	1.93 ± 0.32	0.83 ± 0.22	1.10 ± 0.24

⋆ Bulge sources

SII No. (1)	R.A. (h) (2)	(m) (3)	(J2000) (s) (4)	($^\circ$) (5)	Dec. ($'$) (6)	($''$) (7)	$\sigma_{\rm Pos}$ ($''$) (8)	Cl. (9)	Maxlik (LH) (10)	Rate (B) ($ct \cdot ks^{-1}$) (11)	Rate (S) ($ct \cdot ks^{-1}$) (12)	Rate (H) ($ct \cdot ks^{-1}$) (13)	Rate (H_1) ($ct \cdot ks^{-1}$) (14)	Rate (H_2) ($ct \cdot ks^{-1}$) (15)
370	0	47	14.7	42	21	1	11	1	45.9	5.48 ± 1.11	< 0.54	6.54 ± 0.94	1.81 ± 0.51	4.09 ± 0.75
371	0	47	15.4	41	40	41	9	1	40.0	1.81 ± 0.45	< 0.36	1.94 ± 0.39	0.70 ± 0.25	1.18 ± 0.30
372	0	47	16.2	41	35	46	12	1	16.9	< 1.90	< 0.53	1.42 ± 0.38	< 0.78	0.77 ± 0.27
373	0	47	20.1	41	48	37	10	1	18.0	1.93 ± 0.46	< 3.26	0.85 ± 0.25	< 0.45	0.60 ± 0.21
374	0	47	25.1	42	21	45	10	1	66.2	7.65 ± 1.29	< 0.97	7.22 ± 1.07	2.49 ± 0.63	4.10 ± 0.83
375	0	47	26.9	41	52	53	9	1	52.7	3.35 ± 0.54	< 0.88	2.49 ± 0.40	1.00 ± 0.26	1.48 ± 0.30
376	0	47	27.8	41	24	40	13	1	12.8	< 5.97	< 1.65	3.64 ± 1.34	< 1.07	3.01 ± 1.23
377	0	47	30.6	41	49	24	8	1	81.3	4.39 ± 0.63	< 4.52	2.97 ± 0.46	0.95 ± 0.27	2.11 ± 0.38
378	0	47	30.9	41	40	42	11	1	10.3	< 2.17	< 1.21	< 0.84	< 0.52	< 0.38
379	0	47	31.4	41	35	24	12	1	12.0	< 1.73	< 0.45	1.17 ± 0.40	< 1.00	< 0.68
380	0	47	40.4	42	22	32	5	1	17.4	5.20 ± 1.48	< 1.49	5.80 ± 1.33	< 2.37	< 2.68
381	0	47	42.8	42	3	2	10	1	12.0	< 1.20	< 0.52	< 0.78	< 0.15	0.48 ± 0.18
382	0	47	43.2	42	1	19	9	1	24.6	1.48 ± 0.41	< 0.54	1.19 ± 0.30	0.60 ± 0.21	0.67 ± 0.23
383	0	47	43.8	42	24	16	5	1	17.5	< 5.17	< 1.31	4.65 ± 1.31	< 1.35	< 3.45
384	0	47	44.5	42	22	37	5	1	15.8	< 6.19	< 1.70	7.36 ± 1.60	< 3.10	< 2.63
385	0	47	45.0	42	11	3	11	1	10.9	< 2.25	< 1.47	1.22 ± 0.40	< 0.74	0.75 ± 0.29
386	0	47	47.9	42	19	33	8	1	145.6	12.77 ± 1.63	< 1.19	12.11 ± 1.45	2.96 ± 0.74	8.89 ± 1.25
387	0	47	49.4	41	53	26	10	1	16.9	< 1.13	< 0.31	0.89 ± 0.28	< 0.24	0.78 ± 0.25
388	0	47	49.9	41	42	9	11	1	41.4	7.02 ± 1.15	< 1.63	13.74 ± 1.37	4.06 ± 0.78	7.97 ± 1.05
389	0	47	51.7	42	7	24	9	1	19.9	2.46 ± 0.59	< 3.90	1.23 ± 0.36	0.80 ± 0.28	< 0.69
390	0	47	53.9	41	35	38	16	1	11.8	< 3.40	3.07 ± 0.94	< 0.45	< 0.27	< 0.36
391	0	48	0.3	41	40	15	7	1	442.6	27.75 ± 2.07	< 3.14	25.92 ± 1.97	10.22 ± 1.22	16.23 ± 1.58
392	0	48	4.2	41	56	48	10	1	13.1	2.11 ± 0.58	< 1.74	< 0.85	< 0.56	< 0.37
393	0	48	23.6	42	10	43	11	1	14.8	3.61 ± 1.02	< 3.18	1.91 ± 0.64	< 0.45	1.71 ± 0.58
394	0	48	24.6	41	57	18	6	1	614.1	35.30 ± 2.16	21.89 ± 1.77	14.28 ± 1.31	8.11 ± 0.99	6.24 ± 0.87
395	0	48	58.4	42	23	47	9	4	250.2	9.21 ± 0.99	< 0.52	15.95 ± 1.07	6.21 ± 0.69	9.84 ± 0.81
396	0	49	30.6	41	58	23	13	1	22.1	6.87 ± 2.29	< 1.91	6.12 ± 1.85	< 2.66	< 5.62

Table 6. Total list of all ROSAT PSPC X-ray sources in M31 merged from the source lists of both surveys. The different symbols in front of the RXJ numbers in column (1) are explained at the top of the table. The meaning of the different columns is described in Sect. 3.3. The listed count rate errors are purely statistical. The systematic errors are expected to be less than ∼ 15%. Count rates for bulge sources (marked with ⋆) may be uncertain due to confusion. For sources not detected in a considered energy band, 1σ upper limits have been calculated indicated by a '<'-symbol in front of the upper limit value. A conversion of count rates into fluxes depends on the assumed spectral shape. For M31-sources a power law with photon index $\Gamma = -2.0$ and $N_{\rm H} = 9 \times 10^{20}$ cm^{-2} may be used, leading to a conversion factor 1 ct ks^{-1} = 3.00×10^{-14} erg cm^{-2} s^{-1} in the 0.1 - 2.0 keV band (B-band). For foreground stars, the application of this conversion factor leads to an overestimation of the flux.

[a] Foreground star [b] Galaxy [c] Supersoft source candidate [d] Globular cluster [e] SNR
⋆ bulge source ∼ Variable source (ref. Tables 2, 3 and footnote in Sect. 4.1.1) † Source with uncertain count rate.

RXJ No. (1)	SI No. (2)	R.A. (h) (3)	(m) (4)	(J2000) (s) (5)	Dec. (°) (6)	(′) (7)	(″) (8)	$\sigma_{\rm Pos}$ (″) (9)	Cl. (10)	Maxlik (LH) (11)	Rate (B) ($ct \cdot ks^{-1}$) (12)	Rate (S) ($ct \cdot ks^{-1}$) (13)	Rate (H) ($ct \cdot ks^{-1}$) (14)	Rate (H_1) ($ct \cdot ks^{-1}$) (15)	Rate (H_2) ($ct \cdot ks^{-1}$) (16)
[d]RX J0036.3+4053		0	36	21.7	40	53	37	13	4	69.7	< 0.61	< 0.20	5.73 ± 0.65	< 1.70	4.22 ± 0.53
RX J0036.7+4109		0	36	43.0	41	9	2	19	4	27.1	< 0.43	< 0.16	3.18 ± 0.71	< 0.87	3.56 ± 0.61
RX J0036.8+4008		0	36	49.8	40	8	52	12	1	45.0	10.62 ± 1.82	< 3.50	7.46 ± 1.43	< 3.59	3.74 ± 1.04
RX J0036.8+4055		0	36	49.6	40	55	12	18	4	11.8	< 0.13	< 0.14	1.72 ± 0.42	< 0.99	< 1.20
RX J0036.9+4026		0	36	57.4	40	26	10	12	1	12.2	< 2.13	< 0.62	1.34 ± 0.43	< 0.81	< 1.30
RX J0037.1+4022		0	37	11.4	40	22	10	11	1	10.5	< 1.65	< 0.70	< 1.13	< 0.63	< 0.55
RX J0037.2+4045	1	0	37	17.4	40	45	23	6	2	26.7	2.14 ± 0.80	0.95 ± 0.80	< 0.87	< 0.12	< 0.80
RX J0037.3+4029	2-	0	37	18.7	40	29	47	8	1	82.4	3.43 ± 0.65	< 0.30	3.90 ± 0.60	2.02 ± 0.43	1.79 ± 0.41
[a]RX J0037.3+4043		0	37	22.5	40	43	49	9	1	86.3	10.19 ± 1.34	5.09 ± 0.98	4.93 ± 0.90	2.97 ± 0.69	1.82 ± 0.56
RX J0037.4+4013		0	37	26.2	40	13	7	10	1	20.6	2.16 ± 0.60	< 0.79	1.63 ± 0.43	< 0.54	1.22 ± 0.36
[c]RX J0037.4+4015	3	0	37	25.3	40	15	16	6	2	15.1	< 0.31	< 0.31	0.01 ± 0.00	< 0.01	< 0.01
RX J0037.5+4009	4-	0	37	34.6	40	9	55	7	1	238.8	11.48 ± 1.16	< 1.25	9.49 ± 0.97	3.63 ± 0.61	5.63 ± 0.75
†RX J0037.6+3938	5+	0	37	36.5	39	38	56	6	3	177.2	2.11 ± 1.04	< 0.01	2.26 ± 1.12	< 0.01	2.15 ± 1.07
RX J0037.6+4025		0	37	41.5	40	25	45	10	1	15.9	< 1.62	< 0.59	0.78 ± 0.25	< 0.36	0.51 ± 0.19
RX J0037.7+4004	7-	0	37	43.5	40	4	55	11	1	44.0	19.11 ± 2.03	< 2.32	14.48 ± 1.49	4.25 ± 0.89	8.80 ± 1.15
RX J0037.7+4023		0	37	43.3	40	23	44	8	1	52.3	2.97 ± 0.54	< 1.30	2.12 ± 0.39	1.64 ± 0.34	< 0.62
RX J0037.7+4037	6-	0	37	42.6	40	37	50	10	1	15.9	< 1.86	< 0.73	0.90 ± 0.28	< 0.45	0.58 ± 0.22
[a]RX J0038.0+4026	8+	0	38	1.1	40	26	28	5	1	847.8	19.87 ± 0.83	11.64 ± 0.63	7.61 ± 0.50	4.05 ± 0.45	3.90 ± 0.26
RX J0038.3+4018	9+	0	38	22.1	40	18	26	5	1	35.5	1.34 ± 0.29	0.37 ± 0.26	1.07 ± 0.16	0.16 ± 0.11	0.79 ± 0.09
RX J0038.3+4040		0	38	20.1	40	40	29	10	1	17.2	< 1.39	< 0.50	0.75 ± 0.23	< 0.22	0.60 ± 0.20
RX J0038.3+4056		0	38	21.3	40	56	40	9	1	52.1	7.23 ± 1.16	3.23 ± 0.92	3.99 ± 0.80	1.42 ± 0.50	2.49 ± 0.63
†RX J0038.4+3959	11	0	38	28.0	39	59	52	18	2	10.5	< 0.29	< 0.03	0.27 ± 0.15	< 0.00	< 0.24
∼[a]RX J0038.4+4012	10+	0	38	24.1	40	12	57	5	1	706.2	12.61 ± 0.66	1.91 ± 0.29	9.39 ± 0.52	3.50 ± 0.33	6.95 ± 0.47
[b]RX J0038.4+4136		0	38	27.7	41	36	55	23	4	14.6	< 0.17	< 0.17	< 2.86	< 0.46	< 0.68
[c]RX J0038.5+4014	12	0	38	32.1	40	14	39	11	1	14.1	0.80 ± 0.28	0.70 ± 0.26	< 0.03	< 0.03	< 0.01
RX J0038.5+4024	13	0	38	34.7	40	24	30	5	1	10.4	0.46 ± 0.20	< 0.04	0.38 ± 0.03	< 0.05	< 0.34
RX J0038.5+4128	14-	0	38	34.5	41	28	51	8	4	2093.6	55.28 ± 0.96	< 0.40	63.69 ± 1.42	21.82 ± 0.91	35.02 ± 1.17
RX J0038.6+4010	16+	0	38	38.1	40	10	33	8	1	26.6	1.98 ± 0.36	1.20 ± 0.31	0.88 ± 0.22	0.31 ± 0.15	0.51 ± 0.14
RX J0038.6+4015	15	0	38	37.6	40	15	19	7	1	12.0	1.04 ± 0.26	0.54 ± 0.19	0.39 ± 0.14	0.26 ± 0.13	0.15 ± 0.07
[c]RX J0038.6+4019	18+	0	38	40.9	40	20	0	5	1	49.3	1.73 ± 0.29	1.54 ± 0.26	< 0.05	< 0.02	< 0.04
[a]RX J0038.6+4026	17+	0	38	38.6	40	26	15	5	1	154.0	3.76 ± 0.37	0.93 ± 0.28	2.94 ± 0.26	< 1.73	< 1.21
RX J0038.6+4043		0	38	39.0	40	43	25	10	1	11.7	< 0.80	< 0.25	< 0.77	< 0.18	0.44 ± 0.17
RX J0038.6+4044	19-	0	38	40.8	40	44	57	9	1	20.3	1.46 ± 0.39	< 0.98	0.78 ± 0.24	< 0.18	0.69 ± 0.21
RX J0038.6+4056		0	38	38.6	40	56	54	11	1	26.0	2.59 ± 0.71	< 0.48	2.57 ± 0.57	< 0.82	2.25 ± 0.53
RX J0038.8+4008	20-	0	38	48.2	40	8	3	10	1	23.9	1.50 ± 0.44	< 0.60	1.39 ± 0.33	< 1.20	0.64 ± 0.21
RX J0038.8+4038	21-	0	38	48.6	40	38	12	8	1	39.5	1.28 ± 0.31	< 0.26	1.18 ± 0.24	0.43 ± 0.15	0.73 ± 0.19
RX J0038.8+4044	19-	0	38	50.1	40	44	18	8	1	111.0	3.28 ± 0.49	< 0.45	3.25 ± 0.43	< 0.87	2.70 ± 0.38
RX J0038.9+3955		0	38	56.0	39	55	51	10	1	26.2	2.52 ± 0.74	< 0.66	2.07 ± 0.59	< 0.73	1.57 ± 0.50
RX J0038.9+4016	22	0	38	55.4	40	16	53	7	1	11.9	0.93 ± 0.24	< 0.42	< 0.47	< 0.32	< 0.21
RX J0038.9+4029	23	0	38	55.6	40	29	8	5	1	14.8	0.72 ± 0.21	0.18 ± 0.17	0.45 ± 0.07	0.19 ± 0.14	< 0.35
RX J0038.9+4034	25-	0	38	56.3	40	34	52	9	1	43.3	1.69 ± 0.34	< 0.50	1.35 ± 0.25	< 0.42	1.03 ± 0.21
RX J0038.9+4058	24	0	38	56.8	40	58	56	5	2	10.5	1.05 ± 0.44	0.82 ± 0.33	< 0.12	< 0.10	< 0.03
RX J0039.0+4047		0	39	3.6	40	47	43	9	1	10.9	< 1.03	< 0.37	0.59 ± 0.20	< 0.30	0.39 ± 0.15
RX J0039.1+4006	27-	0	39	9.1	40	6	23	12	1	12.8	< 0.85	< 0.36	< 0.87	< 0.19	0.58 ± 0.21
RX J0039.1+4012	28	0	39	10.6	40	12	22	5	1	15.6	1.10 ± 0.26	< 0.19	< 0.85	< 0.47	< 0.40
RX J0039.1+4026	26	0	39	6.6	40	26	55	5	1	10.7	0.25 ± 0.16	0.07 ± 0.05	0.20 ± 0.17	0.02 ± 0.01	< 0.17

[a] Foreground star [b] Galaxy [c] Supersoft source candidate [d] Globular cluster [e] SNR
⋆ bulge source ∼ Variable source (ref. Tables 2, 3 and footnote in Sect. 4.1.1) † Source with uncertain count rate.

RXJ No. (1)	SI No. (2)	R.A. (h) (3)	(m) (4)	(J2000) (s) (5)	Dec. (°) (6)	(′) (7)	(″) (8)	σ_{Pos} (″) (9)	Cl. (10)	Maxlik (LH) (11)	Rate (B) ($ct \cdot ks^{-1}$) (12)	Rate (S) ($ct \cdot ks^{-1}$) (13)	Rate (H) ($ct \cdot ks^{-1}$) (14)	Rate (H_1) ($ct \cdot ks^{-1}$) (15)	Rate (H_2) ($ct \cdot ks^{-1}$) (16)
RX J0039.1+4035		0	39	11.6	40	35	34	10	1	16.8	< 1.11	< 0.30	0.66 ± 0.18	0.51 ± 0.16	< 0.23
RX J0039.2+4001	31-	0	39	16.5	40	1	6	9	1	25.0	2.21 ± 0.61	< 2.02	1.69 ± 0.44	< 0.96	1.53 ± 0.42
RX J0039.2+4008	29+	0	39	16.4	40	8	28	5	1	83.0	3.16 ± 0.39	0.44 ± 0.33	3.04 ± 0.28	0.97 ± 0.27	< 1.84
RX J0039.2+4013		0	39	12.8	40	13	8	10	1	14.9	< 1.36	< 0.63	0.56 ± 0.19	< 0.20	0.46 ± 0.16
RX J0039.2+4051		0	39	16.6	40	51	17	8	1	35.4	1.64 ± 0.38	< 0.42	1.33 ± 0.28	< 0.78	0.84 ± 0.21
RX J0039.2+4102	30-	0	39	17.9	41	3	0	10	1	33.8	1.62 ± 0.47	< 0.26	2.17 ± 0.45	< 1.00	1.40 ± 0.36
RX J0039.3+4023	33	0	39	23.0	40	23	28	5	1	10.9	0.29 ± 0.16	< 0.03	0.27 ± 0.16	< 0.05	0.20 ± 0.14
RX J0039.3+4047	32	0	39	21.4	40	47	41	14	2	30.2	< 0.26	0.22 ± 0.07	< 0.01	< 0.01	< 0.00
RX J0039.4+4029	34	0	39	24.7	40	29	57	5	1	23.9	0.49 ± 0.18	< 0.02	0.41 ± 0.15	< 0.15	< 0.31
RX J0039.4+4035	36+	0	39	29.9	40	35	54	5	1	25.9	0.63 ± 0.23	< 0.03	0.56 ± 0.21	< 0.19	< 0.37
RX J0039.4+4050	35+	0	39	25.1	40	50	39	8	1	34.8	2.93 ± 0.36	1.52 ± 0.24	1.37 ± 0.26	0.85 ± 0.21	0.40 ± 0.11
RX J0039.4+4105		0	39	25.0	41	5	20	11	1	12.3	< 1.80	< 0.54	0.98 ± 0.32	< 0.47	0.66 ± 0.26
[b]RX J0039.5+4008	37	0	39	33.3	40	8	43	5	1	18.2	0.71 ± 0.26	< 0.06	0.61 ± 0.24	< 0.03	0.60 ± 0.22
RX J0039.5+4109	38-	0	39	34.6	41	9	34	8	1	93.4	5.04 ± 0.81	< 0.53	4.87 ± 0.72	1.09 ± 0.36	3.75 ± 0.63
[a]RX J0039.6+4011	40-	0	39	38.3	40	11	6	9	1	26.2	1.86 ± 0.41	< 0.93	1.04 ± 0.25	0.65 ± 0.20	0.45 ± 0.16
RX J0039.6+4035	43-	0	39	39.9	40	35	37	9	1	31.6	1.18 ± 0.28	< 0.33	1.00 ± 0.21	< 0.50	0.66 ± 0.16
RX J0039.6+4048	42-	0	39	38.0	40	48	3	9	1	18.7	1.02 ± 0.30	< 1.18	0.78 ± 0.20	< 0.38	0.54 ± 0.16
[c]RX J0039.6+4054	39	0	39	38.5	40	54	9	7	2	10.6	< 0.44	0.45 ± 0.32	< 0.02	< 0.01	< 0.01
†RX J0039.6+4148	41	0	39	39.6	41	48	10	12	3	28.8	< 0.05	< 0.00	0.04 ± 0.01	< 0.00	< 0.04
RX J0039.7+4030	45+	0	39	47.1	40	30	5	5	1	51.2	2.03 ± 0.30	1.84 ± 0.28	0.15 ± 0.10	0.15 ± 0.10	< 0.01
[a]RX J0039.7+4039	44-	0	39	42.6	40	39	48	9	1	24.5	1.03 ± 0.26	< 0.34	0.79 ± 0.18	0.62 ± 0.16	< 0.31
RX J0039.7+4116		0	39	43.0	41	16	3	20	1	15.0	< 11.52	< 0.87	4.67 ± 1.13	< 2.19	3.11 ± 0.87
RX J0039.8+4009	50+	0	39	53.6	40	9	2	5	1	112.2	4.05 ± 0.41	0.61 ± 0.32	3.65 ± 0.29	1.18 ± 0.28	< 1.99
RX J0039.8+4013	48	0	39	52.6	40	13	14	5	1	11.9	0.74 ± 0.22	< 0.04	< 0.67	< 0.01	< 0.64
RX J0039.8+4048	49	0	39	53.3	40	48	2	5	1	14.7	0.87 ± 0.21	0.30 ± 0.20	0.56 ± 0.06	0.26 ± 0.23	< 0.32
RX J0039.8+4053	46	0	39	50.4	40	53	38	8	1	10.2	1.07 ± 0.25	0.88 ± 0.21	0.12 ± 0.10	< 0.03	0.09 ± 0.06
RX J0039.8+4055	47	0	39	50.7	40	55	28	10	1	12.0	0.68 ± 0.23	0.25 ± 0.22	0.48 ± 0.11	< 0.03	0.41 ± 0.06
RX J0039.8+4110		0	39	48.8	41	10	8	9	1	22.6	< 2.03	< 0.35	1.51 ± 0.39	< 0.88	0.88 ± 0.29
RX J0039.9+3929		0	39	58.1	39	29	33	37	4	10.3	< 0.70	< 0.55	< 3.01	< 1.01	< 3.21
RX J0039.9+4016	54+	0	39	58.3	40	16	33	5	1	36.1	1.45 ± 0.26	0.36 ± 0.29	< 1.18	< 0.26	< 0.92
RX J0039.9+4027	53+	0	39	58.1	40	27	20	5	1	105.3	2.39 ± 0.30	0.28 ± 0.21	2.29 ± 0.24	< 1.28	< 0.99
RX J0039.9+4041	51-	0	39	56.1	40	41	6	7	1	100.5	2.44 ± 0.34	< 0.36	1.91 ± 0.26	1.15 ± 0.20	0.76 ± 0.17
RX J0039.9+4050	52	0	39	57.7	40	50	33	6	1	10.3	0.87 ± 0.21	0.53 ± 0.17	0.41 ± 0.16	0.17 ± 0.04	0.22 ± 0.14
RX J0039.9+4111		0	39	56.4	41	11	39	10	1	14.0	< 1.55	< 0.33	1.15 ± 0.36	< 1.27	< 0.53
RX J0040.0+4025	56	0	40	1.2	40	25	19	5	1	17.8	0.89 ± 0.22	< 0.05	< 0.78	< 0.35	< 0.52
RX J0040.0+4031	55+	0	40	0.0	40	31	58	5	1	222.1	3.89 ± 0.37	0.25 ± 0.21	3.98 ± 0.34	1.06 ± 0.20	2.26 ± 0.20
RX J0040.0+4033	57	0	40	1.5	40	33	7	5	1	17.7	0.46 ± 0.20	< 0.11	0.30 ± 0.15	0.03 ± 0.02	0.28 ± 0.15
RX J0040.0+4043	59	0	40	2.8	40	43	55	6	1	11.9	0.94 ± 0.22	0.57 ± 0.16	0.24 ± 0.09	< 0.06	0.23 ± 0.09
RX J0040.0+4051	60	0	40	4.0	40	51	42	5	1	20.1	0.90 ± 0.21	0.24 ± 0.14	0.54 ± 0.12	0.13 ± 0.08	0.44 ± 0.10
RX J0040.0+4053	61+	0	40	5.8	40	53	2	5	1	18.4	0.75 ± 0.20	< 0.13	0.51 ± 0.09	0.24 ± 0.14	< 0.42
RX J0040.0+4100	58+	0	40	1.6	41	0	51	7	1	30.9	2.04 ± 0.32	0.65 ± 0.22	1.29 ± 0.21	0.88 ± 0.16	0.50 ± 0.17
[a]RX J0040.1+4006	65-	0	40	7.6	40	6	28	14	1	11.5	< 2.23	< 1.24	< 1.27	< 0.18	< 1.34
RX J0040.1+4021	62	0	40	6.6	40	21	52	5	1	10.2	0.46 ± 0.19	< 0.09	0.37 ± 0.16	0.31 ± 0.15	< 0.04
[a]RX J0040.1+4044	63	0	40	8.7	40	44	42	9	1	11.7	0.80 ± 0.22	0.75 ± 0.21	< 0.03	< 0.02	< 0.01
[a]RX J0040.1+4047	64	0	40	9.2	40	47	7	5	1	27.0	1.19 ± 0.23	0.41 ± 0.22	0.85 ± 0.09	0.17 ± 0.10	< 0.58
RX J0040.1+4047	66	0	40	10.6	40	47	44	5	1	36.2	1.43 ± 0.24	0.55 ± 0.18	0.82 ± 0.15	0.32 ± 0.12	0.47 ± 0.09
RX J0040.1+4059		0	40	11.3	40	59	30	9	1	16.7	< 1.32	< 0.37	0.78 ± 0.22	< 0.40	0.51 ± 0.18
RX J0040.2+3953	72-	0	40	17.7	39	53	54	8	1	99.8	9.65 ± 1.45	< 2.27	7.97 ± 1.26	4.25 ± 0.91	3.67 ± 0.87
[a]RX J0040.2+4015	70+	0	40	15.7	40	15	16	5	1	22.2	1.33 ± 0.27	0.69 ± 0.44	< 0.74	< 0.29	< 0.39
RX J0040.2+4033		0	40	13.9	40	33	52	8	1	59.8	1.84 ± 0.32	< 0.26	1.59 ± 0.25	0.81 ± 0.19	0.90 ± 0.18
∼RX J0040.2+4034	69	0	40	13.9	40	34	49	5	1	14294.	76.09 ± 1.10	4.87 ± 0.30	65.96 ± 0.98	24.87 ± 0.59	43.88 ± 0.84
RX J0040.2+4038	68	0	40	12.3	40	38	24	7	1	11.2	0.87 ± 0.22	0.56 ± 0.18	0.25 ± 0.10	< 0.06	0.21 ± 0.07
[b]RX J0040.2+4050	67-	0	40	13.5	40	50	10	5	1	16287.	118.14 ± 1.78	1.72 ± 0.36	124.12 ± 1.94	23.39 ± 0.87	103.45 ± 1.86
RX J0040.3+4003		0	40	21.5	40	3	20	13	1	10.6	< 1.87	< 0.38	< 1.90	< 0.28	1.07 ± 0.35
RX J0040.3+4011	71	0	40	19.2	40	11	51	11	1	10.1	0.70 ± 0.27	0.64 ± 0.28	0.12 ± 0.10	< 0.01	< 0.10
RX J0040.3+4036	74+	0	40	22.3	40	36	11	5	1	54.8	1.25 ± 0.22	< 0.12	1.08 ± 0.18	0.49 ± 0.11	0.58 ± 0.14

[a] Foreground star   [b] Galaxy   [c] Supersoft source candidate   [d] Globular cluster   [e] SNR
⋆ bulge source   ∼ Variable source (ref. Tables 2, 3 and footnote in Sect. 4.1.1)   † Source with uncertain count rate.

RXJ No. (1)	SI No. (2)	R.A. (h) (3)	(m) (4)	(J2000) (s) (5)	Dec. (°) (6)	(′) (7)	(″) (8)	$\sigma_{\rm Pos}$ (″) (9)	Cl. (10)	Maxlik (LH) (11)	Rate (B) ($ct \cdot ks^{-1}$) (12)	Rate (S) ($ct \cdot ks^{-1}$) (13)	Rate (H) ($ct \cdot ks^{-1}$) (14)	Rate (H_1) ($ct \cdot ks^{-1}$) (15)	Rate (H_2) ($ct \cdot ks^{-1}$) (16)
[d]RX J0040.3+4043	73+	0	40	20.2	40	43	57	5	1	9790.0	51.61 ± 1.07	2.24 ± 0.26	49.81 ± 1.05	14.05 ± 0.55	33.80 ± 0.84
RX J0040.3+4053	75+	0	40	23.7	40	53	4	5	1	49.1	1.44 ± 0.23	0.39 ± 0.19	1.14 ± 0.14	< 0.52	< 0.48
[c]RX J0040.4+4009	78	0	40	26.3	40	9	1	9	1	20.5	0.85 ± 0.32	0.85 ± 0.33	< 0.03	< 0.03	< 0.00
RX J0040.4+4013	81	0	40	28.6	40	13	44	8	1	26.6	0.50 ± 0.27	0.39 ± 0.23	< 0.03	< 0.00	< 0.03
RX J0040.4+4029	76+	0	40	24.5	40	29	46	5	1	228.1	4.00 ± 0.38	< 0.13	3.61 ± 0.31	1.00 ± 0.20	3.14 ± 0.29
RX J0040.4+4034		0	40	25.3	40	34	30	10	1	11.2	< 0.82	< 0.35	< 0.60	< 0.19	0.35 ± 0.12
RX J0040.4+4047	77	0	40	25.4	40	47	46	5	1	25.4	0.72 ± 0.17	< 0.09	0.61 ± 0.14	0.16 ± 0.09	0.49 ± 0.12
[a]RX J0040.4+4050	80	0	40	27.6	40	50	13	5	1	16.3	1.02 ± 0.21	< 0.57	< 0.53	< 0.21	< 0.30
[d]RX J0040.4+4129	79-	0	40	25.8	41	29	12	12	1	35.6	8.58 ± 1.51	< 1.31	7.79 ± 1.28	< 1.64	6.94 ± 1.18
RX J0040.5+3957		0	40	35.6	39	57	18	12	1	10.4	2.55 ± 0.80	< 3.27	< 0.99	< 0.44	< 0.60
RX J0040.5+4001		0	40	32.1	40	1	12	11	1	16.0	2.12 ± 0.63	< 1.23	1.49 ± 0.46	< 1.14	< 0.99
RX J0040.5+4022	84	0	40	34.0	40	22	47	5	1	11.5	0.88 ± 0.23	< 0.15	< 0.67	< 0.28	< 0.41
[d]RX J0040.5+4033		0	40	32.4	40	33	28	16	1	12.4	< 1.08	< 0.42	< 0.73	< 0.16	< 0.94
[a]RX J0040.5+4034	82	0	40	30.4	40	34	34	7	1	13.7	1.30 ± 0.30	0.76 ± 0.20	0.35 ± 0.16	0.31 ± 0.16	< 0.06
RX J0040.5+4100	83	0	40	32.9	41	0	42	5	1	36.8	1.72 ± 0.28	0.51 ± 0.20	1.11 ± 0.16	0.26 ± 0.12	0.98 ± 0.13
RX J0040.6+4015	87	0	40	39.1	40	15	53	5	1	19.2	1.39 ± 0.31	1.01 ± 0.29	0.50 ± 0.15	0.12 ± 0.10	0.38 ± 0.11
RX J0040.6+4022		0	40	41.0	40	22	29	11	1	12.8	< 1.26	< 0.49	0.68 ± 0.21	< 0.45	0.44 ± 0.16
RX J0040.6+4047	86	0	40	37.8	40	47	2	8	1	11.0	0.94 ± 0.21	< 0.53	< 0.49	< 0.19	< 0.30
RX J0040.6+4108		0	40	41.8	41	8	8	19	1	10.8	< 1.64	< 0.45	< 2.27	< 0.30	< 1.40
RX J0040.6+4119	85-	0	40	38.1	41	19	39	14	1	11.1	< 3.20	< 2.72	< 1.70	< 0.77	< 1.05
RX J0040.7+3937		0	40	44.3	39	37	1	12	4	135.1	11.01 ± 1.57	< 0.85	15.23 ± 1.32	6.17 ± 0.88	8.30 ± 0.97
†RX J0040.7+3937	91	0	40	45.3	39	37	32	6	3	90.1	4.58 ± 0.90	< 0.01	4.96 ± 0.98	3.22 ± 1.08	< 1.60
∼RX J0040.7+3959		0	40	42.3	39	59	7	8	1	50.8	5.54 ± 1.01	< 1.89	3.97 ± 0.77	2.55 ± 0.63	1.54 ± 0.47
[c]RX J0040.7+4015	88	0	40	43.2	40	15	18	7	1	33.7	1.26 ± 0.32	1.17 ± 0.31	< 0.03	< 0.03	< 0.01
RX J0040.7+4027	93	0	40	46.5	40	27	18	10	1	12.2	1.22 ± 0.30	1.11 ± 0.26	< 0.19	0.16 ± 0.15	< 0.01
RX J0040.7+4032	89+	0	40	43.2	40	32	41	5	1	13.2	0.74 ± 0.22	0.19 ± 0.16	0.46 ± 0.10	< 0.30	< 0.25
RX J0040.7+4048	90	0	40	44.0	40	48	50	5	1	17.8	0.60 ± 0.16	< 0.10	0.43 ± 0.07	< 0.05	< 0.40
RX J0040.7+4051	92+	0	40	45.8	40	51	31	5	1	74.6	1.81 ± 0.24	0.36 ± 0.17	1.36 ± 0.15	0.51 ± 0.16	1.02 ± 0.08
[e]RX J0040.7+4055	94	0	40	47.6	40	55	24	5	1	18.7	0.95 ± 0.20	0.32 ± 0.17	0.53 ± 0.06	< 0.30	< 0.29
[a]RX J0040.8+4011	95+	0	40	48.8	40	11	25	5	1	548.0	14.10 ± 0.73	11.73 ± 0.63	1.66 ± 0.28	0.71 ± 0.22	1.07 ± 0.20
RX J0040.8+4021	100-	0	40	51.6	40	21	12	9	1	15.5	< 1.04	< 0.23	0.75 ± 0.22	< 0.58	< 0.53
RX J0040.8+4030	96+	0	40	48.9	40	30	27	6	1	38.9	1.63 ± 0.29	0.51 ± 0.27	1.26 ± 0.17	0.47 ± 0.20	< 0.69
RX J0040.8+4049	97	0	40	49.2	40	49	27	5	1	19.3	0.57 ± 0.16	< 0.06	0.50 ± 0.14	0.12 ± 0.07	0.36 ± 0.12
RX J0040.8+4132	99-	0	40	53.3	41	32	46	11	1	20.0	2.26 ± 0.67	< 0.90	2.03 ± 0.54	< 1.20	1.32 ± 0.44
RX J0040.8+4153	98-	0	40	48.0	41	53	2	15	4	35.2	< 0.81	< 0.11	3.59 ± 0.53	1.21 ± 0.31	3.60 ± 0.49
RX J0040.9+4003		0	40	58.6	40	3	45	11	1	10.6	< 2.23	< 0.67	1.08 ± 0.39	< 0.75	< 0.82
[a]RX J0040.9+4056	101	0	40	57.1	40	56	43	5	1	27.1	1.15 ± 0.22	0.38 ± 0.16	0.65 ± 0.11	0.44 ± 0.04	0.26 ± 0.12
RX J0041.0+4022	102	0	41	0.3	40	22	3	9	1	16.4	1.43 ± 0.34	< 1.11	< 0.21	< 0.03	< 0.20
RX J0041.0+4027	103+	0	41	5.7	40	27	6	5	1	46.0	1.88 ± 0.35	< 0.03	1.78 ± 0.16	0.38 ± 0.21	< 1.50
RX J0041.0+4123		0	41	4.8	41	23	58	10	1	24.4	2.86 ± 0.60	< 1.87	2.12 ± 0.48	1.19 ± 0.33	< 1.32
∼RX J0041.1+4002	104-	0	41	6.9	40	2	51	10	1	45.4	5.57 ± 1.01	< 1.49	4.08 ± 0.80	1.42 ± 0.47	3.04 ± 0.70
RX J0041.1+4050		0	41	7.3	40	50	57	9	1	20.8	1.11 ± 0.27	< 0.44	0.72 ± 0.18	< 0.33	0.47 ± 0.13
RX J0041.1+4054	105+	0	41	11.9	40	54	16	5	1	88.3	1.93 ± 0.25	0.36 ± 0.16	1.39 ± 0.16	0.40 ± 0.13	1.22 ± 0.13
RX J0041.2+4016		0	41	15.9	40	16	48	9	1	23.4	1.73 ± 0.46	< 0.60	1.26 ± 0.32	< 0.78	0.71 ± 0.24
RX J0041.2+4049		0	41	14.7	40	49	1	12	1	10.7	1.00 ± 0.27	< 1.12	< 0.27	< 0.11	< 0.22
RX J0041.2+4101	106-	0	41	15.8	41	1	7	8	1	46.7	1.81 ± 0.33	< 0.40	1.37 ± 0.24	< 0.65	0.92 ± 0.19
[b]RX J0041.3+4012	110	0	41	23.8	40	12	17	18	2	13.3	1.48 ± 0.48	< 0.22	1.13 ± 0.33	0.36 ± 0.22	0.83 ± 0.26
[a]RX J0041.3+4051	107+	0	41	18.3	40	51	57	5	1	435.8	5.51 ± 0.37	1.05 ± 0.20	4.14 ± 0.29	1.79 ± 0.24	2.80 ± 0.22
RX J0041.3+4103	108	0	41	20.9	41	3	38	5	1	12.9	1.02 ± 0.32	0.27 ± 0.23	0.71 ± 0.20	0.20 ± 0.16	0.54 ± 0.14
[a]RX J0041.3+4109	109	0	41	23.3	41	9	37	30	2	14.2	0.57 ± 0.37	0.49 ± 0.34	0.03 ± 0.02	< 0.02	< 0.01
[a]RX J0041.4+4025		0	41	28.5	40	25	51	9	1	17.6	< 1.37	< 0.36	0.91 ± 0.26	< 0.44	0.58 ± 0.20
RX J0041.4+4053	112+	0	41	26.3	40	53	23	5	1	179.9	3.01 ± 0.29	0.48 ± 0.18	2.65 ± 0.25	1.06 ± 0.20	1.44 ± 0.12
RX J0041.4+4058	111+	0	41	25.9	40	58	42	5	1	560.5	7.23 ± 0.46	0.31 ± 0.16	6.05 ± 0.37	2.23 ± 0.26	5.27 ± 0.37
RX J0041.4+4102	113	0	41	27.6	41	2	32	6	1	11.4	0.72 ± 0.28	< 0.06	0.70 ± 0.22	< 0.40	< 0.32
RX J0041.4+4136		0	41	24.8	41	36	51	11	1	12.4	< 1.51	< 0.49	1.07 ± 0.34	0.80 ± 0.28	< 0.37
RX J0041.5+4028		0	41	34.6	40	28	56	10	1	14.3	< 1.50	< 0.70	0.71 ± 0.22	< 0.21	0.57 ± 0.19

[a] Foreground star [b] Galaxy [c] Supersoft source candidate [d] Globular cluster [e] SNR
⋆ bulge source ∼ Variable source (ref. Tables 2, 3 and footnote in Sect. 4.1.1) † Source with uncertain count rate.

RXJ No. (1)	SI No. (2)	R.A. (h) (3)	(m) (4)	(J2000) (s) (5)	Dec. (°) (6)	(′) (7)	(″) (8)	$\sigma_{\rm Pos}$ (″) (9)	Cl. (10)	Maxlik (LH) (11)	Rate (B) ($ct\cdot ks^{-1}$) (12)	Rate (S) ($ct\cdot ks^{-1}$) (13)	Rate (H) ($ct\cdot ks^{-1}$) (14)	Rate (H_1) ($ct\cdot ks^{-1}$) (15)	Rate (H_2) ($ct\cdot ks^{-1}$) (16)
[c]RX J0041.5+4040	114	0	41	30.2	40	40	4	6	1	13.1	0.32 ± 0.18	0.28 ± 0.17	< 0.01	< 0.01	< 0.00
∼RX J0041.5+4105		0	41	31.3	41	5	55	6	1	901.2	12.36 ± 0.69	< 0.19	11.92 ± 0.64	2.84 ± 0.32	9.27 ± 0.56
[e]RX J0041.5+4106	116	0	41	35.8	41	6	57	5	1	23.8	1.18 ± 0.30	< 0.15	0.87 ± 0.10	< 0.45	< 0.51
RX J0041.5+4117	115+	0	41	34.1	41	17	38	8	1	22.2	1.85 ± 0.38	0.50 ± 0.38	1.46 ± 0.12	0.31 ± 0.20	< 1.04
RX J0041.5+4140		0	41	35.9	41	40	6	11	1	14.3	< 1.95	< 0.51	1.03 ± 0.35	0.91 ± 0.30	< 0.28
RX J0041.6+4031		0	41	41.1	40	31	22	10	1	28.4	1.75 ± 0.42	< 0.54	1.46 ± 0.30	0.64 ± 0.20	0.72 ± 0.21
RX J0041.6+4100		0	41	41.3	41	0	10	5	1	16.5	< 2.12	< 0.33	1.76 ± 0.36	< 0.16	0.56 ± 0.16
∼RX J0041.6+4101	118-	0	41	37.6	41	1	13	8	1	85.8	3.10 ± 0.40	< 1.31	2.30 ± 0.30	0.71 ± 0.18	1.56 ± 0.24
[a]RX J0041.6+4103	119-	0	41	41.4	41	3	32	8	1	46.6	1.84 ± 0.33	< 0.36	1.45 ± 0.25	0.66 ± 0.17	0.80 ± 0.19
[a]RX J0041.6+4112	117	0	41	36.5	41	12	18	5	1	21.6	1.21 ± 0.30	< 0.13	1.13 ± 0.16	0.44 ± 0.30	< 0.63
RX J0041.7+4021		0	41	44.7	40	22	0	5	1	52.1	19.66 ± 1.52	< 3.94	5.15 ± 0.70	2.37 ± 0.48	2.58 ± 0.49
RX J0041.7+4034	123+	0	41	45.6	40	34	39	5	1	24.5	1.18 ± 0.27	0.48 ± 0.23	0.63 ± 0.10	0.32 ± 0.25	< 0.40
RX J0041.7+4036		0	41	45.7	40	36	24	10	1	10.6	< 0.98	< 0.92	< 0.56	< 0.12	0.33 ± 0.13
[a]RX J0041.7+4105	121+	0	41	43.4	41	5	5	5	1	135.6	3.85 ± 0.44	0.88 ± 0.34	3.33 ± 0.35	< 1.64	< 1.47
RX J0041.7+4107	124	0	41	46.2	41	7	15	8	1	10.0	0.63 ± 0.25	< 0.06	0.56 ± 0.11	< 0.39	< 0.20
RX J0041.7+4121		0	41	44.1	41	21	19	10	1	26.2	1.11 ± 0.33	< 0.62	1.60 ± 0.34	< 0.14	0.92 ± 0.23
RX J0041.7+4126		0	41	45.2	41	26	25	8	1	49.2	2.37 ± 0.46	< 0.55	1.91 ± 0.35	0.77 ± 0.23	1.01 ± 0.25
RX J0041.7+4131		0	41	47.2	41	31	55	9	1	53.5	3.08 ± 0.56	< 0.54	3.00 ± 0.46	0.95 ± 0.27	1.62 ± 0.34
∼[d]RX J0041.7+4134	122-	0	41	43.2	41	34	22	6	1	3463.9	53.70 ± 1.83	< 1.12	51.53 ± 1.75	14.74 ± 0.94	37.07 ± 1.49
RX J0041.7+4217	120	0	41	43.0	42	17	45	20	3	11.5	< 0.06	< 0.03	0.03 ± 0.02	< 0.00	< 0.03
∼RX J0041.8+4015	129-	0	41	49.9	40	15	26	8	1	62.0	7.02 ± 1.04	2.80 ± 0.76	3.60 ± 0.68	< 2.33	2.20 ± 0.51
∼[b]RX J0041.8+4021	134-	0	41	52.6	40	21	24	6	1	3614.5	90.56 ± 2.85	10.27 ± 1.06	76.44 ± 2.59	36.93 ± 1.80	41.22 ± 1.91
RX J0041.8+4028		0	41	48.7	40	28	14	10	1	13.0	< 1.08	< 0.42	0.73 ± 0.25	< 0.27	0.61 ± 0.21
RX J0041.8+4046	131	0	41	51.5	40	46	52	7	1	14.7	0.50 ± 0.21	0.44 ± 0.21	< 0.08	< 0.05	< 0.03
[c]RX J0041.8+4059	128	0	41	49.9	40	59	21	9	1	12.3	0.49 ± 0.24	0.46 ± 0.24	0.02 ± 0.01	< 0.01	< 0.00
∼RX J0041.8+4101	127+	0	41	49.8	41	1	9	5	1	710.7	11.73 ± 0.71	1.28 ± 0.30	9.54 ± 0.58	3.52 ± 0.41	7.37 ± 0.52
RX J0041.8+4110	133	0	41	52.4	41	10	40	5	1	39.8	1.72 ± 0.33	< 0.18	1.69 ± 0.23	< 0.82	< 0.83
RX J0041.8+4113	130+	0	41	50.7	41	13	36	5	1	34.9	1.61 ± 0.33	< 0.06	1.45 ± 0.08	0.21 ± 0.16	< 1.25
RX J0041.8+4114	132-	0	41	51.9	41	14	49	8	1	46.2	1.85 ± 0.36	< 0.40	1.84 ± 0.31	0.63 ± 0.18	1.21 ± 0.25
∼RX J0041.8+4122	126+	0	41	49.2	41	22	23	5	1	217.3	6.11 ± 0.58	< 0.17	6.27 ± 0.58	1.70 ± 0.32	4.49 ± 0.48
RX J0041.8+4151	125-	0	41	51.3	41	51	53	11	1	14.3	3.28 ± 0.91	< 1.80	1.94 ± 0.66	< 1.43	< 1.17
[e]RX J0041.9+4046		0	41	55.6	40	46	49	15	1	15.1	< 2.96	< 0.17	2.82 ± 0.42	< 0.92	1.22 ± 0.25
RX J0041.9+4133		0	41	54.7	41	33	38	8	1	45.1	2.10 ± 0.44	< 0.48	1.76 ± 0.34	0.78 ± 0.23	0.91 ± 0.24
RX J0042.0+4024	137-	0	42	3.0	40	24	16	10	1	45.9	3.24 ± 0.68	< 0.62	3.79 ± 0.64	1.56 ± 0.41	2.06 ± 0.47
RX J0042.0+4028		0	42	3.2	40	28	56	8	1	46.0	2.19 ± 0.47	< 0.37	1.84 ± 0.37	0.77 ± 0.24	1.03 ± 0.28
[a]RX J0042.0+4031		0	42	2.6	40	31	18	10	1	16.0	< 1.40	< 0.49	0.77 ± 0.24	< 0.52	< 0.57
[a]RX J0042.0+4033		0	42	3.3	40	33	8	10	1	12.3	< 1.15	< 0.39	0.67 ± 0.22	< 0.66	< 0.32
[a]RX J0042.0+4041	135+	0	42	1.0	40	41	15	5	1	331.0	5.96 ± 0.44	4.91 ± 0.39	0.76 ± 0.16	0.51 ± 0.12	0.28 ± 0.11
RX J0042.0+4046	136-	0	42	2.7	40	46	15	8	1	42.1	1.50 ± 0.32	< 0.44	1.06 ± 0.22	< 0.83	0.91 ± 0.19
[d]RX J0042.0+4102	138+	0	42	5.4	41	2	51	5	1	60.0	1.94 ± 0.34	< 0.11	1.67 ± 0.26	0.48 ± 0.17	1.16 ± 0.18
[a]RX J0042.1+4016		0	42	9.6	40	16	47	9	1	36.0	4.96 ± 1.07	< 1.17	3.77 ± 0.83	1.66 ± 0.55	2.06 ± 0.60
RX J0042.1+4053	143	0	42	11.2	40	53	32	9	1	15.5	0.95 ± 0.26	0.44 ± 0.18	0.38 ± 0.14	0.33 ± 0.13	0.13 ± 0.11
RX J0042.1+4100	139+	0	42	7.1	41	0	19	5	1	76.2	2.07 ± 0.34	< 0.15	1.81 ± 0.29	0.46 ± 0.16	1.45 ± 0.26
RX J0042.1+4104	140+	0	42	8.2	41	4	38	5	1	72.4	2.16 ± 0.35	< 0.05	2.07 ± 0.26	0.70 ± 0.23	1.48 ± 0.14
∼RX J0042.1+4110	144+	0	42	11.4	41	10	54	5	1	144.5	4.20 ± 0.46	0.75 ± 0.34	3.60 ± 0.34	0.80 ± 0.23	2.59 ± 0.22
∼RX J0042.1+4118	141-	0	42	9.0	41	18	19	5	1	970.6	35.01 ± 1.21	< 0.32	27.80 ± 1.01	5.76 ± 0.48	21.32 ± 0.88
RX J0042.1+4120	142+	0	42	9.3	41	20	40	5	1	64.7	2.68 ± 0.42	0.34 ± 0.30	2.23 ± 0.28	0.22 ± 0.16	1.89 ± 0.21
∼RX J0042.2+4019		0	42	15.2	40	19	45	6	1	3894.8	150.77 ± 4.58	14.56 ± 1.57	125.26 ± 4.09	43.66 ± 2.43	80.55 ± 3.27
∼RX J0042.2+4039	148-	0	42	13.5	40	39	25	6	1	329.3	8.12 ± 0.71	< 1.30	6.62 ± 0.59	2.20 ± 0.34	4.45 ± 0.48
RX J0042.2+4048	156-	0	42	16.3	40	48	18	11	1	13.9	< 1.22	< 0.43	0.84 ± 0.22	0.57 ± 0.17	< 0.27
∼RX J0042.2+4055	153+	0	42	16.4	40	55	55	5	1	545.2	10.13 ± 0.69	0.59 ± 0.28	9.43 ± 0.62	3.32 ± 0.40	6.60 ± 0.52
∼[d]RX J0042.2+4101	150+	0	42	15.6	41	1	16	5	1	3624.9	35.60 ± 1.18	0.66 ± 0.27	38.05 ± 1.25	5.87 ± 0.49	30.64 ± 1.10
[a]RX J0042.2+4105	147	0	42	13.0	41	5	57	5	1	16.3	1.19 ± 0.29	0.43 ± 0.24	0.67 ± 0.11	< 0.44	< 0.28
RX J0042.2+4109	149	0	42	14.7	41	9	24	7	1	11.8	0.97 ± 0.28	0.59 ± 0.22	0.28 ± 0.13	0.12 ± 0.11	0.22 ± 0.10
∼RX J0042.2+4112	155-	0	42	17.7	41	12	29	5	1	2282.0	33.74 ± 0.95	3.22 ± 0.51	35.36 ± 1.11	13.32 ± 0.68	21.68 ± 0.87
RX J0042.2+4115	145+	0	42	12.1	41	15	0	5	1	46.9	1.37 ± 0.32	< 0.20	1.15 ± 0.23	0.33 ± 0.17	0.79 ± 0.15

[a] Foreground star   [b] Galaxy   [c] Supersoft source candidate   [d] Globular cluster   [e] SNR
$\star$ bulge source $\sim$ Variable source (ref. Tables 2, 3 and footnote in Sect. 4.1.1)   † Source with uncertain count rate.

RXJ No. (1)	SI No. (2)	R.A. (h) (3)	(m) (4)	(J2000) (s) (5)	(°) (6)	(′) (7)	Dec. (″) (8)	σ_{Pos} (″) (9)	Cl. (10)	Maxlik (LH) (11)	Rate (B) ($ct \cdot ks^{-1}$) (12)	Rate (S) ($ct \cdot ks^{-1}$) (13)	Rate (H) ($ct \cdot ks^{-1}$) (14)	Rate (H_1) ($ct \cdot ks^{-1}$) (15)	Rate (H_2) ($ct \cdot ks^{-1}$) (16)
RX J0042.2+4117	151	0	42	15.9	41	17	17	5	1	472.7	8.13 ± 0.60	0.39 ± 0.22	6.78 ± 0.48	1.35 ± 0.25	6.04 ± 0.46
$\sim$[a]RX J0042.2+4118	146-	0	42	12.4	41	18	31	5	1	1492.6	36.25 ± 1.21	< 0.38	33.07 ± 1.10	8.65 ± 0.60	29.48 ± 1.04
RX J0042.2+4120	152-	0	42	15.6	41	20	31	8	1	47.9	2.06 ± 0.37	< 0.27	1.79 ± 0.30	0.56 ± 0.17	1.18 ± 0.24
RX J0042.2+4131	154+	0	42	17.0	41	31	12	8	1	12.5	0.82 ± 0.37	0.30 ± 0.19	0.50 ± 0.31	0.04 ± 0.03	0.46 ± 0.31
RX J0042.3+4019		0	42	22.9	40	19	42	7	1	815.9	94.42 ± 4.08	6.63 ± 1.45	48.60 ± 2.78	16.05 ± 1.63	30.90 ± 2.20
RX J0042.3+4019	159	0	42	19.7	40	19	48	5	2	5459.9	136.24 ± 1.23	18.99 ± 0.50	114.45 ± 1.09	48.72 ± 0.68	79.06 ± 1.02
RX J0042.3+4044		0	42	22.6	40	44	18	9	1	35.1	1.26 ± 0.32	< 0.48	0.96 ± 0.23	< 0.19	0.90 ± 0.21
RX J0042.3+4059	162+	0	42	22.1	40	59	26	5	1	686.1	10.93 ± 0.68	1.19 ± 0.32	10.27 ± 0.64	3.43 ± 0.40	7.20 ± 0.53
RX J0042.3+4104	161	0	42	20.5	41	4	48	5	1	10.5	0.98 ± 0.28	0.63 ± 0.25	0.37 ± 0.15	0.30 ± 0.11	< 0.10
RX J0042.3+4107	164+	0	42	23.0	41	7	31	5	1	63.5	2.27 ± 0.35	0.47 ± 0.25	2.02 ± 0.29	< 0.90	< 0.81
RX J0042.3+4112	160	0	42	20.3	41	12	10	5	1	26.2	11.22 ± 0.73	0.88 ± 0.25	9.63 ± 0.64	3.45 ± 0.34	6.17 ± 0.54
$\sim$[d]RX J0042.3+4113	158+	0	42	19.3	41	13	59	5	1	1416.1	18.74 ± 0.87	1.79 ± 0.30	14.45 ± 0.69	5.07 ± 0.45	12.14 ± 0.69
$\star$RX J0042.3+4113	165+	0	42	24.0	41	13	46	5	1	870.2	12.31 ± 0.76	1.46 ± 0.30	9.58 ± 0.61	2.62 ± 0.34	7.83 ± 0.57
$\star$RX J0042.3+4115	163+	0	42	22.8	41	15	36	5	1	6200.4	59.95 ± 1.52	3.58 ± 0.43	59.84 ± 1.55	17.86 ± 0.85	42.88 ± 1.32
[a]RX J0042.3+4126		0	42	20.3	41	26	41	9	1	27.9	1.69 ± 0.37	< 0.40	1.37 ± 0.28	< 0.63	0.91 ± 0.23
[b]RX J0042.3+4129	157+	0	42	18.1	41	29	17	8	1	24.3	1.27 ± 0.43	0.35 ± 0.27	0.88 ± 0.32	< 0.05	0.77 ± 0.30
RX J0042.3+4147		0	42	20.2	41	47	46	12	1	10.1	< 1.12	< 0.39	0.79 ± 0.30	< 0.47	< 0.72
RX J0042.4+3947		0	42	24.8	39	47	38	26	4	10.2	< 0.78	< 0.32	< 3.91	< 0.85	2.58 ± 0.67
RX J0042.4+4028	169-	0	42	25.0	40	28	30	14	1	12.3	< 2.00	< 0.35	< 2.31	< 0.33	< 2.18
[c]RX J0042.4+4044	171	0	42	27.6	40	44	32	5	1	54.3	1.69 ± 0.32	1.59 ± 0.31	< 0.06	< 0.03	< 0.03
[a]RX J0042.4+4055	170	0	42	27.0	40	55	24	5	1	62.1	1.36 ± 0.33	< 0.08	1.29 ± 0.33	< 0.01	1.33 ± 0.33
[d]RX J0042.4+4057	168+	0	42	25.1	40	57	23	5	1	24.0	1.19 ± 0.31	0.31 ± 0.28	0.86 ± 0.12	< 0.09	0.82 ± 0.03
$\sim$RX J0042.4+4104	173-	0	42	29.1	41	4	35	6	1	1118.4	17.85 ± 0.83	< 1.17	15.22 ± 0.74	5.04 ± 0.43	10.24 ± 0.60
[a]RX J0042.4+4108		0	42	29.2	41	8	26	8	1	43.0	2.41 ± 0.39	< 2.06	1.59 ± 0.28	0.64 ± 0.18	0.98 ± 0.21
RX J0042.4+4110	166	0	42	24.6	41	10	19	6	1	17.4	1.38 ± 0.33	0.75 ± 0.16	0.60 ± 0.28	< 0.32	< 0.33
$\sim$RX J0042.4+4112	172+	0	42	28.5	41	12	19	5	1	1782.2	22.09 ± 0.94	2.12 ± 0.39	21.65 ± 0.93	6.24 ± 0.51	13.09 ± 0.65
$\star$RX J0042.4+4114		0	42	29.7	41	14	30	5	1	317.8	154.67 ± 1.01	7.28 ± 0.68	97.14 ± 1.08	35.21 ± 1.10	42.28 ± 1.04
$\star$RX J0042.4+4119		0	42	27.6	41	19	21	5	1	131.9	9.20 ± 0.62	< 0.40	8.01 ± 0.59	2.25 ± 0.34	5.37 ± 0.48
RX J0042.4+4125	167-	0	42	26.4	41	25	54	7	1	128.8	4.21 ± 0.50	< 0.25	3.95 ± 0.43	0.85 ± 0.21	3.02 ± 0.37
[a]RX J0042.4+4129	174-	0	42	29.6	41	29	3	8	1	51.7	1.52 ± 0.35	< 0.39	1.63 ± 0.28	0.54 ± 0.17	1.15 ± 0.23
RX J0042.4+4145		0	42	26.9	41	45	30	10	1	15.3	< 1.04	< 0.22	1.06 ± 0.31	< 0.56	0.66 ± 0.23
RX J0042.5+4040		0	42	35.0	40	40	35	11	1	12.9	< 1.26	< 0.44	0.82 ± 0.25	< 0.41	0.60 ± 0.21
$\sim$RX J0042.5+4048	179-	0	42	34.5	40	48	40	7	1	171.8	3.91 ± 0.46	< 0.33	3.54 ± 0.39	1.34 ± 0.24	2.28 ± 0.31
[d]RX J0042.5+4103	178	0	42	33.0	41	3	30	5	1	256.7	4.99 ± 0.47	0.44 ± 0.24	4.93 ± 0.45	1.30 ± 0.25	3.24 ± 0.33
$\star$RX J0042.5+4113	177+	0	42	32.7	41	13	18	5	1	685.1	15.50 ± 0.83	5.76 ± 0.57	8.79 ± 0.53	3.81 ± 0.56	< 5.09
$\star$RX J0042.5+4116	176+	0	42	31.4	41	16	18	5	1	1780.0	22.43 ± 0.79	1.86 ± 0.26	19.79 ± 0.72	8.58 ± 0.45	13.49 ± 0.66
[d]$\star$RX J0042.5+4119	175+	0	42	31.2	41	19	34	5	1	774.5	12.31 ± 0.74	0.25 ± 0.18	10.33 ± 0.61	3.64 ± 0.39	8.92 ± 0.63
$\star$RX J0042.5+4119	182	0	42	35.5	41	19	47	5	1	454.4	6.75 ± 0.60	0.26 ± 0.19	5.89 ± 0.52	1.61 ± 0.26	4.62 ± 0.48
RX J0042.5+4121		0	42	33.5	41	21	49	10	1	18.0	1.30 ± 0.34	< 0.24	1.16 ± 0.26	0.85 ± 0.21	< 0.41
[d]RX J0042.5+4132	180-	0	42	34.4	41	32	53	6	1	287.1	6.30 ± 0.58	< 0.45	5.68 ± 0.51	0.91 ± 0.21	4.93 ± 0.47
RX J0042.5+4155	183-	0	42	32.2	41	55	45	9	1	38.1	3.64 ± 0.77	< 1.11	2.61 ± 0.56	1.61 ± 0.44	0.88 ± 0.34
RX J0042.6+4043	185-	0	42	39.5	40	43	20	8	1	75.2	3.96 ± 0.53	1.36 ± 0.36	2.43 ± 0.37	1.44 ± 0.28	0.97 ± 0.24
$\sim$[b]RX J0042.6+4052	188+	0	42	41.4	40	52	1	5	1	9660.5	121.17 ± 1.99	8.62 ± 0.55	99.99 ± 1.70	36.82 ± 1.02	72.92 ± 1.56
RX J0042.6+4110	186+	0	42	39.0	41	10	14	5	1	39.8	1.35 ± 0.32	0.35 ± 0.22	0.96 ± 0.22	0.46 ± 0.37	< 0.48
$\star$RX J0042.6+4113	187-	0	42	40.4	41	13	29	5	1	701.9	112.89 ± 0.87	7.23 ± 0.65	61.78 ± 0.87	26.80 ± 1.00	32.18 ± 1.09
$\star$RX J0042.6+4114	181-	0	42	36.7	41	14	1	5	1	611.8	171.71 ± 0.99	10.17 ± 0.76	93.39 ± 1.05	29.82 ± 0.93	33.16 ± 0.92
$\star$RX J0042.6+4114	189	0	42	41.6	41	14	40	5	1	554.2	14.01 ± 0.65	2.46 ± 0.31	12.69 ± 0.63	6.42 ± 0.56	5.70 ± 0.23
[d]$\star$RX J0042.6+4115	184+	0	42	38.6	41	15	58	5	1	9797.5	157.95 ± 1.41	13.51 ± 0.42	139.51 ± 1.30	49.60 ± 0.71	83.12 ± 1.01
$\star$RX J0042.6+4118	190-	0	42	41.9	41	18	26	5	1	215.8	81.41 ± 0.78	4.20 ± 0.57	47.10 ± 0.80	19.54 ± 0.86	22.07 ± 0.93
RX J0042.6+4159	183-	0	42	39.4	41	59	52	13	1	19.2	3.04 ± 0.84	< 1.04	3.74 ± 0.81	1.38 ± 0.48	< 1.14
RX J0042.6+4203		0	42	41.8	42	3	16	13	1	13.1	< 3.45	< 1.00	2.01 ± 0.66	< 1.23	< 1.79
RX J0042.7+4008		0	42	43.5	40	8	34	24	4	10.4	< 0.84	< 0.12	< 1.82	< 1.18	1.33 ± 0.33
RX J0042.7+4058	199+	0	42	48.0	40	58	40	5	1	12.7	0.40 ± 0.23	0.06 ± 0.05	0.29 ± 0.20	0.03 ± 0.02	0.33 ± 0.25
RX J0042.7+4107	196	0	42	44.9	41	7	18	8	1	12.6	1.04 ± 0.31	1.03 ± 0.31	< 0.06	< 0.05	< 0.01
$\star$RX J0042.7+4111	195+	0	42	44.7	41	11	36	5	1	1109.9	15.43 ± 0.79	1.53 ± 0.30	12.48 ± 0.65	4.78 ± 0.44	7.72 ± 0.49
$\star$RX J0042.7+4114	197	0	42	45.5	41	14	15	5	1	114.9	13.31 ± 0.76	4.18 ± 0.43	10.38 ± 0.71	< 4.24	< 4.64

^{a} Foreground star ^{b} Galaxy ^{c} Supersoft source candidate ^{d} Globular cluster ^{e} SNR
$\star$ bulge source $\sim$ Variable source (ref. Tables 2, 3 and footnote in Sect. 4.1.1) † Source with uncertain count rate.

RXJ No. (1)	SI No. (2)	R.A. (h) (3)	(m) (4)	(J2000) (s) (5)	(°) (6)	(′) (7)	Dec. (″) (8)	$\sigma_{\rm Pos}$ (″) (9)	Cl. (10)	Maxlik (LH) (11)	Rate (B) ($ct \cdot ks^{-1}$) (12)	Rate (S) ($ct \cdot ks^{-1}$) (13)	Rate (H) ($ct \cdot ks^{-1}$) (14)	Rate (H_1) ($ct \cdot ks^{-1}$) (15)	Rate (H_2) ($ct \cdot ks^{-1}$) (16)
$\star$RX J0042.7+4115	193	0	42	43.3	41	15	45	5	1	1556.9	85.12 ± 1.11	11.75 ± 0.40	62.04 ± 0.87	32.54 ± 0.57	42.51 ± 0.89
$\star$RX J0042.7+4116	198+	0	42	46.0	41	16	15	5	1	3575.0	111.62 ± 1.06	12.67 ± 0.35	87.92 ± 0.89	44.95 ± 0.60	51.27 ± 0.76
$\star$RX J0042.7+4119	192	0	42	43.1	41	19	46	5	1	54.3	3.47 ± 0.46	1.39 ± 0.27	1.91 ± 0.35	< 0.99	< 1.00
$\star$RX J0042.7+4120	191	0	42	42.9	41	20	31	5	1	54.5	2.39 ± 0.43	0.79 ± 0.25	1.44 ± 0.32	0.45 ± 0.16	1.11 ± 0.31
RX J0042.7+4121		0	42	44.1	41	21	28	11	1	31.1	5.61 ± 0.64	< 0.59	3.46 ± 0.46	< 2.41	1.55 ± 0.30
RX J0042.7+4128	194+	0	42	44.3	41	28	10	5	1	126.9	4.33 ± 0.50	0.74 ± 0.24	3.39 ± 0.41	0.95 ± 0.21	2.79 ± 0.40
RX J0042.8+4008	202	0	42	49.3	40	8	35	7	3	15.3	6.34 ± 0.64	3.86 ± 0.47	2.12 ± 0.38	0.89 ± 0.47	< 1.18
RX J0042.8+4013	209-	0	42	53.2	40	13	20	11	4	135.7	< 1.81	< 0.09	7.40 ± 0.58	4.00 ± 0.42	5.53 ± 0.47
RX J0042.8+4048		0	42	53.6	40	48	18	10	1	10.4	< 0.95	< 0.35	< 0.73	< 0.39	0.36 ± 0.14
RX J0042.8+4053		0	42	52.7	40	53	27	10	1	11.6	< 0.92	< 0.29	0.58 ± 0.18	< 0.35	< 0.51
RX J0042.8+4104	204	0	42	51.7	41	4	44	5	1	23.2	1.53 ± 0.32	0.72 ± 0.18	0.60 ± 0.20	< 0.32	< 0.39
$\star$RX J0042.8+4115	200+	0	42	48.1	41	15	25	5	1	2846.5	64.95 ± 0.92	12.17 ± 0.43	56.56 ± 0.88	23.73 ± 0.64	30.49 ± 0.55
$\star$RX J0042.8+4115	208-	0	42	53.3	41	15	49	5	1	1250.4	253.68 ± 1.13	30.40 ± 1.09	136.85 ± 1.07	45.88 ± 1.01	45.55 ± 1.03
$\star$RX J0042.8+4115	210+	0	42	53.9	41	15	53	5	1	2150.3	42.38 ± 1.08	12.90 ± 0.62	31.57 ± 0.94	15.36 ± 0.63	12.70 ± 0.56
$\star$RX J0042.8+4118	206+	0	42	52.4	41	18	49	5	1	2880.7	36.16 ± 1.21	3.73 ± 0.47	33.67 ± 1.16	12.36 ± 0.68	20.11 ± 0.90
RX J0042.8+4125	201+	0	42	48.7	41	25	22	5	1	863.1	14.75 ± 0.84	0.43 ± 0.23	14.44 ± 0.81	2.31 ± 0.32	11.82 ± 0.73
$\sim^{e}$RX J0042.8+4125	203	0	42	51.7	41	25	39	5	1	103.3	13.54 ± 0.90	0.36 ± 0.26	12.74 ± 0.83	3.52 ± 0.39	9.84 ± 0.78
†RX J0042.8+4129	207	0	42	52.7	41	29	51	5	3	104.0	16.45 ± 0.94	< 0.04	17.71 ± 1.01	< 5.61	< 9.48
$\sim^{d}$RX J0042.8+4131	205+	0	42	52.1	41	31	8	5	1	6833.2	69.55 ± 1.68	2.66 ± 0.41	73.59 ± 1.80	17.55 ± 0.86	55.43 ± 1.56
RX J0042.8+4149		0	42	53.7	41	49	32	5	1	13.2	< 2.38	< 0.92	1.59 ± 0.40	< 1.31	< 0.65
RX J0042.9+4059	212	0	42	55.6	40	59	39	5	1	16.2	0.90 ± 0.28	< 0.17	0.76 ± 0.24	0.57 ± 0.19	0.10 ± 0.09
RX J0042.9+4111	213+	0	42	57.7	41	11	3	5	1	1058.9	14.34 ± 0.77	0.79 ± 0.25	12.59 ± 0.67	4.94 ± 0.49	9.66 ± 0.60
$\star$RX J0042.9+4113		0	42	54.5	41	13	36	5	1	98.0	65.09 ± 0.82	4.70 ± 0.57	8.44 ± 0.53	6.73 ± 0.52	1.46 ± 0.27
$\star$RX J0042.9+4113	214	0	42	58.3	41	13	28	5	1	400.2	7.77 ± 0.61	1.51 ± 0.33	6.60 ± 0.54	2.29 ± 0.31	3.67 ± 0.38
$\star$RX J0042.9+4117		0	42	56.1	41	17	1	5	1	298.8	31.59 ± 0.48	15.27 ± 0.86	92.18 ± 1.06	35.71 ± 1.03	40.83 ± 1.09
$^{d}\star$RX J0042.9+4119	217+	0	42	59.4	41	19	25	5	1	641.0	13.66 ± 0.81	2.99 ± 0.45	11.40 ± 0.72	4.91 ± 0.44	6.51 ± 0.57
$\star$RX J0042.9+4120	215	0	42	58.8	41	20	5	5	1	251.0	7.31 ± 0.65	3.07 ± 0.35	4.38 ± 0.56	1.70 ± 0.16	2.67 ± 0.53
^{e}RX J0042.9+4125	211-	0	42	54.4	41	25	55	6	1	606.8	11.39 ± 0.72	< 0.36	12.22 ± 0.69	3.96 ± 0.40	8.20 ± 0.56
$\sim$RX J0042.9+4146	216-	0	42	57.8	41	46	6	7	1	212.7	7.64 ± 0.72	2.11 ± 0.47	5.17 ± 0.55	3.04 ± 0.42	2.16 ± 0.36
RX J0043.0+4044		0	43	1.9	40	44	58	9	1	57.5	2.99 ± 0.54	< 0.48	2.83 ± 0.43	0.94 ± 0.25	1.74 ± 0.33
^{a}RX J0043.0+4110	221	0	43	3.4	41	10	21	5	1	33.4	1.64 ± 0.32	0.44 ± 0.27	1.25 ± 0.19	0.44 ± 0.20	< 0.73
$\star$RX J0043.0+4113		0	43	1.5	41	13	55	5	1	138.3	57.23 ± 0.95	< 2.66	9.58 ± 0.58	4.96 ± 0.45	4.49 ± 0.44
$^{d}\star$RX J0043.0+4115	220+	0	43	2.8	41	15	24	5	1	2605.0	33.50 ± 1.16	3.78 ± 0.40	26.04 ± 0.95	10.69 ± 0.60	16.69 ± 0.80
$^{d}\star$RX J0043.0+4117	223+	0	43	4.1	41	17	59	5	1	1379.9	23.11 ± 0.99	4.63 ± 0.53	20.22 ± 0.93	6.31 ± 0.49	10.98 ± 0.62
^{d}RX J0043.0+4121	222+	0	43	3.8	41	21	22	5	1	235.9	7.57 ± 0.65	1.55 ± 0.34	6.21 ± 0.57	2.48 ± 0.33	3.80 ± 0.48
^{d}RX J0043.0+4130	218+	0	43	1.8	41	30	15	5	1	431.7	7.62 ± 0.59	< 0.13	6.93 ± 0.52	1.84 ± 0.30	6.08 ± 0.51
RX J0043.1+4045	224	0	43	7.1	40	45	8	9	2	30.4	0.96 ± 0.54	0.04 ± 0.03	0.90 ± 0.53	< 0.39	< 0.46
$\sim$RX J0043.1+4048		0	43	11.8	40	48	35	7	1	169.0	5.53 ± 0.62	< 1.03	4.31 ± 0.50	1.70 ± 0.31	2.62 ± 0.39
RX J0043.1+4059	227+	0	43	10.2	40	59	16	5	1	41.9	1.72 ± 0.37	< 0.15	1.58 ± 0.27	0.23 ± 0.17	1.40 ± 0.22
$\sim$RX J0043.1+4112	225+	0	43	8.1	41	12	44	5	1	69.9	3.06 ± 0.41	1.14 ± 0.30	1.80 ± 0.25	0.61 ± 0.21	1.21 ± 0.14
^{d}RX J0043.1+4114	228+	0	43	10.7	41	14	47	5	1	2616.3	32.13 ± 1.13	3.07 ± 0.38	27.07 ± 0.99	8.86 ± 0.57	17.58 ± 0.79
$\sim$RX J0043.1+4118	226-	0	43	9.5	41	19	0	5	1	1217.7	28.17 ± 0.91	2.91 ± 0.54	24.21 ± 0.94	12.81 ± 0.74	15.33 ± 0.75
RX J0043.1+4145		0	43	7.7	41	45	51	8	1	28.9	1.55 ± 0.38	< 0.57	1.12 ± 0.26	< 0.38	0.85 ± 0.22
RX J0043.1+4152	219-	0	43	8.8	41	52	8	9	1	22.5	1.40 ± 0.42	< 0.43	1.10 ± 0.29	< 0.62	0.92 ± 0.28
†RX J0043.1+4155		0	43	10.7	41	55	41	10	1	18.4	< 1.68	< 0.47	1.03 ± 0.30	< 0.33	0.82 ± 0.26
RX J0043.2+4054	230+	0	43	14.0	40	54	26	7	1	14.8	0.48 ± 0.32	0.07 ± 0.05	0.35 ± 0.27	0.04 ± 0.02	0.34 ± 0.29
RX J0043.2+4103	233+	0	43	16.0	41	3	46	5	1	28.4	1.10 ± 0.29	< 0.10	0.95 ± 0.26	0.25 ± 0.13	0.76 ± 0.25
^{d}RX J0043.2+4107	229+	0	43	13.9	41	7	21	5	1	746.9	11.52 ± 0.70	1.06 ± 0.30	11.52 ± 0.70	2.66 ± 0.34	8.07 ± 0.56
^{d}RX J0043.2+4112		0	43	17.2	41	12	28	12	1	12.7	1.53 ± 0.38	< 0.34	< 1.43	0.87 ± 0.22	< 0.28
RX J0043.2+4117		0	43	13.4	41	17	15	5	1	73.1	11.08 ± 0.69	3.55 ± 0.53	6.00 ± 0.55	3.04 ± 0.39	2.60 ± 0.37
RX J0043.2+4117	232	0	43	15.6	41	17	54	5	1	104.4	4.42 ± 0.54	1.20 ± 0.28	2.86 ± 0.41	1.79 ± 0.40	1.30 ± 0.18
RX J0043.2+4118	234	0	43	16.5	41	18	34	5	1	192.5	7.08 ± 0.63	1.86 ± 0.37	5.22 ± 0.51	2.61 ± 0.37	2.89 ± 0.38
RX J0043.2+4123		0	43	15.6	41	23	41	9	1	75.6	6.34 ± 0.63	4.29 ± 0.49	< 2.94	< 1.97	< 0.64
RX J0043.2+4125	231	0	43	15.1	41	25	9	5	1	12.8	1.12 ± 0.30	0.40 ± 0.21	0.58 ± 0.16	0.24 ± 0.14	0.37 ± 0.09
^{d}RX J0043.2+4127		0	43	17.2	41	27	44	6	1	1165.6	17.30 ± 0.81	< 0.88	15.37 ± 0.73	5.61 ± 0.44	9.78 ± 0.59
RX J0043.3+4048		0	43	19.4	40	48	38	10	1	21.6	< 1.85	< 0.52	1.39 ± 0.33	< 0.53	0.90 ± 0.25

[a] Foreground star [b] Galaxy [c] Supersoft source candidate [d] Globular cluster [e] SNR
⋆ bulge source ∼ Variable source (ref. Tables 2, 3 and footnote in Sect. 4.1.1) † Source with uncertain count rate.

RXJ No. (1)	SI No. (2)	R.A. (h) (3)	(m) (4)	(J2000) (s) (5)	Dec. (°) (6)	(′) (7)	(″) (8)	$\sigma_{\rm Pos}$ (″) (9)	Cl. (10)	Maxlik (LH) (11)	Rate (B) ($ct \cdot ks^{-1}$) (12)	Rate (S) ($ct \cdot ks^{-1}$) (13)	Rate (H) ($ct \cdot ks^{-1}$) (14)	Rate (H_1) ($ct \cdot ks^{-1}$) (15)	Rate (H_2) ($ct \cdot ks^{-1}$) (16)
RX J0043.3+4057	237	0	43	21.8	40	57	58	5	1	19.1	1.33 ± 0.37	0.32 ± 0.31	1.14 ± 0.25	< 0.54	< 0.46
[a]RX J0043.3+4114		0	43	23.8	41	14	19	10	1	10.5	< 1.26	< 0.26	0.72 ± 0.21	< 0.75	< 0.42
∼RX J0043.3+4117		0	43	21.0	41	17	49	5	1	114.2	16.60 ± 0.94	2.17 ± 0.42	12.21 ± 0.81	2.95 ± 0.37	3.50 ± 0.44
∼RX J0043.3+4120	235+	0	43	18.6	41	20	24	5	1	196.3	6.74 ± 0.62	1.55 ± 0.30	4.57 ± 0.48	4.43 ± 0.50	0.97 ± 0.26
RX J0043.3+4131	238-	0	43	23.0	41	31	47	8	1	35.7	1.68 ± 0.33	< 0.52	1.22 ± 0.24	< 0.43	0.98 ± 0.21
RX J0043.3+4159	236-	0	43	18.0	41	59	8	7	1	185.4	7.12 ± 0.84	< 0.45	6.65 ± 0.74	2.12 ± 0.43	4.53 ± 0.61
RX J0043.4+4107	241+	0	43	28.6	41	7	47	5	1	306.7	6.25 ± 0.55	< 0.12	6.20 ± 0.52	1.52 ± 0.28	4.71 ± 0.44
∼[e]RX J0043.4+4118	240-	0	43	26.7	41	18	27	7	1	271.8	11.96 ± 0.76	< 1.71	7.20 ± 0.54	5.13 ± 0.44	1.90 ± 0.30
∼RX J0043.4+4126		0	43	26.6	41	26	14	7	1	218.4	5.87 ± 0.52	< 0.39	4.78 ± 0.43	1.26 ± 0.23	3.53 ± 0.37
RX J0043.4+4136	239	0	43	26.1	41	36	49	5	1	20.4	1.05 ± 0.28	< 0.08	0.98 ± 0.10	0.17 ± 0.14	< 0.77
RX J0043.4+4153		0	43	25.9	41	53	12	14	1	10.3	< 1.47	< 0.51	< 1.45	< 0.26	1.07 ± 0.30
RX J0043.4+4211	242	0	43	29.6	42	11	3	5	2	17.6	1.76 ± 0.63	1.47 ± 0.52	< 0.31	< 0.08	< 0.24
RX J0043.4+4222		0	43	28.4	42	22	12	14	4	24.5	< 0.21	< 0.15	2.46 ± 0.44	< 1.29	1.88 ± 0.36
RX J0043.5+4056		0	43	34.4	40	56	30	7	1	219.6	6.06 ± 0.59	< 0.91	4.62 ± 0.47	2.40 ± 0.34	2.21 ± 0.32
RX J0043.5+4110	243+	0	43	31.9	41	10	38	5	1	130.8	2.97 ± 0.41	< 0.03	3.02 ± 0.36	0.33 ± 0.16	2.76 ± 0.33
RX J0043.5+4113	244+	0	43	34.1	41	13	21	5	1	1522.4	23.55 ± 1.01	2.45 ± 0.42	23.29 ± 1.02	6.97 ± 0.51	13.22 ± 0.72
[a]RX J0043.5+4116		0	43	32.9	41	16	14	12	1	39.9	10.76 ± 1.01	3.58 ± 0.50	< 2.20	< 0.71	< 0.43
RX J0043.5+4204		0	43	32.3	42	4	58	12	1	10.0	< 1.91	< 0.77	< 1.59	< 0.37	0.91 ± 0.35
[c]RX J0043.5+4207	245	0	43	35.9	42	7	30	5	2	26.0	2.15 ± 0.55	2.19 ± 0.58	< 0.09	< 0.05	< 0.03
[b]RX J0043.6+4054	246-	0	43	40.3	40	54	36	9	1	55.3	4.08 ± 0.59	< 2.45	2.38 ± 0.38	< 1.20	1.42 ± 0.28
[d]RX J0043.6+4114	247-	0	43	36.7	41	14	42	6	1	1048.8	19.14 ± 0.87	4.72 ± 0.71	15.26 ± 0.74	4.94 ± 0.42	10.03 ± 0.60
[e]RX J0043.6+4126	249-	0	43	38.7	41	26	52	8	1	78.0	3.53 ± 0.44	< 0.61	2.57 ± 0.33	1.68 ± 0.26	0.80 ± 0.20
[a]RX J0043.6+4138	248	0	43	38.9	41	38	51	5	1	12.7	0.91 ± 0.27	0.22 ± 0.21	0.63 ± 0.15	0.16 ± 0.13	0.48 ± 0.08
RX J0043.6+4153		0	43	41.6	41	53	13	11	1	15.5	< 1.41	< 0.42	1.09 ± 0.29	0.72 ± 0.22	< 0.42
RX J0043.6+4201		0	43	38.7	42	1	26	10	1	21.8	1.81 ± 0.53	< 0.58	1.63 ± 0.40	< 0.69	1.21 ± 0.33
RX J0043.7+4112	251+	0	43	44.1	41	12	19	5	1	34.9	1.58 ± 0.38	< 0.10	1.60 ± 0.33	0.92 ± 0.28	0.59 ± 0.14
∼RX J0043.7+4124		0	43	44.1	41	24	8	9	1	60.0	3.72 ± 0.50	< 0.36	2.55 ± 0.35	1.43 ± 0.30	1.35 ± 0.25
RX J0043.7+4127	252	0	43	44.4	41	27	24	7	1	14.1	1.12 ± 0.32	0.48 ± 0.45	< 0.74	< 0.44	< 0.17
[d]RX J0043.7+4128	250-	0	43	43.0	41	28	52	8	1	48.0	2.54 ± 0.39	< 0.58	1.92 ± 0.30	< 0.72	1.40 ± 0.25
∼[d]RX J0043.7+4136	253+	0	43	45.8	41	36	54	5	1	398.2	7.04 ± 0.56	0.57 ± 0.24	6.04 ± 0.46	2.46 ± 0.37	4.29 ± 0.36
RX J0043.8+4016		0	43	52.5	40	16	29	20	4	10.4	< 0.13	< 0.13	< 1.95	< 0.59	< 1.37
RX J0043.8+4049		0	43	49.7	40	49	49	12	1	15.8	< 1.74	< 0.43	1.37 ± 0.37	< 0.70	< 1.03
[a]RX J0043.8+4106	257-	0	43	53.7	41	6	13	9	1	25.6	1.36 ± 0.34	< 0.43	1.15 ± 0.26	0.55 ± 0.17	0.57 ± 0.18
[e]RX J0043.8+4111		0	43	53.1	41	11	53	11	1	10.3	< 1.20	< 0.56	< 0.72	0.56 ± 0.18	< 0.13
RX J0043.8+4116	256-	0	43	53.2	41	16	54	6	1	1565.6	23.50 ± 0.96	1.32 ± 0.32	20.69 ± 0.88	7.17 ± 0.51	13.57 ± 0.71
RX J0043.8+4121	254	0	43	49.7	41	21	14	5	1	15.3	1.11 ± 0.30	< 0.15	0.87 ± 0.14	0.26 ± 0.19	< 0.62
RX J0043.8+4124	255	0	43	50.0	41	24	5	5	1	10.1	0.92 ± 0.27	< 0.29	< 0.57	< 0.23	< 0.37
[d]RX J0043.8+4127		0	43	48.6	41	27	46	48	1	10.0	< 1.98	< 0.47	< 0.97	< 0.27	0.51 ± 0.17
RX J0043.9+4045	260-	0	43	54.6	40	45	38	9	1	53.9	3.17 ± 0.70	< 0.61	3.36 ± 0.62	0.91 ± 0.34	2.40 ± 0.52
[e]RX J0043.9+4113	262+	0	43	56.4	41	13	34	13	1	13.7	1.12 ± 0.40	0.79 ± 0.44	< 0.40	< 0.28	< 0.09
∼[d]RX J0043.9+4122	261+	0	43	56.2	41	22	3	5	1	191.3	4.82 ± 0.48	0.59 ± 0.25	3.92 ± 0.37	1.19 ± 0.26	2.91 ± 0.29
[a]RX J0043.9+4127	263+	0	43	56.9	41	27	22	5	1	38.1	1.60 ± 0.31	< 0.05	1.33 ± 0.19	0.55 ± 0.24	< 0.92
RX J0043.9+4130		0	43	57.6	41	30	53	8	1	31.5	1.41 ± 0.30	< 0.42	1.03 ± 0.21	< 0.42	0.73 ± 0.17
RX J0043.9+4151	259	0	43	54.6	41	51	48	8	1	10.4	1.29 ± 0.36	0.82 ± 0.29	0.36 ± 0.16	0.38 ± 0.15	< 0.03
[e]RX J0043.9+4152	258+	0	43	54.1	41	52	58	10	1	24.6	1.01 ± 0.32	< 0.17	0.93 ± 0.25	0.47 ± 0.10	0.38 ± 0.21
[b]RX J0043.9+4157	265-	0	43	58.8	41	57	17	8	1	28.3	< 1.35	< 0.28	0.97 ± 0.26	< 0.20	0.88 ± 0.23
RX J0043.9+4212	264	0	43	57.5	42	12	46	6	2	11.3	1.31 ± 0.52	< 0.67	< 0.66	< 0.39	< 0.23
RX J0044.0+4056		0	44	0.9	40	56	13	10	1	52.8	2.73 ± 0.55	< 0.82	2.81 ± 0.46	0.77 ± 0.24	1.82 ± 0.34
[c]RX J0044.0+4118	268	0	44	4.8	41	18	20	5	1	54.3	2.46 ± 0.42	2.47 ± 0.43	< 0.08	< 0.03	< 0.04
RX J0044.0+4121	267-	0	44	4.5	41	21	18	9	1	16.7	< 1.15	< 0.46	< 0.71	< 0.11	0.61 ± 0.17
RX J0044.0+4139	266	0	44	2.4	41	39	26	5	1	12.5	0.71 ± 0.26	< 0.10	0.55 ± 0.21	0.13 ± 0.12	0.50 ± 0.21
[e]RX J0044.0+4149		0	44	4.3	41	49	5	12	1	10.2	< 1.33	< 0.43	0.82 ± 0.24	< 0.68	< 0.46
RX J0044.0+4152	269-	0	44	5.8	41	52	1	10	1	17.2	< 1.41	< 1.10	0.67 ± 0.21	< 0.14	0.67 ± 0.19
RX J0044.1+4156	270+	0	44	9.0	41	56	33	6	1	40.4	1.63 ± 0.35	0.46 ± 0.28	1.28 ± 0.24	0.28 ± 0.15	0.85 ± 0.15
RX J0044.1+4205	273-	0	44	10.2	42	5	5	10	1	15.4	1.74 ± 0.48	< 0.81	1.10 ± 0.32	< 0.57	0.76 ± 0.26
RX J0044.2+4026	271-	0	44	15.3	40	26	50	20	4	23.5	< 0.48	< 0.10	2.30 ± 0.41	1.28 ± 0.30	1.18 ± 0.31

[a] Foreground star   [b] Galaxy   [c] Supersoft source candidate   [d] Globular cluster   [e] SNR
⋆ bulge source   ∼ Variable source (ref. Tables 2, 3 and footnote in Sect. 4.1.1)   † Source with uncertain count rate.

RXJ No. (1)	SI No. (2)	R.A. (h) (3)	(m) (4)	(J2000) (s) (5)	(°) (6)	Dec. (′) (7)	(″) (8)	$\sigma_{\rm Pos}$ (″) (9)	Cl. (10)	Maxlik (LH) (11)	Rate (B) ($ct \cdot ks^{-1}$) (12)	Rate (S) ($ct \cdot ks^{-1}$) (13)	Rate (H) ($ct \cdot ks^{-1}$) (14)	Rate (H_1) ($ct \cdot ks^{-1}$) (15)	Rate (H_2) ($ct \cdot ks^{-1}$) (16)
RX J0044.2+4111		0	44	16.4	41	11	14	10	1	12.1	< 0.90	< 0.36	< 0.68	< 0.09	0.46 ± 0.16
RX J0044.2+4117	275	0	44	14.0	41	17	57	11	1	10.5	0.95 ± 0.35	0.88 ± 0.31	< 0.01	< 0.01	< 0.00
[e]RX J0044.2+4119	274	0	44	13.6	41	19	50	5	1	16.7	1.34 ± 0.32	< 0.27	1.06 ± 0.10	0.44 ± 0.34	< 0.62
[a]RX J0044.2+4126		0	44	15.9	41	26	22	10	1	14.3	1.22 ± 0.30	< 0.75	0.60 ± 0.18	< 0.37	< 0.48
RX J0044.2+4131	272+	0	44	12.4	41	31	45	5	1	24.7	1.16 ± 0.27	< 0.04	1.08 ± 0.18	0.45 ± 0.23	< 0.78
RX J0044.2+4157		0	44	13.8	41	57	51	9	1	14.3	< 0.99	< 0.56	< 0.60	< 0.10	0.54 ± 0.18
RX J0044.2+4206	273-	0	44	14.9	42	6	34	12	1	12.0	< 1.88	< 0.62	1.25 ± 0.36	< 0.51	1.00 ± 0.31
RX J0044.2+4208		0	44	13.7	42	8	44	11	1	10.1	< 1.46	< 0.66	< 1.08	< 0.82	< 0.91
RX J0044.2+4214		0	44	13.8	42	14	4	11	1	17.4	< 3.01	< 1.14	1.48 ± 0.47	< 0.53	1.35 ± 0.41
RX J0044.3+4134		0	44	20.2	41	34	12	10	1	10.2	0.98 ± 0.28	< 0.74	< 0.63	< 0.22	< 0.44
RX J0044.3+4136	277	0	44	20.2	41	36	52	5	1	15.6	1.16 ± 0.29	< 0.58	< 0.53	< 0.37	< 0.19
∼RX J0044.3+4145	278-	0	44	22.3	41	45	7	8	1	86.4	3.07 ± 0.42	< 0.60	2.40 ± 0.32	0.73 ± 0.18	1.65 ± 0.26
RX J0044.3+4228	276	0	44	18.6	42	28	51	5	2	20.6	3.08 ± 0.87	1.04 ± 0.59	1.77 ± 0.54	0.98 ± 0.43	0.82 ± 0.34
RX J0044.4+4115		0	44	29.5	41	15	31	14	1	11.2	< 1.92	< 0.41	1.08 ± 0.29	< 0.98	< 0.43
∼[d]RX J0044.4+4121	282+	0	44	29.4	41	21	36	5	1	2135.4	29.77 ± 1.12	2.51 ± 0.37	26.14 ± 1.01	8.06 ± 0.55	16.52 ± 0.78
RX J0044.4+4131	279+	0	44	24.9	41	31	49	5	1	43.9	1.56 ± 0.31	< 0.12	1.32 ± 0.26	0.24 ± 0.13	1.12 ± 0.23
[d]RX J0044.4+4136	281+	0	44	25.6	41	36	28	5	1	113.2	3.26 ± 0.41	< 0.12	3.37 ± 0.36	1.57 ± 1.25	< 1.59
RX J0044.4+4200	280+	0	44	25.0	42	0	5	5	1	13.7	1.17 ± 0.31	0.45 ± 0.28	0.62 ± 0.04	< 0.50	< 0.13
RX J0044.5+4207		0	44	31.8	42	7	31	10	1	10.2	< 1.47	< 0.81	< 0.78	< 0.23	0.49 ± 0.18
RX J0044.5+4210		0	44	35.7	42	10	47	12	1	10.1	< 1.52	< 0.62	< 1.18	< 0.46	< 0.86
†RX J0044.6+4041	285	0	44	37.6	40	41	9	8	2	18.1	3.84 ± 1.16	< 0.10	3.50 ± 1.09	1.39 ± 0.15	2.56 ± 1.21
[e]RX J0044.6+4125	284	0	44	36.3	41	25	15	7	1	20.3	1.51 ± 0.33	0.62 ± 0.35	1.01 ± 0.10	0.44 ± 0.39	< 0.53
RX J0044.6+4145		0	44	36.7	41	45	8	10	1	13.6	< 0.79	< 0.36	< 0.82	< 0.15	0.51 ± 0.15
RX J0044.6+4152	283	0	44	36.1	41	52	24	5	1	12.0	0.78 ± 0.25	< 0.11	0.59 ± 0.20	0.43 ± 0.24	0.28 ± 0.04
RX J0044.7+4113		0	44	42.0	41	13	42	10	1	11.2	< 1.05	< 0.60	< 0.64	< 0.14	0.51 ± 0.18
RX J0044.7+4122	287-	0	44	47.5	41	22	52	8	1	36.7	1.51 ± 0.33	< 0.35	1.24 ± 0.25	0.48 ± 0.16	0.74 ± 0.19
†RX J0044.7+4242	286+	0	44	44.1	42	42	53	5	2	80.9	3.94 ± 1.13	< 0.06	4.06 ± 1.18	< 1.23	< 2.43
RX J0044.8+4117		0	44	52.0	41	17	11	10	1	13.5	< 1.01	< 0.30	0.60 ± 0.19	< 0.29	0.41 ± 0.15
RX J0044.8+4127	289-	0	44	52.0	41	27	17	7	1	116.2	2.94 ± 0.38	< 0.36	2.24 ± 0.30	0.41 ± 0.14	1.79 ± 0.26
[e]RX J0044.8+4129	288+	0	44	49.7	41	29	6	5	1	34.6	2.42 ± 0.41	0.55 ± 0.39	1.78 ± 0.06	0.47 ± 0.26	< 1.28
∼RX J0044.8+4225		0	44	52.0	42	25	10	9	1	24.3	4.85 ± 1.11	< 1.41	3.04 ± 0.77	< 1.72	1.91 ± 0.60
[a]RX J0044.8+4229		0	44	48.2	42	29	54	12	1	11.2	< 5.17	< 1.95	< 4.17	2.83 ± 1.01	< 0.67
RX J0044.9+4059	293-	0	44	56.5	40	59	11	8	1	58.1	3.12 ± 0.65	< 0.56	2.78 ± 0.53	1.11 ± 0.34	1.64 ± 0.41
RX J0044.9+4123		0	44	57.4	41	23	38	7	1	62.2	1.80 ± 0.34	< 0.22	1.66 ± 0.28	0.48 ± 0.16	1.18 ± 0.23
RX J0044.9+4134	291-	0	44	55.1	41	34	38	10	1	16.5	< 1.12	< 0.42	0.54 ± 0.17	< 0.14	0.55 ± 0.16
RX J0044.9+4159	292+	0	44	57.0	41	59	35	5	1	268.0	6.30 ± 0.51	1.96 ± 0.36	4.88 ± 0.42	2.08 ± 0.36	2.66 ± 0.20
RX J0044.9+4229	290	0	44	54.5	42	29	53	11	2	36.1	3.51 ± 0.68	1.39 ± 0.50	2.09 ± 0.45	1.06 ± 0.31	0.87 ± 0.28
RX J0045.0+4114		0	45	0.4	41	14	38	10	1	11.9	< 1.50	< 0.58	0.63 ± 0.21	< 0.25	0.46 ± 0.17
RX J0045.0+4126		0	45	0.8	41	26	48	10	1	11.2	< 0.87	< 0.25	0.52 ± 0.17	< 0.37	< 0.38
RX J0045.1+4100	293-	0	45	10.1	41	0	15	12	1	12.9	2.17 ± 0.62	< 1.76	1.05 ± 0.37	< 0.53	0.67 ± 0.28
RX J0045.1+4145	296-	0	45	10.4	41	45	53	8	1	29.1	1.59 ± 0.34	< 1.17	1.14 ± 0.24	< 0.79	0.78 ± 0.18
[a]RX J0045.1+4202	295+	0	45	9.8	42	2	36	5	1	30.3	1.58 ± 0.31	0.43 ± 0.26	0.99 ± 0.11	< 0.63	< 0.56
RX J0045.1+4215	294+	0	45	9.1	42	15	47	5	1	285.2	8.77 ± 0.71	0.53 ± 0.31	7.88 ± 0.61	2.94 ± 0.36	4.51 ± 0.45
RX J0045.2+4123	299	0	45	17.2	41	23	15	7	1	10.5	1.03 ± 0.36	< 0.18	0.89 ± 0.33	0.26 ± 0.18	0.55 ± 0.24
[e]RX J0045.2+4136	297-	0	45	13.2	41	36	11	8	1	33.7	1.49 ± 0.31	< 0.71	1.03 ± 0.21	0.66 ± 0.17	0.35 ± 0.13
[a]RX J0045.2+4217		0	45	17.1	42	17	10	10	1	11.0	< 1.86	< 0.98	< 0.91	< 0.21	0.47 ± 0.19
RX J0045.2+4220	298-	0	45	12.3	42	20	26	9	1	16.8	< 1.83	< 0.44	1.18 ± 0.36	< 0.73	0.64 ± 0.25
RX J0045.3+4232	300	0	45	21.4	42	32	36	18	2	10.2	0.92 ± 0.53	< 0.20	0.69 ± 0.32	0.38 ± 0.20	0.29 ± 0.24
RX J0045.4+4120		0	45	28.0	41	20	37	8	1	39.3	1.57 ± 0.36	< 0.33	1.32 ± 0.28	< 0.39	1.03 ± 0.24
RX J0045.4+4129	306-	0	45	27.8	41	29	38	7	1	126.7	3.68 ± 0.46	< 0.49	2.93 ± 0.37	0.87 ± 0.21	2.05 ± 0.31
[d]RX J0045.4+4132	302-	0	45	26.5	41	32	45	8	1	50.7	1.81 ± 0.35	< 0.22	1.77 ± 0.29	0.45 ± 0.15	1.41 ± 0.25
RX J0045.4+4138	305+	0	45	28.2	41	38	56	5	1	23.4	1.61 ± 0.34	< 0.14	1.25 ± 0.17	0.45 ± 0.22	< 1.06
[e]RX J0045.4+4146		0	45	28.3	41	46	4	10	1	11.2	< 1.21	< 1.47	< 0.48	< 0.11	0.36 ± 0.13
RX J0045.4+4154		0	45	28.7	41	54	6	6	1	2703.3	29.63 ± 0.98	2.87 ± 0.37	23.80 ± 0.85	18.78 ± 0.75	4.91 ± 0.39
RX J0045.4+4156	303	0	45	27.4	41	56	30	5	1	26.6	1.25 ± 0.29	0.56 ± 0.41	< 0.69	< 0.07	< 0.56
RX J0045.4+4200	301	0	45	26.9	42	0	27	5	1	26.0	0.95 ± 0.27	< 0.12	0.69 ± 0.19	0.18 ± 0.11	0.64 ± 0.20

[a] Foreground star [b] Galaxy [c] Supersoft source candidate [d] Globular cluster [e] SNR
⋆ bulge source ∼ Variable source (ref. Tables 2, 3 and footnote in Sect. 4.1.1) † Source with uncertain count rate.

RXJ No. (1)	SI No. (2)	R.A. (h) (3)	(m) (4)	(J2000) (s) (5)	Dec. (°) (6)	(′) (7)	(″) (8)	$\sigma_{\rm Pos}$ (″) (9)	Cl. (10)	Maxlik (LH) (11)	Rate (B) ($ct \cdot ks^{-1}$) (12)	Rate (S) ($ct \cdot ks^{-1}$) (13)	Rate (H) ($ct \cdot ks^{-1}$) (14)	Rate (H_1) ($ct \cdot ks^{-1}$) (15)	Rate (H_2) ($ct \cdot ks^{-1}$) (16)
RX J0045.4+4210	304-	0	45	27.4	42	10	56	9	1	27.5	< 1.69	< 0.26	1.18 ± 0.27	< 0.58	0.88 ± 0.22
RX J0045.4+4219	307	0	45	29.8	42	19	8	7	1	11.8	1.19 ± 0.33	0.35 ± 0.25	0.79 ± 0.20	0.67 ± 0.16	0.21 ± 0.15
RX J0045.5+4156	311	0	45	35.0	41	56	1	5	1	17.8	0.62 ± 0.22	< 0.06	< 0.47	< 0.05	< 0.49
RX J0045.5+4201		0	45	30.4	42	1	45	11	1	10.0	< 0.76	< 0.38	< 0.50	< 0.12	0.37 ± 0.13
RX J0045.5+4201	308	0	45	32.0	42	1	19	5	1	18.5	0.72 ± 0.24	< 0.07	0.64 ± 0.23	0.22 ± 0.08	0.45 ± 0.23
[c]RX J0045.5+4207	309-	0	45	31.8	42	7	6	8	1	147.7	7.75 ± 0.69	7.41 ± 0.66	< 0.45	< 0.32	< 0.18
[a]RX J0045.5+4210	310	0	45	33.0	42	10	54	5	1	12.5	1.61 ± 0.35	0.73 ± 0.37	< 0.88	< 0.48	< 0.46
RX J0045.5+4217	313-	0	45	34.5	42	17	55	9	1	22.9	< 1.36	< 0.37	0.90 ± 0.28	< 0.20	0.90 ± 0.26
RX J0045.5+4227		0	45	32.6	42	27	48	11	1	13.3	< 3.12	< 3.44	1.30 ± 0.50	< 0.34	1.16 ± 0.45
RX J0045.6+4042	314	0	45	40.0	40	42	35	11	3	15.3	< 0.15	< 0.13	0.04 ± 0.02	< 0.02	< 0.02
RX J0045.6+4119	315-	0	45	38.2	41	19	30	10	1	21.6	< 1.57	< 0.38	1.12 ± 0.29	< 0.59	0.69 ± 0.22
RX J0045.6+4127		0	45	41.1	41	27	49	8	1	34.3	1.58 ± 0.36	< 1.21	1.13 ± 0.25	< 0.62	0.67 ± 0.19
∼RX J0045.6+4208	316-	0	45	40.2	42	8	5	6	1	1122.7	25.83 ± 1.11	11.23 ± 0.79	13.77 ± 0.77	6.70 ± 0.54	7.01 ± 0.55
RX J0045.6+4212		0	45	38.3	42	12	39	10	1	11.8	1.43 ± 0.40	< 0.98	0.64 ± 0.21	< 0.25	0.50 ± 0.18
RX J0045.6+4231		0	45	38.1	42	31	53	12	1	10.5	4.59 ± 1.40	< 3.50	< 3.01	< 2.07	< 1.30
†RX J0045.6+4241	312+	0	45	36.3	42	41	56	9	2	60.0	3.92 ± 0.84	< 0.19	3.45 ± 0.75	0.97 ± 0.20	2.83 ± 0.81
RX J0045.7+4120	315-	0	45	42.9	41	20	25	8	1	51.6	2.18 ± 0.44	< 0.50	1.78 ± 0.34	0.92 ± 0.24	0.83 ± 0.23
RX J0045.7+4123		0	45	42.1	41	23	52	9	1	19.5	< 1.13	< 0.24	0.86 ± 0.24	< 0.66	< 0.56
∼[d]RX J0045.7+4139	318-	0	45	45.4	41	39	37	5	1	17930.	134.43 ± 1.96	4.71 ± 0.47	133.47 ± 2.10	38.77 ± 1.15	95.71 ± 1.82
RX J0045.7+4158	317	0	45	44.8	41	58	56	5	1	27.3	1.07 ± 0.27	< 0.10	0.90 ± 0.15	0.23 ± 0.13	0.65 ± 0.06
RX J0045.7+4223		0	45	42.6	42	23	28	10	1	13.1	2.01 ± 0.60	< 1.43	0.93 ± 0.34	< 0.32	0.74 ± 0.28
RX J0045.8+4136	319	0	45	49.6	41	36	3	10	1	23.4	0.74 ± 0.35	0.72 ± 0.32	< 0.05	< 0.03	< 0.03
RX J0045.8+4237	320	0	45	53.4	42	37	33	5	2	12.9	0.79 ± 0.56	< 0.44	0.41 ± 0.31	0.10 ± 0.04	< 0.25
RX J0045.9+4148	322+	0	45	56.8	41	48	33	5	1	170.9	3.26 ± 0.39	0.35 ± 0.29	3.17 ± 0.32	0.24 ± 0.12	2.44 ± 0.24
[a]RX J0045.9+4156	321+	0	45	56.3	41	56	39	5	1	29.7	1.83 ± 0.33	1.67 ± 0.32	0.24 ± 0.12	0.17 ± 0.10	< 0.06
[a]RX J0045.9+4203	323-	0	45	57.6	42	3	10	8	1	65.3	3.03 ± 0.42	< 1.50	1.89 ± 0.28	0.83 ± 0.19	1.06 ± 0.21
RX J0045.9+4212		0	45	56.0	42	12	32	9	1	20.2	1.39 ± 0.39	< 2.41	0.91 ± 0.25	< 0.28	0.72 ± 0.21
[a]RX J0045.9+4226	324+	0	45	58.7	42	26	52	5	1	59.4	2.59 ± 0.43	0.42 ± 0.27	2.01 ± 0.30	0.68 ± 0.24	1.67 ± 0.26
RX J0046.0+4133		0	46	0.2	41	33	10	10	1	17.5	1.06 ± 0.31	< 0.37	0.79 ± 0.22	< 0.46	0.47 ± 0.16
[a]RX J0046.0+4136	325	0	46	1.0	41	36	55	11	1	20.9	0.33 ± 0.32	< 0.24	< 0.10	< 0.06	< 0.03
RX J0046.0+4141	327	0	46	5.6	41	41	41	8	1	20.3	1.39 ± 0.35	0.82 ± 0.25	0.40 ± 0.17	< 0.24	< 0.23
RX J0046.0+4151	326+	0	46	4.8	41	51	47	5	1	17.3	0.71 ± 0.25	< 0.14	< 0.59	< 0.07	< 0.53
RX J0046.0+4220	328	0	46	5.8	42	20	32	5	1	11.0	0.86 ± 0.28	< 0.32	< 0.61	< 0.35	< 0.25
RX J0046.1+4136	330	0	46	10.1	41	36	26	9	1	10.2	< 0.25	< 0.06	0.18 ± 0.09	< 0.18	< 0.03
RX J0046.1+4154	329	0	46	9.4	41	54	37	5	1	10.5	0.72 ± 0.27	0.52 ± 0.24	0.23 ± 0.15	0.02 ± 0.01	0.21 ± 0.15
RX J0046.1+4158	334-	0	46	11.6	41	58	58	10	1	15.2	< 1.21	< 0.42	0.53 ± 0.16	< 0.15	0.49 ± 0.14
RX J0046.1+4203	331-	0	46	10.9	42	3	53	9	1	40.7	1.67 ± 0.35	< 0.37	1.28 ± 0.25	< 0.54	0.88 ± 0.19
RX J0046.1+4208	332+	0	46	11.9	42	8	30	5	1	123.3	3.84 ± 0.45	0.96 ± 0.33	2.64 ± 0.27	0.78 ± 0.23	1.98 ± 0.16
RX J0046.2+4124	337-	0	46	15.7	41	24	9	13	1	11.6	< 1.29	< 0.46	1.00 ± 0.32	< 0.73	< 0.55
[c]RX J0046.2+4138	341	0	46	17.8	41	38	48	9	1	28.1	1.12 ± 0.40	0.99 ± 0.37	< 0.05	< 0.03	< 0.02
RX J0046.2+4143	339	0	46	16.4	41	43	9	12	1	15.8	1.36 ± 0.35	0.57 ± 0.38	< 0.80	< 0.44	< 0.31
[c]RX J0046.2+4144	335	0	46	15.6	41	44	36	5	1	51.2	2.15 ± 0.39	1.92 ± 0.35	< 0.07	< 0.02	< 0.07
RX J0046.2+4150	333+	0	46	13.4	41	50	48	5	1	32.8	1.48 ± 0.31	0.57 ± 0.30	0.97 ± 0.13	0.25 ± 0.15	< 0.62
[a]RX J0046.2+4154	338	0	46	16.3	41	54	19	5	1	13.0	0.78 ± 0.26	< 0.19	< 0.48	< 0.13	< 0.38
RX J0046.2+4205	340	0	46	17.2	42	5	11	5	1	27.5	2.37 ± 0.41	0.51 ± 0.26	1.84 ± 0.31	0.50 ± 0.17	1.36 ± 0.27
RX J0046.2+4221	336+	0	46	16.0	42	21	38	5	1	24.5	1.27 ± 0.31	0.40 ± 0.23	0.73 ± 0.15	< 0.07	0.83 ± 0.15
RX J0046.3+4201	344	0	46	19.2	42	1	28	5	1	28.0	2.22 ± 0.41	0.66 ± 0.29	1.68 ± 0.33	0.30 ± 0.13	1.17 ± 0.25
RX J0046.3+4214	345-	0	46	19.9	42	14	36	9	1	13.2	< 0.89	< 0.24	0.70 ± 0.22	< 0.47	< 0.53
RX J0046.3+4225	343	0	46	19.0	42	25	34	5	1	21.1	1.33 ± 0.31	0.49 ± 0.27	0.82 ± 0.14	0.24 ± 0.15	< 0.62
RX J0046.3+4238	342	0	46	18.2	42	38	33	5	2	28.3	3.10 ± 0.64	0.94 ± 0.49	2.03 ± 0.38	1.41 ± 0.28	0.72 ± 0.29
RX J0046.4+4116		0	46	25.6	41	16	30	13	1	16.0	2.42 ± 0.73	< 1.76	1.83 ± 0.54	< 1.30	< 1.23
RX J0046.4+4155	347	0	46	24.2	41	55	30	5	1	15.1	1.17 ± 0.29	0.35 ± 0.25	0.67 ± 0.06	0.31 ± 0.22	< 0.46
∼[d]RX J0046.4+4201	349-	0	46	26.7	42	1	51	6	1	3781.8	37.64 ± 1.15	< 1.28	34.53 ± 1.06	10.53 ± 0.59	24.08 ± 0.88
∼RX J0046.4+4204	348-	0	46	24.2	42	4	38	6	1	1690.2	33.17 ± 1.16	< 0.71	29.36 ± 1.02	6.85 ± 0.50	22.29 ± 0.88
RX J0046.4+4209	346-	0	46	24.3	42	9	53	9	1	29.4	1.79 ± 0.42	< 1.12	2.45 ± 0.46	< 0.48	1.16 ± 0.27
RX J0046.5+4207		0	46	34.1	42	7	29	10	1	15.3	< 1.44	< 0.47	0.70 ± 0.20	< 1.24	0.52 ± 0.17

[a] Foreground star [b] Galaxy [c] Supersoft source candidate [d] Globular cluster [e] SNR
⋆ bulge source ∼ Variable source (ref. Tables 2, 3 and footnote in Sect. 4.1.1) † Source with uncertain count rate.

RXJ No. (1)	SI No. (2)	R.A. (h) (3)	(m) (4)	(J2000) (s) (5)	Dec. (°) (6)	(′) (7)	(″) (8)	$\sigma_{\rm Pos}$ (″) (9)	Cl. (10)	Maxlik (LH) (11)	Rate (B) ($ct \cdot ks^{-1}$) (12)	Rate (S) ($ct \cdot ks^{-1}$) (13)	Rate (H) ($ct \cdot ks^{-1}$) (14)	Rate (H_1) ($ct \cdot ks^{-1}$) (15)	Rate (H_2) ($ct \cdot ks^{-1}$) (16)
†RX J0046.5+4244	350+	0	46	31.7	42	44	42	14	2	15.8	< 0.44	< 0.03	0.43 ± 0.25	< 0.13	< 0.29
RX J0046.6+4129		0	46	36.6	41	29	0	11	1	12.7	< 1.45	< 0.52	0.80 ± 0.27	< 0.57	< 0.60
RX J0046.6+4146		0	46	38.0	41	46	17	11	1	11.5	< 0.92	< 0.42	< 0.61	< 0.12	0.40 ± 0.14
[a]RX J0046.6+4225	351+	0	46	40.3	42	25	19	5	1	48.2	1.95 ± 0.34	0.50 ± 0.27	1.44 ± 0.19	0.52 ± 0.21	< 0.90
RX J0046.7+4149		0	46	46.9	41	49	8	10	1	12.6	< 1.14	< 0.47	0.59 ± 0.19	< 0.58	< 0.40
[b]RX J0046.7+4208	353+	0	46	47.9	42	8	53	5	1	63.5	1.94 ± 0.34	0.29 ± 0.25	1.56 ± 0.20	0.44 ± 0.19	1.36 ± 0.13
[a]RX J0046.7+4230	352-	0	46	44.8	42	30	38	10	1	16.7	< 5.19	< 1.39	2.76 ± 0.84	< 2.21	< 1.66
RX J0046.8+4219	354	0	46	52.8	42	19	45	5	1	13.6	1.07 ± 0.28	0.31 ± 0.23	0.81 ± 0.17	0.30 ± 0.18	< 0.41
RX J0046.9+4152		0	46	56.8	41	52	33	9	1	33.3	0.98 ± 0.29	< 0.27	0.83 ± 0.21	< 0.12	0.87 ± 0.20
RX J0046.9+4220	355+	0	46	55.7	42	20	46	5	1	1749.8	19.39 ± 0.88	1.11 ± 0.27	17.52 ± 0.80	6.07 ± 0.47	10.78 ± 0.61
RX J0047.0+4141		0	47	0.8	41	41	7	10	1	19.0	< 1.47	< 0.40	0.98 ± 0.27	0.65 ± 0.22	< 0.46
RX J0047.0+4151		0	47	1.0	41	51	24	9	1	23.7	1.21 ± 0.33	< 0.48	0.88 ± 0.22	< 0.29	0.70 ± 0.19
[a]RX J0047.0+4157	356+	0	47	3.2	41	57	55	8	1	17.9	1.79 ± 0.43	0.95 ± 0.31	0.71 ± 0.26	0.64 ± 0.24	< 0.08
[a]RX J0047.0+4201	358	0	47	3.7	42	1	47	15	1	10.5	0.90 ± 0.33	0.85 ± 0.32	< 0.07	< 0.06	< 0.01
RX J0047.0+4204	357-	0	47	3.4	42	4	55	8	1	43.7	1.89 ± 0.37	< 0.53	1.39 ± 0.27	< 0.58	1.05 ± 0.23
RX J0047.0+4222	359	0	47	5.6	42	22	18	8	1	14.5	0.47 ± 0.24	< 0.04	0.46 ± 0.11	< 0.33	< 0.14
RX J0047.1+4218	360	0	47	8.6	42	18	11	5	1	18.1	0.94 ± 0.27	0.39 ± 0.31	< 0.59	< 0.10	< 0.50
RX J0047.2+4135	365-	0	47	16.2	41	35	46	12	1	16.9	< 1.90	< 0.53	1.42 ± 0.38	< 0.78	0.77 ± 0.27
RX J0047.2+4140	363-	0	47	15.4	41	40	41	9	1	40.0	1.81 ± 0.45	< 0.36	1.94 ± 0.39	0.70 ± 0.25	1.18 ± 0.30
RX J0047.2+4158	364	0	47	17.0	41	58	19	11	1	13.4	0.93 ± 0.40	0.86 ± 0.39	< 0.16	< 0.07	0.09 ± 0.03
[a]RX J0047.2+4202	362-	0	47	13.8	42	2	13	8	1	68.9	3.67 ± 0.50	1.47 ± 0.37	1.93 ± 0.32	0.83 ± 0.22	1.10 ± 0.24
RX J0047.2+4220	361+	0	47	14.2	42	20	39	5	1	62.4	2.51 ± 0.38	0.45 ± 0.27	2.08 ± 0.27	0.76 ± 0.25	1.29 ± 0.10
RX J0047.2+4221	366	0	47	17.9	42	21	16	5	1	46.3	1.75 ± 0.34	0.59 ± 0.28	1.30 ± 0.23	0.53 ± 0.21	0.71 ± 0.07
RX J0047.3+4148		0	47	20.1	41	48	37	10	1	18.0	1.93 ± 0.46	< 3.26	0.85 ± 0.25	< 0.45	0.60 ± 0.21
RX J0047.4+4124		0	47	27.8	41	24	40	13	1	12.8	< 5.97	< 1.65	3.64 ± 1.34	< 1.07	3.01 ± 1.23
∼RX J0047.4+4152		0	47	26.9	41	52	53	9	1	52.7	3.35 ± 0.54	< 0.88	2.49 ± 0.40	1.00 ± 0.26	1.48 ± 0.30
RX J0047.4+4208	368	0	47	24.2	42	8	44	5	1	22.6	1.35 ± 0.30	0.47 ± 0.26	0.76 ± 0.07	0.38 ± 0.28	< 0.52
RX J0047.4+4213	370	0	47	26.3	42	13	47	5	1	16.2	0.55 ± 0.22	< 0.12	0.42 ± 0.19	< 0.05	0.38 ± 0.17
[a]RX J0047.4+4220	372	0	47	28.7	42	20	53	5	1	13.9	0.61 ± 0.24	< 0.29	< 0.34	< 0.03	< 0.28
[a]RX J0047.4+4221	369+	0	47	26.2	42	21	52	5	1	192.2	4.45 ± 0.46	0.80 ± 0.28	3.71 ± 0.38	1.90 ± 0.19	1.45 ± 0.29
RX J0047.4+4230	371	0	47	27.3	42	30	21	7	1	17.5	2.08 ± 0.42	0.85 ± 0.35	1.03 ± 0.16	0.55 ± 0.38	< 0.68
RX J0047.4+4248	367	0	47	24.1	42	48	32	35	2	19.4	< 0.12	< 0.02	0.10 ± 0.07	< 0.02	< 0.07
RX J0047.5+4135		0	47	31.4	41	35	24	12	1	12.0	< 1.73	< 0.45	1.17 ± 0.40	< 1.00	< 0.68
RX J0047.5+4140		0	47	30.9	41	40	42	11	1	10.3	< 2.17	< 1.21	< 0.84	< 0.52	< 0.38
RX J0047.5+4149	373-	0	47	30.6	41	49	24	8	1	81.3	4.39 ± 0.63	< 4.52	2.97 ± 0.46	0.95 ± 0.27	2.11 ± 0.38
†RX J0047.6+4132	374	0	47	36.0	41	32	8	8	2	12.4	< 0.32	0.04 ± 0.01	< 0.25	< 0.27	< 0.02
[c]RX J0047.6+4205	376	0	47	38.5	42	5	7	10	1	12.9	1.05 ± 0.36	0.99 ± 0.35	< 0.04	< 0.02	< 0.02
RX J0047.6+4208	375	0	47	36.5	42	8	42	5	1	15.0	0.85 ± 0.29	0.28 ± 0.27	0.54 ± 0.07	< 0.08	< 0.50
RX J0047.7+4159	377	0	47	42.3	42	0	0	12	1	11.8	1.23 ± 0.44	1.15 ± 0.41	< 0.12	< 0.07	< 0.05
[a]RX J0047.7+4201	381-	0	47	43.2	42	1	19	9	1	24.6	1.48 ± 0.41	< 0.54	1.19 ± 0.30	0.60 ± 0.21	0.67 ± 0.23
RX J0047.7+4202	382+	0	47	44.5	42	2	46	9	1	19.3	0.75 ± 0.35	< 0.06	0.62 ± 0.31	0.18 ± 0.05	0.55 ± 0.36
RX J0047.7+4210	380	0	47	42.6	42	10	17	5	1	21.6	1.21 ± 0.30	< 0.23	0.98 ± 0.13	< 0.53	< 0.51
RX J0047.7+4211		0	47	45.0	42	11	3	11	1	10.9	< 2.25	< 1.47	1.22 ± 0.40	< 0.74	0.75 ± 0.29
RX J0047.7+4211	378	0	47	42.5	42	11	40	5	1	15.3	1.41 ± 0.34	0.58 ± 0.32	< 0.71	< 0.44	< 0.38
RX J0047.7+4222		0	47	44.5	42	22	37	5	1	15.8	< 6.19	< 1.70	7.36 ± 1.60	< 3.10	< 2.63
RX J0047.7+4222	379+	0	47	42.5	42	22	22	5	1	63.7	2.20 ± 0.38	< 0.14	1.95 ± 0.28	0.72 ± 0.24	1.34 ± 0.18
RX J0047.7+4224	383+	0	47	45.4	42	24	28	5	1	70.4	3.34 ± 0.48	0.99 ± 0.38	2.54 ± 0.33	0.84 ± 0.26	1.53 ± 0.16
RX J0047.8+4135		0	47	53.9	41	35	38	16	1	11.8	< 3.40	3.07 ± 0.94	< 0.45	< 0.27	< 0.36
∼RX J0047.8+4142		0	47	49.9	41	42	9	11	1	41.4	7.02 ± 1.15	< 1.63	13.74 ± 1.37	4.06 ± 0.78	7.97 ± 1.05
RX J0047.8+4153		0	47	49.4	41	53	26	10	1	16.9	< 1.13	< 0.31	0.89 ± 0.28	< 0.24	0.78 ± 0.25
RX J0047.8+4207		0	47	51.7	42	7	24	9	1	19.9	2.46 ± 0.59	< 3.90	1.23 ± 0.36	0.80 ± 0.28	< 0.69
RX J0047.8+4219	384+	0	47	48.4	42	19	25	5	1	399.2	7.87 ± 0.62	0.78 ± 0.31	7.85 ± 0.60	1.63 ± 0.27	5.02 ± 0.43
RX J0048.0+4140	385-	0	48	0.3	41	40	15	7	1	442.6	27.75 ± 2.07	< 3.14	25.92 ± 1.97	10.22 ± 1.22	16.23 ± 1.58
RX J0048.0+4156		0	48	4.2	41	56	48	10	1	13.1	2.11 ± 0.58	< 1.74	< 0.85	< 0.56	< 0.37
RX J0048.0+4218	386	0	48	4.6	42	18	6	9	1	16.4	1.24 ± 0.37	0.48 ± 0.28	0.65 ± 0.19	0.26 ± 0.18	0.50 ± 0.12
†RX J0048.1+4149	387	0	48	6.8	41	49	56	6	2	18.8	1.01 ± 0.79	0.21 ± 0.07	< 0.68	< 0.32	< 0.38

[a] Foreground star   [b] Galaxy   [c] Supersoft source candidate   [d] Globular cluster   [e] SNR
$\star$ bulge source $\sim$ Variable source (ref. Tables 2, 3 and footnote in Sect. 4.1.1)   † Source with uncertain count rate.

RXJ No. (1)	SI No. (2)	R.A. (J2000) (h) (3)	(m) (4)	(s) (5)	Dec. (°) (6)	(′) (7)	(″) (8)	$\sigma_{\rm Pos}$ (″) (9)	Cl. (10)	Maxlik (LH) (11)	Rate (B) ($ct \cdot ks^{-1}$) (12)	Rate (S) ($ct \cdot ks^{-1}$) (13)	Rate (H) ($ct \cdot ks^{-1}$) (14)	Rate (H_1) ($ct \cdot ks^{-1}$) (15)	Rate (H_2) ($ct \cdot ks^{-1}$) (16)
†RX J0048.3+4134	388	0	48	19.1	41	34	37	36	2	63.8	4.94 ± 1.15	< 0.61	4.09 ± 0.84	0.76 ± 0.39	3.68 ± 0.83
RX J0048.3+4210	389+	0	48	23.7	42	10	25	6	1	18.2	0.84 ± 0.37	0.15 ± 0.14	0.69 ± 0.35	< 0.10	0.63 ± 0.34
$\sim$[a]RX J0048.4+4157	390-	0	48	24.6	41	57	18	6	1	614.1	35.30 ± 2.16	21.89 ± 1.77	14.28 ± 1.31	8.11 ± 0.99	6.24 ± 0.87
†RX J0048.4+4203	391	0	48	28.4	42	3	10	10	2	22.4	0.58 ± 0.49	0.02 ± 0.01	0.59 ± 0.52	< 0.18	< 0.43
RX J0048.9+4223	392-	0	48	58.4	42	23	47	9	4	250.2	9.21 ± 0.99	< 0.52	15.95 ± 1.07	6.21 ± 0.69	9.84 ± 0.81
†RX J0049.1+4200	393	0	49	6.7	42	0	7	16	2	32.4	0.70 ± 0.65	0.13 ± 0.02	< 0.60	< 0.24	< 0.38
†RX J0049.2+4254	394	0	49	13.5	42	54	1	11	3	14.6	< 0.09	0.02 ± 0.01	< 0.07	< 0.00	< 0.06
RX J0049.5+4158		0	49	30.6	41	58	23	13	1	22.1	6.87 ± 2.29	< 1.91	6.12 ± 1.85	< 2.66	< 5.62
RX J0049.5+4211	395	0	49	35.8	42	11	48	8	2	16.4	1.90 ± 0.85	< 0.21	1.41 ± 0.44	0.55 ± 0.41	1.12 ± 0.31
RX J0049.7+4220	396	0	49	45.1	42	20	9	27	2	11.6	3.68 ± 1.03	1.59 ± 0.66	1.80 ± 0.68	0.50 ± 0.43	1.47 ± 0.61

Table 7. Table of the identifications of ROSAT PSPC sources with *Einstein* sources listed by TF. $F_{\rm R}$ gives the ROSAT source flux using the *Einstein* spectral model of TF and $F_{\rm E}$ gives the *Einstein* source flux of the correlated *Einstein* source (see Sect. 4.1.2). The distance between two correlating sources is given in arcseconds ($''$) as well as in units of the combined positional error (σ) of both sources. The last column gives the flux ratio between the ROSAT and the *Einstein* measurements, showing possible long term variabilities between the epochs of the two observations. Sources with ROSAT numbers preceeded by a $\star$ belong to the bulge region.

ROSAT No.	$F_{\rm R}$ ($\times 10^{13}$) (cgs)	*Einstein* No.	$F_{\rm E}$ ($\times 10^{13}$) (cgs)	Distance ($''$)	Distance (σ)	$F_{\rm R}/F_{\rm E}$
RX J0039.4+4035	0.17 ± 0.06	1	0.60 ± 0.26	59.1	1.31	0.28 ± 0.16
RX J0040.0+4031	1.04 ± 0.10	2	1.64 ± 0.42	31.7	0.70	0.63 ± 0.17
RX J0040.2+4050	31.64 ± 0.48	3	25.38 ± 2.50	3.6	0.59	1.25 ± 0.12
RX J0040.3+4043	13.82 ± 0.29	4	16.35 ± 2.09	3.4	0.58	0.85 ± 0.11
RX J0040.4+4029	1.07 ± 0.10	5	0.99 ± 0.28	13.4	0.30	1.08 ± 0.33
RX J0040.4+4129	2.30 ± 0.41	6	1.06 ± 0.35	9.5	0.20	2.17 ± 0.81
RX J0040.7+4051	0.49 ± 0.07	7	0.66 ± 0.26	6.0	0.13	0.74 ± 0.30
RX J0041.4+4058	1.94 ± 0.12	8	1.77 ± 0.50	24.6	0.54	1.09 ± 0.32
RX J0041.7+4134	14.38 ± 0.49	9	8.72 ± 1.08	1.8	0.29	1.65 ± 0.21
RX J0041.8+4021	24.25 ± 0.76	11	15.54 ± 0.88	5.4	0.12	1.56 ± 0.10
RX J0041.8+4113	0.43 ± 0.09	10	0.90 ± 0.24	32.9	0.73	0.48 ± 0.16
RX J0042.2+4019	40.38 ± 1.23	15	48.83 ± 1.61	2.9	0.06	0.83 ± 0.04
RX J0042.2+4039	2.18 ± 0.19	13	1.64 ± 0.38	18.4	0.41	1.33 ± 0.33
RX J0042.2+4055	2.71 ± 0.18	18	1.67 ± 0.48	1.9	0.32	1.62 ± 0.48
RX J0042.2+4101	9.53 ± 0.32	16	3.88 ± 0.75	0.7	0.12	2.46 ± 0.48
RX J0042.2+4112	9.04 ± 0.25	19	4.26 ± 0.54	8.0	1.37	2.12 ± 0.28
RX J0042.2+4117	2.18 ± 0.16	17	1.26 ± 0.38	5.0	0.86	1.73 ± 0.54
RX J0042.2+4118	9.71 ± 0.32	14	3.23 ± 0.51	9.5	1.63	3.01 ± 0.49
$\star$RX J0042.3+4113	5.02 ± 0.23	20	4.93 ± 0.54	9.1	1.55	1.02 ± 0.12
$\star$RX J0042.3+4115	16.06 ± 0.41	23	6.88 ± 0.61	1.0	0.17	2.33 ± 0.21
RX J0042.4+4104	4.78 ± 0.22	28	3.07 ± 0.71	6.4	0.99	1.56 ± 0.37
RX J0042.4+4112	5.92 ± 0.25	27	3.38 ± 0.52	5.2	0.89	1.75 ± 0.28
RX J0042.4+4125	1.13 ± 0.13	30	1.71 ± 0.47	38.7	0.85	0.66 ± 0.20
RX J0042.5+4103	1.34 ± 0.13	37	2.61 ± 0.85	65.8	1.45	0.51 ± 0.17
$\star$RX J0042.5+4113	4.15 ± 0.22	34	3.05 ± 0.50	7.1	1.22	1.36 ± 0.23
$\star$RX J0042.5+4116	6.01 ± 0.21	32	3.62 ± 0.51	6.8	1.16	1.66 ± 0.24
$\star$RX J0042.5+4119	3.30 ± 0.20	33	0.83 ± 0.28	9.2	1.58	3.97 ± 1.35
RX J0042.5+4132	1.69 ± 0.16	38	1.56 ± 0.29	5.0	0.11	1.08 ± 0.23
RX J0042.6+4052	32.45 ± 0.53	51	9.16 ± 1.01	11.6	1.98	3.54 ± 0.40
$\star$RX J0042.6+4114	3.75 ± 0.17	48	0.97 ± 0.27	9.1	1.56	3.87 ± 1.09
$\star$RX J0042.6+4115	42.30 ± 0.38	41	41.28 ± 1.22	6.9	1.19	1.02 ± 0.03
$\star$RX J0042.7+4111	4.13 ± 0.21	58	1.59 ± 0.44	3.7	0.63	2.60 ± 0.73
$\star$RX J0042.7+4115	22.80 ± 0.30	52	1.62 ± 0.31	4.5	0.77	14.07 ± 2.71
$\star$RX J0042.7+4116	29.89 ± 0.28	59	1.81 ± 0.34	8.6	1.47	16.51 ± 3.14
$\star$RX J0042.8+4115	17.39 ± 0.25	63	8.04 ± 0.63	5.6	0.96	2.16 ± 0.17
$\star$RX J0042.8+4118	9.68 ± 0.33	68	5.64 ± 0.58	6.4	1.09	1.72 ± 0.19
RX J0042.8+4125	3.95 ± 0.22	62	3.44 ± 0.84	6.2	1.06	1.15 ± 0.29
RX J0042.8+4131	18.62 ± 0.45	67	11.95 ± 1.10	4.6	0.78	1.56 ± 0.15
RX J0042.9+4111	3.84 ± 0.21	73	3.13 ± 0.51	5.4	0.92	1.23 ± 0.21
$\star$RX J0042.9+4117	8.46 ± 0.13	72	0.77 ± 0.27	10.6	1.83	10.99 ± 3.82
$\star$RX J0042.9+4119	3.66 ± 0.22	76	1.64 ± 0.46	4.6	0.78	2.23 ± 0.64
RX J0042.9+4125	3.05 ± 0.19	70	3.77 ± 0.34	2.3	0.05	0.81 ± 0.09
$\star$RX J0043.0+4115	8.97 ± 0.31	79	3.26 ± 0.42	1.7	0.30	2.75 ± 0.36
$\star$RX J0043.0+4117	6.19 ± 0.27	80	1.92 ± 0.35	9.1	1.56	3.22 ± 0.61
RX J0043.1+4048	1.48 ± 0.17	81	1.04 ± 0.42	52.4	1.15	1.43 ± 0.60

ROSAT No.	F_R ($\times10^{13}$) (cgs)	*Einstein* No.	F_E ($\times10^{13}$) (cgs)	Distance ($''$)	(σ)	F_R/F_E
RX J0043.1+4114	8.60 ± 0.30	83	7.51 ± 0.61	5.8	1.00	1.15 ± 0.10
RX J0043.1+4118	7.54 ± 0.24	82	2.03 ± 0.31	2.4	0.41	3.72 ± 0.58
RX J0043.2+4107	3.08 ± 0.19	85	4.27 ± 0.94	5.4	0.93	0.72 ± 0.16
RX J0043.3+4117	4.44 ± 0.25	88	1.31 ± 0.34	32.7	0.72	3.39 ± 0.89
RX J0043.3+4120	1.80 ± 0.17	87	2.15 ± 0.52	5.0	0.85	0.84 ± 0.22
RX J0043.3+4159	1.91 ± 0.22	86	0.96 ± 0.29	12.1	0.27	1.99 ± 0.64
RX J0043.4+4107	1.67 ± 0.15	90	1.64 ± 0.28	15.3	0.34	1.02 ± 0.20
RX J0043.4+4118	3.20 ± 0.20	89	2.48 ± 0.60	15.5	1.99	1.29 ± 0.32
RX J0043.5+4113	6.31 ± 0.27	91	6.24 ± 1.02	8.8	1.51	1.01 ± 0.17
RX J0043.6+4114	5.13 ± 0.23	92	4.73 ± 0.90	9.3	1.41	1.08 ± 0.21
RX J0043.7+4124	1.00 ± 0.13	93	2.86 ± 0.74	6.4	0.68	0.35 ± 0.10
RX J0043.8+4116	6.29 ± 0.26	94	4.05 ± 0.78	5.3	0.82	1.55 ± 0.30
RX J0043.9+4045	0.85 ± 0.19	95	1.64 ± 0.50	61.8	1.34	0.52 ± 0.19
RX J0044.4+4121	7.97 ± 0.30	97	8.59 ± 1.09	2.6	0.45	0.93 ± 0.12
RX J0044.9+4059	0.84 ± 0.17	98	2.07 ± 0.73	47.2	1.03	0.40 ± 0.16
RX J0045.2+4136	0.40 ± 0.08	99	1.03 ± 0.27	52.7	1.15	0.39 ± 0.13
RX J0045.4+4146	0.32 ± 0.32	100	0.71 ± 0.23	70.4	1.53	0.46 ± 0.48
RX J0045.6+4208	6.92 ± 0.30	101	4.99 ± 0.86	0.6	0.09	1.39 ± 0.25
RX J0045.7+4139	36.00 ± 0.52	102	43.18 ± 3.15	8.3	1.37	0.83 ± 0.06
RX J0046.1+4208	1.03 ± 0.12	103	0.95 ± 0.24	28.2	0.62	1.08 ± 0.30
RX J0046.4+4201	10.08 ± 0.31	105	5.52 ± 0.89	2.1	0.34	1.83 ± 0.30
RX J0046.4+4204	8.88 ± 0.31	104	8.56 ± 0.48	15.1	0.33	1.04 ± 0.07
RX J0046.9+4220	5.19 ± 0.24	107	3.54 ± 0.53	55.6	1.23	1.47 ± 0.23
RX J0048.0+4140	7.43 ± 0.55	108	4.46 ± 0.89	44.1	0.97	1.67 ± 0.35

Table 8. Table of all optical and radio identifications.

ROSAT No.	Obj.-Cl.	Identification	Distance ($''$)	(σ)
RX J0036.3+4053	GC	BA87(5)	10.4	0.78
RX J0037.3+4043	Star (F5)	SIMBAD(SAO 36516)	13.0	1.49
RX J0038.0+4026	Star	HA94(38232)	6.1	1.21
RX J0038.4+4012	Star	HA94(9276)	6.9	1.38
RX J0038.4+4136	EO	87GB 003540.8+412038	34.9	1.51
RX J0038.6+4026	Star (K0)	SIMBAD(SAO 36541)	0.8	0.16
RX J0039.5+4008	EO	B3 0036+398	10.2	1.83
RX J0039.6+4011	Star	HA94(7297)	4.1	0.47
RX J0039.7+4039	Star	HA94(81094)	11.0	1.25
RX J0040.1+4006	Star	HA94(2646)	15.9	1.17
RX J0040.1+4044	Star	HA94(101871)	12.7	1.47
RX J0040.1+4047	Star	HA94(111215)	7.0	1.40
RX J0040.2+4015	Star	HA94(13652)	2.4	0.48
RX J0040.2+4050	EO	87GB 003730.5+403346	6.0	1.11
RX J0040.3+4043	GC	MA94a(6)	1.1	0.22
RX J0040.4+4050	Star	HA94(119503)	4.2	0.85
RX J0040.4+4129	GC	BA87(51)	20.4	1.76
RX J0040.5+4033	GC	MA94a(16)	3.8	0.24
RX J0040.5+4034	Star	HA94(61478)	4.0	0.56
RX J0040.7+4055	SNR	DO80(7)	11.3	0.64
RX J0040.8+4011	Star (K2V)	SIMBAD(GJ 28)	5.4	1.04
RX J0040.9+4056	Star	HA94(140092)	4.7	0.94
RX J0041.3+4012	EO	87GB 003844.0+395608	4.8	0.26
RX J0041.3+4051	Star	HA94(125532)	3.6	0.71
RX J0041.3+4109	Star	HA94(213303)	56.0	1.86
RX J0041.4+4025	Star	HA94(37411)	14.9	1.63

ROSAT No.	Obj.-Cl.	Identification	Distance ($''$)	Distance (σ)
RX J0041.5+4106	SNR	MA95(3-041),DO80(11)	3.2	0.45
RX J0041.6+4103	Star	HA94(175678)	14.9	1.90
RX J0041.6+4112	Star	HA94(232216)	8.1	1.61
RX J0041.7+4105	Star	HA94(189885)	0.4	0.08
RX J0041.7+4134	GC	BA87(98)	1.6	0.28
RX J0041.8+4021	EO	MRK 0957	11.0	1.93
RX J0041.9+4046	SNR	MA95(2-021)	26.0	1.67
RX J0042.0+4031	Star	HA94(50780)	8.0	0.82
RX J0042.0+4033	Star	HA94(56227)	17.3	1.78
RX J0042.0+4041	Star (F5)	SIMBAD(HD 3914)	5.5	1.05
RX J0042.0+4102	GC	MA94a(130)	9.0	1.76
RX J0042.1+4016	Star	HA94(16045)	10.1	1.10
RX J0042.2+4101	GC	BA87(138),MA94a(159)	2.0	0.40
RX J0042.2+4105	Star	HA94(196074)	4.1	0.81
RX J0042.2+4118	Star	HA94(266451)	6.4	1.29
RX J0042.3+4113	GC	BA87(142),MA94a(164)	7.3	1.43
RX J0042.3+4126	Star	HA94(302803)	10.5	1.21
RX J0042.3+4129	EO	87GB 003934.6+411250	11.9	1.55
RX J0042.4+4055	Star	HA94(136397)	8.7	1.74
RX J0042.4+4057	GC	BA87(153),MA94a(173)	6.2	1.22
RX J0042.4+4108	Star	HA94(208922)	10.7	1.37
RX J0042.4+4129	Star	HA94(316946)	2.4	0.32
RX J0042.5+4103	GC	BA87(171),MA94a(196)	2.7	0.53
RX J0042.5+4119	GC	BA87(168),BA93(1),MA94a(192)	4.6	0.91
RX J0042.5+4132	GC	BA87(176),MA94a(205)	2.5	0.39
RX J0042.6+4052	EO	NGC 0221 = M32	9.7	1.90
RX J0042.6+4115	GC	BA93(21)	7.0	1.38
RX J0042.8+4125	SNR	DO80(13)	20.4	1.15
RX J0042.8+4131	GC	BA87(196),MA94a(225)	1.6	0.31
RX J0042.9+4119	GC	BA87(203)	7.2	1.42
RX J0042.9+4125	SNR	DO80(13)	14.4	0.79
RX J0043.0+4110	Star	HA94(223193)	3.5	0.70
RX J0043.0+4115	GC	BA87(206)	3.0	0.60
RX J0043.0+4117	GC	BA87(208)	6.1	1.20
RX J0043.0+4121	GC	BA87(207),MA94a(240)	4.3	0.84
RX J0043.0+4130	GC	MA94a(236)	4.1	0.80
RX J0043.1+4114	GC	BA87(214),MA94a(251)	3.0	0.60
RX J0043.2+4107	GC	BA87(220),MA94a(257)	5.5	1.08
RX J0043.2+4112	GC	BA87(226),MA94a(269)	11.5	0.94
RX J0043.2+4127	GC	BA87(225),MA94a(266)	6.0	1.02
RX J0043.3+4114	Star	HA94(239273)	16.0	1.53
RX J0043.4+4118	SNR	MA95(2-032),DO80(15)	14.2	1.63
RX J0043.5+4116	Star	HA94(254312)	1.1	0.09
RX J0043.6+4054	EO	B3 0040+406	11.5	1.31
RX J0043.6+4114	GC	BA87(246),MA94a(299)	7.1	1.18
RX J0043.6+4126	SNR	MA95(3-059),DO80(16)	9.2	1.02
RX J0043.6+4138	Star	HA94(375268)	8.3	1.65
RX J0043.7+4128	GC	MA94a(311)	2.1	0.26
RX J0043.7+4136	GC	MA94a(314)	4.2	0.83
RX J0043.8+4106	Star	HA94(196928)	16.2	1.78
RX J0043.8+4111	SNR	BW93(230A)	10.7	0.85
RX J0043.8+4127	GC	MA94a(317)	39.9	0.83
RX J0043.9+4113	SNR	MA95(2-038),DO80(18),BW93(252)	24.7	1.78
RX J0043.9+4122	GC	BA87(267),MA94a(334)	3.0	0.58
RX J0043.9+4127	Star	HA94(307124)	7.6	1.53
RX J0043.9+4152	SNR	MA95(2-037),DO80(17)	11.7	1.06
RX J0043.9+4157	EO	87GB 004113.4+414049	7.4	0.87

ROSAT No.	Obj.-Cl.	Identification	Distance ($''$)	(σ)
RX J0044.0+4149	SNR	MA95(3-072)	19.5	1.51
RX J0044.2+4119	SNR	MA95(3-079),BW93(327)	9.1	1.28
RX J0044.2+4126	Star	HA94(302441)	7.5	0.75
RX J0044.4+4121	GC	MA94a(387)	1.9	0.36
RX J0044.4+4136	GC	MA94a(380)	5.8	1.14
RX J0044.6+4125	SNR	MA95(3-086),BW93(490A)	4.9	0.58
RX J0044.8+4129	SNR	MA95(B-012),BW93(566)	8.4	1.19
RX J0044.8+4229	Star (G5)	SIMBAD(HD4194)	6.6	0.56
RX J0045.1+4202	Star	HA94(441416)	6.4	1.28
RX J0045.2+4136	SNR	MA95(2-048),BW93(717),DO80(19)	11.9	1.23
RX J0045.2+4217	Star	HA94(466304)	14.8	1.48
RX J0045.4+4132	GC	MA94a(447)	15.5	1.85
RX J0045.4+4146	SNR	MA95(1-013)	17.3	1.54
RX J0045.5+4210	Star	HA94(456238)	7.8	1.48
RX J0045.7+4139	GC	BA87(318),MA94a(468)	5.8	1.08
RX J0045.9+4156	Star	HA94(431022)	6.1	1.21
RX J0045.9+4203	Star	HA94(442137)	8.5	1.10
RX J0045.9+4226	Star	HA94(479836)	8.1	1.61
RX J0046.0+4136	Star	HA94(364424)	20.4	1.78
RX J0046.2+4154	Star	HA94(425498)	6.3	1.26
RX J0046.4+4201	GC	BA87(329),MA94a(487)	3.0	0.53
RX J0046.6+4225	Star	HA94(478682)	3.8	0.76
RX J0046.7+4208	EO	87GB 004359.8+415217	6.1	1.20
RX J0046.7+4230	Star	HA94(483376)	18.9	1.86
RX J0047.0+4157	Star (F)	SIMBAD(HD4444)	1.9	0.22
RX J0047.0+4201	Star	HA94(440331)	9.8	0.66
RX J0047.2+4202	Star	HA94(441062)	14.5	1.92
RX J0047.4+4220	Star	HA94(472654)	7.7	1.54
RX J0047.4+4221	Star	HA94(474007)	5.6	1.12
RX J0047.7+4201	Star	HA94(439698)	12.8	1.46
RX J0048.4+4157	Star (F8)	SIMBAD(SAO 36677)	7.4	1.14